LBL-13873 c.2

Lawrence Berkeley Laboratory
UNIVERSITY OF CALIFORNIA

A DIFFERENCE FOURIER COMPARISON BETWEEN FROZEN HYDRATED AND GLUCOSE EMBEDDED PURPLE MEMBRANE

RECEIVED
LAWRENCE
BERKELEY LABORATORY

FEB 9 1983

LIBRARY AND
DOCUMENTS SECTION

Jules S. Jaffe
(Ph.D. thesis)

November 1982

TWO-WEEK LOAN COPY
This is a Library Circulating Copy which may be borrowed for two weeks. For a personal retention copy, call Tech. Info. Division, Ext. 6782.

Donner Laboratory

Biology & Medicine Division

Prepared for the U.S. Department of Energy under Contract DE-AC03-76SF00098

LBL-13873 c.2

DISCLAIMER

This document was prepared as an account of work sponsored by the United States Government. While this document is believed to contain correct information, neither the United States Government nor any agency thereof, nor the Regents of the University of California, nor any of their employees, makes any warranty, express or implied, or assumes any legal responsibility for the accuracy, completeness, or usefulness of any information, apparatus, product, or process disclosed, or represents that its use would not infringe privately owned rights. Reference herein to any specific commercial product, process, or service by its trade name, trademark, manufacturer, or otherwise, does not necessarily constitute or imply its endorsement, recommendation, or favoring by the United States Government or any agency thereof, or the Regents of the University of California. The views and opinions of authors expressed herein do not necessarily state or reflect those of the United States Government or any agency thereof or the Regents of the University of California.

LBL-13873

A DIFFERENCE FOURIER COMPARISON BETWEEN FROZEN HYDRATED AND GLUCOSE EMBEDDED PURPLE MEMBRANE

Jules S. Jaffe

Lawrence Berkeley Laboratory
University of California
Berkeley, California 94720

This work was supported by the U. S. Department of Energy under contract No. DE-AC03-76SF00098.

ACKNOWLEDGEMENTS

The author would like to express his sincere appreciation and gratitude to the people that have helped to provide a healthy environment for the genesis and development of ideas. Most notably among these, my advisor, Dr. Robert Glaeser, deserves special thanks for his continued support and dedication to the educational goals of his students. Special mention should also be made of Dr. Steven Hayward who contributed, not only the data for the glucose embedded specimens, but also many helpful discussions.

I would also like to thank Dr. Robert Stroud and Dr. Sung Ho Kim for a critical reading of the thesis and Dr. Janet Moore for sharing her ideas as we both completed similar projects.

Other members of Donner Lab who deserve special thanks are Dr. Kenneth Downing, Dr. David Grano, Dr. Bing Jap, Dr. Gina Sosinsky, and Dr. Kenneth Taylor.

Finally, I would like to thank my wife, Janet, for always being there to provide an encouraging perspective.

TABLE OF CONTENTS

ACKNOWLEDGEMENT. iii

TABLE OF CONTENTS. v

ABSTRACT vii

CHAPTER I

PURPLE MEMBRANE. 1

A. Function 1

B. Structure: Static 3

C. Dynamic Probes of the Structure of Purple Membrane . . 17

D. Current Models of Purple Membrane/Future Prospects . . 24

CHAPTER II

PRESERVATION OF BIOLOGICAL SPECIMENS FOR HIGH RESOLUTION ELECTRON MICROSCOPY. 31

A. Introduction 31

B. Techniques for the Preservation of Structure at Intermediate Resolution. 33

C. Techniques for the Preservation of High Resolution Information. 37

D. Physical Parameters Important in High Resolution Specimen Preservation. 41

E. A Method for Obtaining High Resolution Electron Diffraction Patterns of Purple Membrane 45

CHAPTER III

COMPUTER PROCESSING OF DIFFRACTION PATTERNS: SCANNING AND SCALING 51

A. Scanning of Diffraction Patterns 51

B. Processing of Diffraction Patterns 53

C. Response of the Photo-Emulsion to Electrons. 54

D. Scaling of Diffraction Patterns. 59

CHAPTER IV

DIFFERENCE FOURIER TECHNIQUES. 67

A. Methodology and Goals. 67

B. Error Analysis of the Difference Fourier Method. . . . 73

C. Examples of the Use of the Difference Fourier Technique 78

CHAPTER V

RESULTS AND CONCLUSIONS. 90

A. Microscopy 90

B. Data Processing. 91

C. Interpretations. 101

D. Summary. 102

APPENDIX A

A Guide to the Use of the "DIFPROC" System 105

Purpose of System 105

General Description: Input-Output of Flow Chart of Typical Session 105

DIFPROC COMMANDS 110

REFERENCES 112

A Difference Fourier Comparison between Frozen Hydrated and Glucose Embedded Purple Membrane

by
Jules S. Jaffe

ABSTRACT

The purple membrane from Halobacterium halobrium has been studied at liquid nitrogen temperature using electron diffraction. A new technique for preparing purple membranes in the frozen hydrated state has been devised. The increase in reliability that this technique offers over previous methodologies is primariy due to the controlled evaporation of solvent. Diffraction patterns of purple membrane prepared in this manner have been found to extend to a resolution of 3.2A.

In order to visualize any differences that might exist between the frozen hydrated specimens and glucose embedded ones a differnce Fourier analysis has been performed. A set of three (3) frozen hydrated diffraction patterns and three (3) glucose embedded patterns were processed via a system of computer programs that were devised and implemented for this purpose. Various statistical measures were used to analyze the reliability of the final difference maps based on the accuracy of the data. Several new features of the membrane have been revealed as a result of this process. Areas between the trimers seem to be slightly depressed. No large aqueous channels have been revealed, in confirmation with the results of previous investigations. Finally, several interesting features of marginal

statistical significance may indicate areas where significant structure will emerge when more data has been collected and analyzed.

This thesis also contains a summary of our current knowledge of the structure and function of purple membrane. In addition, various aspects of the history of the preservation of biological specimens for high resolution electron microscopy are reviewed.

CHAPTER I

PURPLE MEMBRANE

A. Function

Purple membrane is a specialized area of the plasma membrane of Halobacterium halobium that is dedicated to converting light energy into chemical energy. It is quite amazing, but true, that this single protein molecule can take photons of visible light and use their energy to generate an electrochemical gradient, by translocating protons across the membrane. This proton gradient can then be used to run the various functions of the cell such as the synthesis of ATP and the uptake of various nutrients.

It would thus appear that purple membrane (PM), or its constituent protein, bacteriorhdopsin (bR), would be an important specimen to be used in order to solve an interesting question about a bioenergetic mechanism. That is, how energy is transformed from one form to another. Indeed, the biochemistry, structural biology, and spectroscopy of PM are currently being pursued in a multiplicity of laboratories. In the following it will be shown that the main problems being encountered by many of the researchers are due to the large differences that exist between the analysis of bR and conventional protein analysis. Mostly, this is because of the fact that PM is the first truly intrinsic membrane protein that has been subject to such intensive study. Thus, it seems that the study of PM represents two kinds of frontiers, one in the amount of new information we will learn in studying a membrane protein, the other in the kind of methodology that is

needed to be developed in order to study the system. We shall see that the PM literature is filled with examples of these discoveries. However, I think it is safe to say that the really exciting thing about bacteriorhodopsin is that we are still a long way from understanding how it really works.

The halophilic bacterium in which purple membrane is found occupies a unique ecological niche: it grows well in saturated salt solutions. In fact, when the salt concentration is lowered below 4.3 M the bacteria will lyse, leaving intact a large fraction that is PM. It was in 1967 as part of a careful investigation of the fragments of Halobacterium halobium that Stoeckenius and Rowen [1967] and later Stoeckenius and Kunau [1968] isolated and partly characterized a purple fragment. Subsequently, Oesterhelt and Stoeckenius [1971] were able to show that the purple membrane contained only one polypeptide with a MW of 26,000 and that it was linked to a retinal in a 1:1 ratio via a Shiff base linkage to an ϵ amino group of a lysine. Various structural observations were also made at that time.

The real function of the membrane was not discovered until 1973 [Oesterhelt and Stoeckenius, 1973]. These authors were able to demonstrate that cells that were either anaerobic or starved were able to generate and maintain a proton gradient across the cell membrane as long as they were exposed to light. However, it was not until 1973 that the role of PM in pumping protons was unambigously established by incorporating it into phospholipid vesicles [Racker and Stoeckenius, 1973]. As this system consisted of only pure bR, it was demonstrated

very clearly that upon illumination, the uptake of protons was a result of the action of purple membrane. In addition, inclusion of ATPase in the vesicle preparations resulted in the generation of ATP, which also demonstrated the feasibility of the Mitchell hypothesis.

B. Structure: Static

Purple membrane is composed of three species of molecule; protein, lipid, and a retinal. Analysis of the isolated membrane showed a content of 75 percent protein and 25 percent lipid [Oesterhelt and Stoeckenius, 1971]. As stated above, one polypeptide of molecular weight 26,000 comprises the protein. The choromophore, or retinal, is depicted in Figure 1-1. As first elucidated by Oesterhelt and Stoeckenius [1971] the all trans configuration is shown bonded to a lysine via an ϵ-amino link in a 1:1 ratio with the protein.

The lipid groups of purple membrane extracted in chloroform-methanol contain phosphotidyl glycerophosphate (52 percent), phosphatidyl glycerol (4 percent), and several neutral lipids, largely squalenes (9 percent). Two sulfolipids are also found, phosphatidyglycerosulfate (5 percent) and a glycolipid sulfate (10 percent), which are not present in the red membrane, another part of the bacterial plasma membrane. It is also interesting to note that the phospholipids are in an ether linkage (rather than ester) and that the tail groups contain branched methyls.

Initial structural work on purple membrane [Blaurock and Stoeckenius, 1971] utilized freeze-fracture as well as x-ray diffraction. At that time researchers were able to show that purple membrane consisted

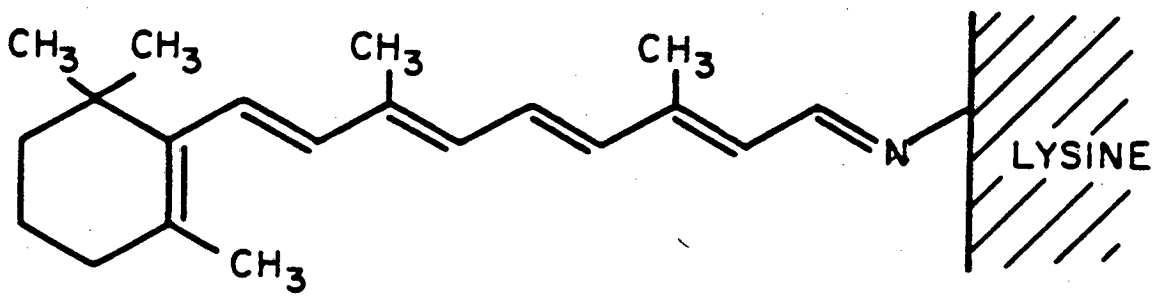

XBL 829-4128

Fig. 1.1 All trans retinal bound to lysine.

of a regular array of particles packed hexagonally, with a unit cell constant of 63Å. Reflections along the meridian established that the membranes stacked *in vacuo* with a 49Å inter-membrane distance. The freeze fracture micrographs revealed a hexagonal appearance on the (A) face and a smoother appearance on the (B). Membranes that were dried onto mica and then shadowed revealed cracks along a hexagonal pattern in support of the hypothesis that purple membrane is a two dimensional crystal *in vivo*.

The primary structure of purple membrane is currently known due to the efforts of Khorana's group at MIT and Ovchinnikov's group in the Soviet Union [Ovchinnikov et al., 1977, 1979]. New methods of protein sequence analysis were necessary to decode the linear sequence of polypeptides. This was due to the extreme hydrophobicity of the membranes [Khorana et al., 1979]. The complete amino acid sequence is shown in Figure 1-2 taken from Khorana [1979]. A very striking thing about this sequence is that over 70 percent of the residues are hydrophobic. It is probable that the long stretches of hydrophobic residues are embedded in the membrane core with some of the more hydrophilic groups extending into the aqueous regions on either side of the membrane. However, a troublesome aspect of this sequence is that there are hydrophilic groups located close to and interspersed with some of these hydrophobic stretches. If these charged groups are to be embedded in the membrane then a large amount of energy would be required to keep them there. A possible solution as proposed by Engelmen et al. [1980] would be to put buried negative and positive

	5		10		15		20		25
Glu Ala Gln Ile	Thr	Gly Arg Pro Glu	Irp	Ile Trp Leu Ala	Leu	Gly Thr Ala Leu	Met	Gly Leu Gly Thr	Leu
	30		35		40		45		50
Tyr Phe Leu Val	Lys	Gly Met Gly Val	Ser	Asp Pro Asp Ala	Lys	Lys Phe Tyr Ala	Ile	Thr Thr Leu Val	Pro
	55		60		65		70		75
Ala Ile Ala Phe	Thr	Met Tyr Leu Ser	Met	Leu Leu Gly Tyr	Gly	Leu Thr Met Val	Pro	Phe Gly Gly Glu	Gln
	80		85		90		95		100
Asn Pro Ile Tyr	Trp	Ala Arg Tyr Ala	Asp	Trp Leu Phe Thr	Thr	Pro Leu Leu Leu	Leu	Asp Leu Ala Leu	Leu
	105		110		115		120		125
Val Asp Ala Asp	Gln	Gly Thr Ile Leu	Ala	Leu Val Gly Ala	Asx	Gly Ile Met Ile	Gly	Thr Gly Leu Val	Gly
	130		135		140		145		150
Ala Leu Thr Lys	Val	Tyr Ser Tyr Arg	Phe	Val Trp Trp Ala	Ile	Ser Thr Ala Ala	Met	Leu Tyr Ile Leu	Tyr
	155		160		165		170		175
Val Leu Phe Phe	Gly	Phe Thr Ser Lys	Ala	Glx Ser Met Arg	Pro	Glu Val Ala Ser	Thr	Phe Lys Val Leu	Arg
	180		185		190		195		200
Asn Val Thr Val	Val	Leu Trp Ser Ala	Tyr	Pro Val Val Trp	Leu	Ile Gly Ser Glu	Gly	Ala Gly Ile Val	Pro
	205		210		215		220		225
Leu Asn Ile Glu	Thr	Leu Leu Phe Met	Val	Leu Asp Val Ser	Ala	Lys Val Gly Phe	Gly	Leu Ile Leu Leu	Arg
	230		235		240		245		250
Ser Arg Ala Ile	Phe	Gly Glu Ala Glu	Ala	Pro Glu Pro Ser	Ala	Gly Asp Gly Ala	Ala	Ala Ala Thr Ser	

Figure 1-2 Complete amino acid sequence of bacteriorhodopsin.

charges next to each other leading to stable ionic interactions. This idea has led these researchers to call bacteriorhodopsin an "inside-out" protein [Engleman and Zaccai, 1980].

A more detailed question about the structure of bR concerns how the polypeptide winds its way through the membrane. Ovchinnikov's group [Ovchinnikov; 1977] treated purple membrane with proteolytic enzymes and were able to cleave off a 17 amino acid fragment at the C terminus that is rich in asparatic and glutamic acid. More extensive treatment was able to cleave between residues 3 and 4 as well as between residues 72 and 73. The fact learned from these studies is that those particular cleaved sites are exposed to the aqueous phase. By preparing oriented vesicles it was also shown [Gerber et al., 1977] that the carboxyl terminus of PM is on the cytoplasmic side. Later results [Ovchinnikov, 1979] revealed that a short loop consisting of residues 65 to 73 could be detached from the membrane. Additionally, harsher treatment was able to cleave the peptide bond between Ser-Met (161-162). In summary, the exposed fragments are then 1-4, 65-73, 161-162, and 230-247 according to Ovchinnikov's group. In addition to doing cleavage experiments, Khorana [1979] performed calculations to determine the secondary structure using a semi-empirical technique [Chou and Fassman; 1978]. The results of the calculations were in general agreement with the cleavage sites indicating probable turns at Arg^{7}-Trp^{10}, Phe-71, and also residues 36-39. Ovchinnikov's cleavage site at residue 162 was not observed by these researchers. An additional site exposed to the aqueous phase [Katre et al., 1981a] has also been observed at Tyr 131/133 via iodination.

The interpretation of this information has been aided by a knowledge of the secondary structure of bacteriorhodopsin obtained from electron microscopy, x-ray diffraction, and spectroscopy. In the case of x-ray diffraction only a limited amount of information about the structure can be learned. At present, large three-dimensional crystals have not been grown of a kind suitable for this method of study. A membrane-profile x-ray diffraction pattern of oriented multilayers [Blaurock et al., 1977] was phased to reveal an asymmetric bilayer [Blaurock and King, 1976]. X-ray patterns also revealed strong diffraction in the equatorial plane at 10Å and 4.6Å and also strong peaks at 5Å and 1.5Å along the meridian, i.e., perpendicular to the membrane [Blaurock, 1975; Henderson; 1975]. The peaks at 10Å, 5Å and 1.5Å were attributed mainly to α-helix content and the peak at 4.6Å mainly to lipids. Closer inspection of the x-ray patterns was consistent with helices oriented with their long axis perpendicular to the plane of the membrane [Henderson, 1975].

Spectroscopic techniques have provided strong hints about the secondary structure of PM. Again, there have been problems in adapting methodologies that have been "tried and true" on the assortment of water soluble proteins. In applying the technique of ultraviolet wavelength circular dichrosism (CD) two problems that can interfer with the results of the observation of such spectra are light scattering and absorption flattening. On the basis of a semi-empirical formula, Long et al. [1977] calculated an α-helical content of 70-80 percent for PM. However, using a technique that corrects experimentally for light scattering Jap et al. [unpublished results] argue that the per-

cent of α-helix content is not more than about 50 percent of the total protein. Estimation of α-helical content was accomplished by using an empirical basis data set derived from water soluble proteins.

Infra-red spectra have also been observed in an attempt to determine more information about the secondary structure. Again, complications arise because of the atypical nature of PM. Polarized infrared spectroscopy [Rothchild and Clark, 1979] of oriented PM was used to demonstrate that the α-helices were in a range of tilt less than 26° away from the membrane normal. However, the frequencies of the Amide I and A peaks were at least 10 cm^{-1} higher than values found for most α-helical polypeptides and proteins. A possible explanation for this deviation, which was cited by these authors, is that the helices are distorted from the normal α-configuration. A detailed explanation of this distortion may include supercoiling of the helices [Henderson and Unwin, 1975], or unusual interactions of the side chain groups.

Very recently, an interesting proposal by Krimm (1982) that the helices may be of the α_{II} type may explain the shifts in the absorbtion bonds as this type of helix will absorb at the experimentally measured frequencies. Also cited in Krimms' paper are several examples of proteins which contain supercoiled helices whose absorbtion bands are more similar to that of normal α-helices. It thus appears reasonable at the present time that the helices are either distorted or of a non-standard type.

Electron crystallographic studies of PM have yielded a great deal of information [Unwin and Henderson, 1975]. Using a low dose technique, these researchers were able to obtain a projected and subsequent 3-dimensional map to a resolution of approximately 7Å in plane of the membrane and 14Å perpendicular to the plane [Henderson and Unwin, 1975]. A projection of the Unwin-Henderson structure to a resolution of 7Å is shown in Figure I-3. In agreement with the x-ray diffraction results, this intermediate resolution map was interpreted as consisting of 7 α-helices oriented approximately perpendicular to the plane of the membrane. The inner row of three helices was considered to be oriented exactly perpendicular to the membrane, approximately 10Å apart, and the outer region was interpreted to be 4 slightly tilted helices. Unfortunately, neither the connections between the helices or the location of the retinal was revealed by this methodology. More recently, Hayward and Stroud [1981] have obtained a high resolution projection of the structure to 3.7Å. This is shown in Figure 1-4. Of special interest in this map is the branched appearance of several of the helices and an indication of some of the possible locations of the lipids.

The absolute orientation of the Unwin and Henderson model in the membrane is of a great deal of interest since the vectorial translocation of protons must ultimately be related to it. Again, the electron crystallographic technique was able to answer this question. The orientation was determined by two different research groups, using two different methodologies. Hayward et al. [1978] were able to observe

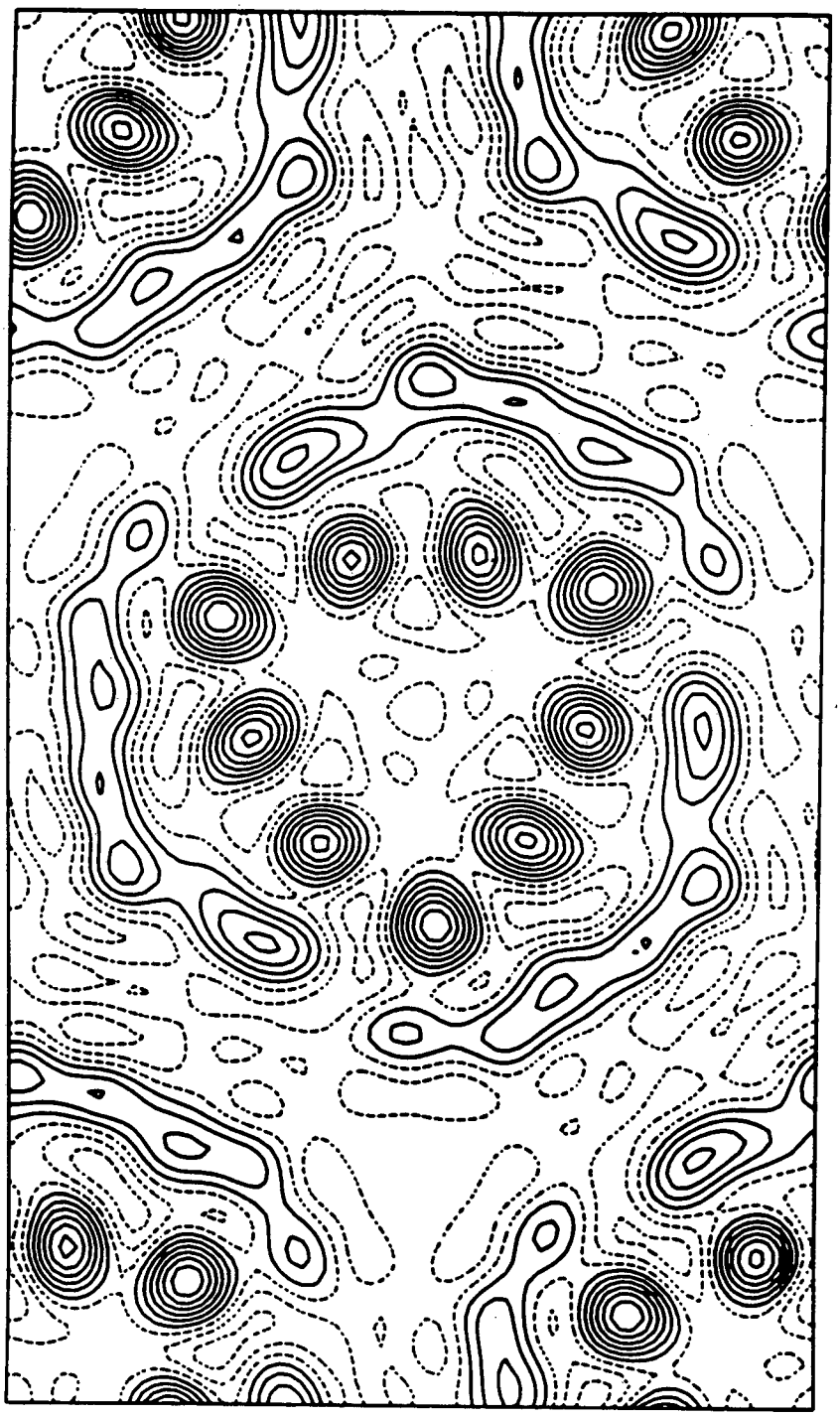

XBL 8211-3269

Fig. 1-3. Projected structure of purple membrane to 7Å (Unwin and Henderson, 1975).

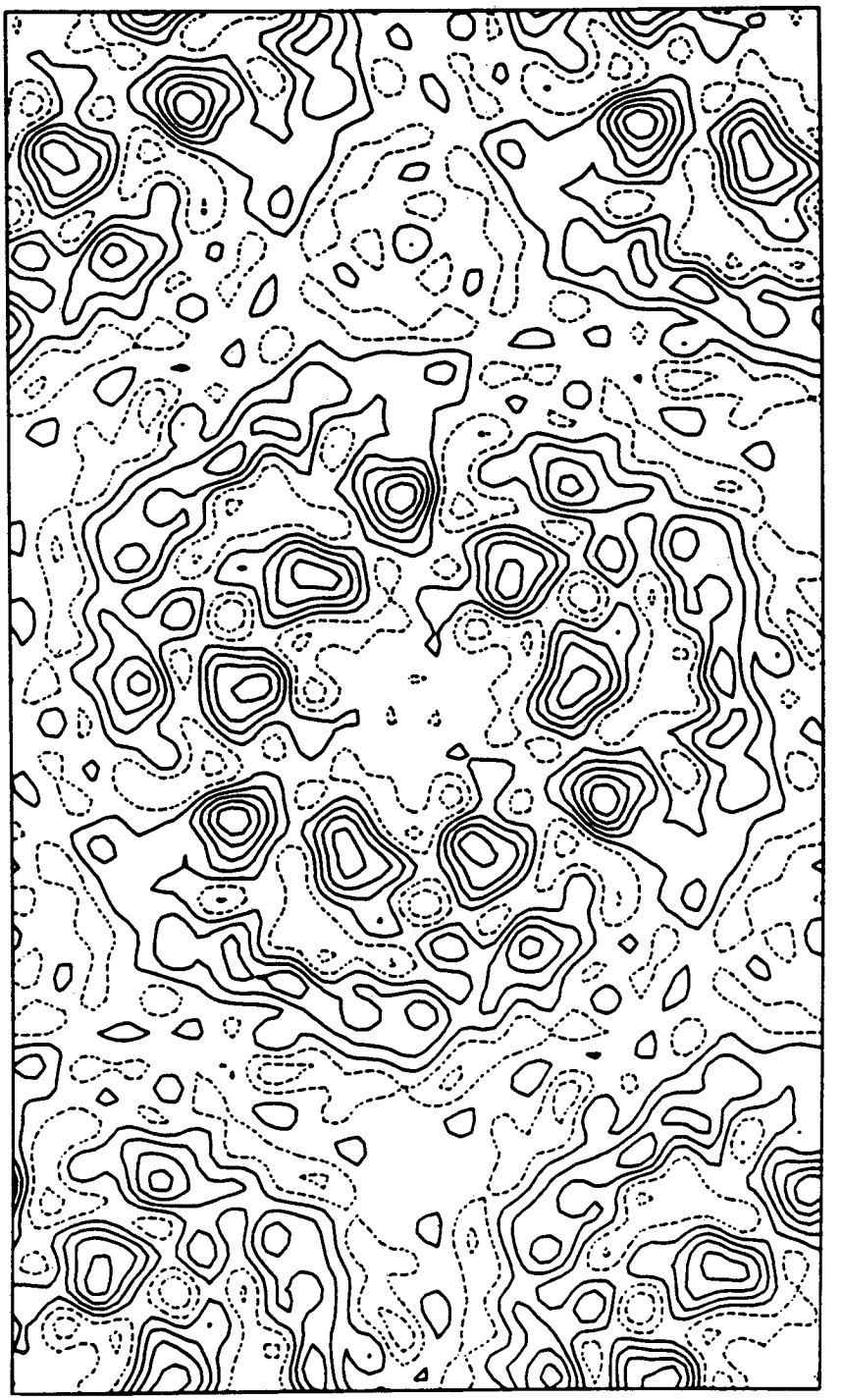

XBL 8211-3270

Fig. 1-4. Structure of purple membrane to 3.7Å (Hayward and Stroud, 1981).

PM attached to polylysine, as a function of pH, via electron microscopy. Observation of the handedness of the diffraction pattern was correlated with the projected structure and the known preference of the membrane for polylysine adhesion [Fisher, 1978]. Henderson et al. [1978] were able to use a ferritin/avidin/biotin labeling technique to correlate the sidedness of the membranes with freeze fracture. It was shown by both groups that the outer slur of helices fans out towards the "cytoplasmic" side, and thus in the three dimensional Unwin and Henderson photograph of the model structure [Henderson and Unwin, 1975] the bottom corresponds to the extracellular surface of the membrane.

Obviously, knowledge of the location of the amino acid residues in the membrane must be correlated with a knowledge of the location and orientation of the retinal group. Assuming that the retinal group is linked to a lysine via a Schiff base, one would like to ask; to which lysine in the amino acid sequence is the retinal linked. This simple question has had a very complicated answer in recent times. Based on the location of a retinal binding polypeptide fragment determined by Bridgen and Walker [1976], Ovchinnikov's group decided that the retinal binding lysine was the 41st amino acid in the sequence. However, the corrected sequence information cast doubt upon whether Lys41 really bound the retinal. In the meantime, all models of PM assumed that Lys41 bound the retinal group. More recently [Lempke and Oesterhelt, 1981; Mullen et al., 1981; Katre et al., 1981b; and Bayley et al., 1981] have suggested that the retinal is located on Lys216 either exclusively, or most of the time, with a possible minor fraction on

Lys41. The main problem with these chemical modification reactions is that an incorrect conclusion may be drawn as a result of a mixed equilibrium that might exist with a minor fraction that is kinetically accessible to the modifying reagent (in this case, $NaBH_4$). Therefore, none of these assignments is definitive. The results of Katre et al. [1981] are extremely interesting. They suggested that the linkage to either Lys41 or Lys216 was dependent on whether the protein was reduced in the dark or light, whether the sample is light or dark adapted, and on temperature. They could not also rule out the isolation of "physiologically irrelevant linkages", but their suggestion would make it possible that Lys41 and Lys216 are close together in the tertiary structure of the protein. However, an interesting experiment by Sigrist and Zahler (1981), reporting that phenylisothiocyanate selectively reacts with LyS-216 with little effect on the spectral properties, leads one to wonder if the retinal is really attached to this amino acid.

Once one has determined where in the amino acid sequence the retinal is located the next question to be answered is: Where in the Unwin and Henderson model (low resolution map) is the retinal. In order to answer this question, researchers have taken basically the same approach, modification of the retinal group. Neutron diffraction of purple membrane with deuterated retinal [King et al., 1979] has led to the conclusion that the retinal is centrally located within the plane of the membrane. Problems encountered with this kind of methodology are related to the experimental availability of only intensities, not phases. Phases for diffraction profiles were calculated that were

consistent with the data and indicative of the above results. Assuming attachment to Lysine 216, and assuming that the C_α of arginine 224 is close to the surface, then the Lysine 216 (and retinal) residue would be located 12Å from the surface, in the central region of the membrane [Bayley et al., 1981]. Neutron diffraction of deuterated retinal may also be used to study the location of the chromophore in the plane of the membrane [King et al., 1980]. Using PM prepared in this way it has been possible to suggest a model for the location of the β-ionine ring and the hydrocarbon chain. This model is shown in Figure 1-5. Again, phasing problems are encountered. In this case, the electron microscopic phases were used to approximate the values of neutron phases. In addition, superposition of certain diffracted intensities in the neutron powder patterns makes interpretation of the neutron results difficult, due to the assumptions needed to calculate the intensities for individual reflections. Surely, the incorrectness of these approximations will decrease the signal due to the deuterated retinal. Whether an incorrect conclusion can be obtained from such a study is currently an open issue.

Henderson has utilized brominated retinals for electron microscopic study to determine the location of the chromophore [Henderson, unpublished results]. Only small changes in electron scattering are anticipated to occur from bromination, and the experiment has proved to be a difficult one as difference maps have, so far, been uninterpretable [Wallace, 1981]. Perhaps the results of Katre et al. that indicate that the retinal can migrate are correct and this has limited the crystallographically obtainable information.

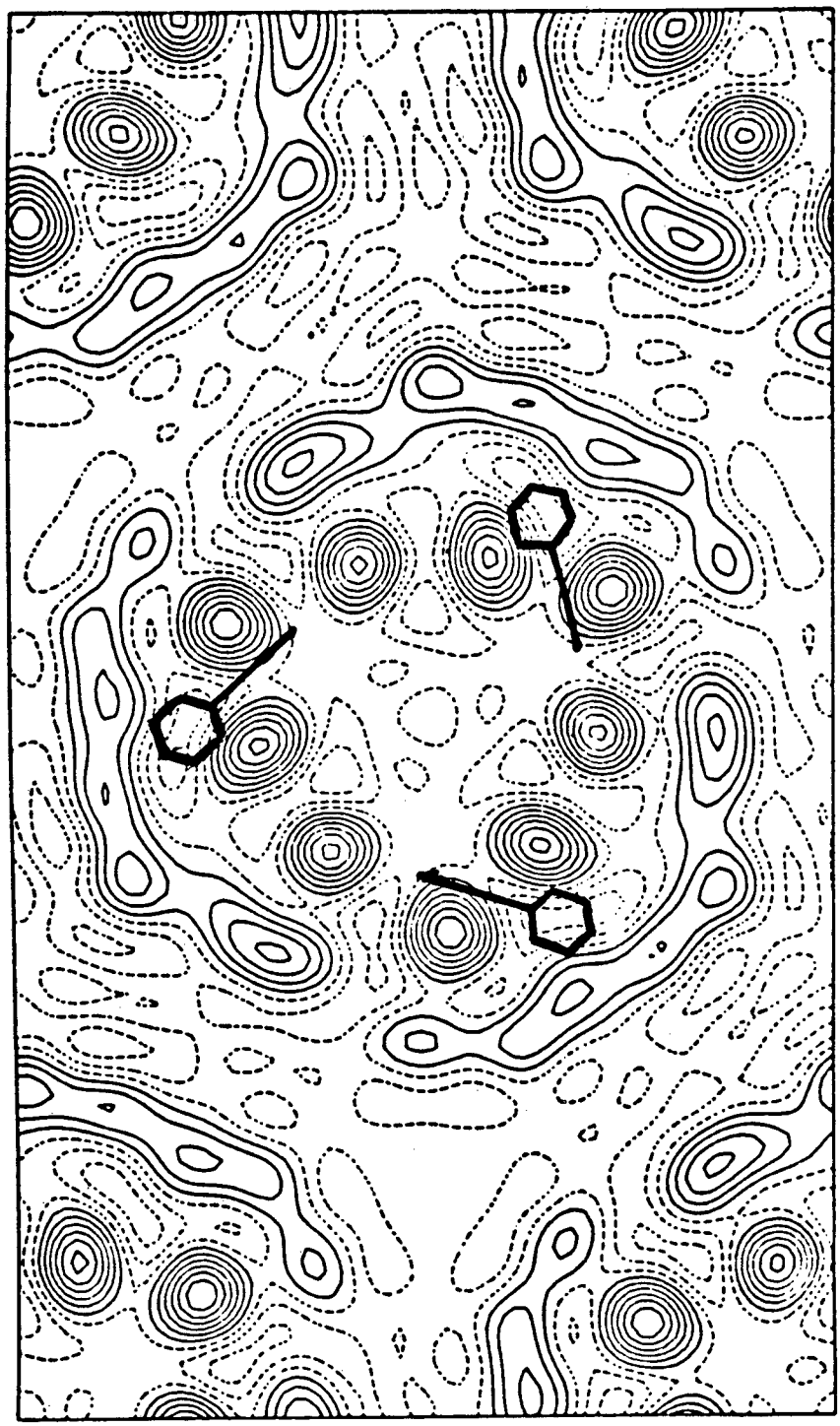

XBL 8211-3268

Fig. 1-5. Location of the chromophore in the plane of the membrane as derived from neutron experiments (King, 1980).

Spectroscopic techniques have also been used to determine the orientation of the hydrocarbon chain and the distance between the retinal groups in trimers. The angle of tilt relative to the membrane plane has been calculated to be approximately 22° [Bogomolni et al., 1977]. Using the presence and absence of excitonic interactions in the CD spectra [Ebrey et al., 1977] the distance between chromophores was calculated to be 9-12Å, in conflict with the neutron data. More recently, a Japanese group [Koyama, et al., 1981] have used fluorescence energy transfer to estimate that the chromophore is situated near the center of the protein in an orientation such that the dipole-dipole interactions with neighboring chromophores is close to a minimum.

Little is known about what relationship the lipids that surround bacteriorhodopsin have to the protein molecule itself. The high resolution map of Hayward and Stroud [1981] indicates probable location of some of the lipid groups. One hopes that the answers to these interesting questions will be found when higher resolution three dimensional data is available.

C. Dynamic Probes of the Structure of Purple Membrane

In contrast to the static picture of PM that has been obtained via the x-ray, electron microscopic, and neutron studies, a great deal of information has been learned about the dynamic changes the molecule undergoes via spectrophotometric techniques. Observation of visible and Raman spectra due to the chromophore have provided detailed information about the conformation of the retinal under conditions of dark adaption and proton cycling.

A lysine-retinal Schiff base would be expected to show an absorbance maximum at 370 nm, however, bacteriophodopsin absorbs maximally at 568 nm (bR 568) with only minor bands at 400 nm [Stoeckenius, 1980]. This large red shift has complicated interpretation of the visible spectra. Keeping bacteriorhodopsin in the dark will shift the absorbance maximum to 558 nm with a small decrease in absorbance. This form is known as br_{558}^{DA} and its reaction kinetics have been shown to be too slow to participate directly in the photocycle. Illumination with moderate light intensity will convert bR to the light adapted state within a few seconds. Extraction of retinal from bR_{568}^{LA} yields nearly exclusively all-trans retinal while bR_{558}^{DA} yields equal amounts of 13-cis and all-trans isomers [Oesterhelt et al., 1973]. It has been presumed that this transformation reflects some lability in the chromophore rather than having functional significance.

A general mechanism of how proton translocation is accomplished certainly involves a cyclic isomerization of the chromophore that either directly or indirectly participates in this process. Dissection of the individual steps in the photocycle have been complicated by the overlap of the spectra of the intermediates and the rapidity of the sequence of events. By altering the chemical environment and/or running the photocycle at low temperature, intermediate lifetimes can be extended into the observational realm.

Concentrated salt solutions saturated with diethyl ether were used [Oesterhelt and Hess, 1973] to produce a bleached form of PM. This form was found to exhibit a maximal absorbance at 412 nm and it was found to regenerate to the 570 nm form in the dark with a half time of

13 sec at 20°C. A release of protons was observed concomitantly with the formation of the 412 nm complex and an uptake upon regeneration to the 570 nm form. Low temperature trapping of the 412 complex can also be accomplished by cooling a suspension of membranes during illumination [Stoeckenius and Lozier, 1974]. An additional intermediate that is indefinitely stable at 77°K and that absorbs maximally at 610 (K610) has been identified [Lozier, Boglomoni, and Stoekenius, 1975], by illuminating bR_{570}^{LA} with 500 nm light. Subsequent illumination with 650 nm light will completely regenerate the BR570. Before regenerating to the 570 species, two more intermediates are formed, one with an absorbtion of 550 (L550) and the other with an absorbtion of 415 (M415).

Current thinking about the photocycle is summarized in Figure 1-6 taken from Braiman and Mathies [1982]. Flash spectroscopy has lead to the discovery of the sequence of events in the photocycle which confirmed some of the earlier results. As can be seen, the primary photoproduct K_{590} has a rise time of less than 10 pico-seconds. Resonance Raman spectra in coordination with the synthesis of several model compounds has provided evidence that K exists in a primarily 13-cis form. However, the presence of unusually strong "low wavenumber" lines indicates the chromophore is in a distorted conformation [Braiman and Mathies, 1980]. It is interesting to note that the remainder of the photocycle does not require the presence of light. This implies that the energy necessary for completion of the cycle is somehow stored in the conformational state of K_{590}. Evidence that the Br_{570} state contains an all-trans chromophore [Braiman and

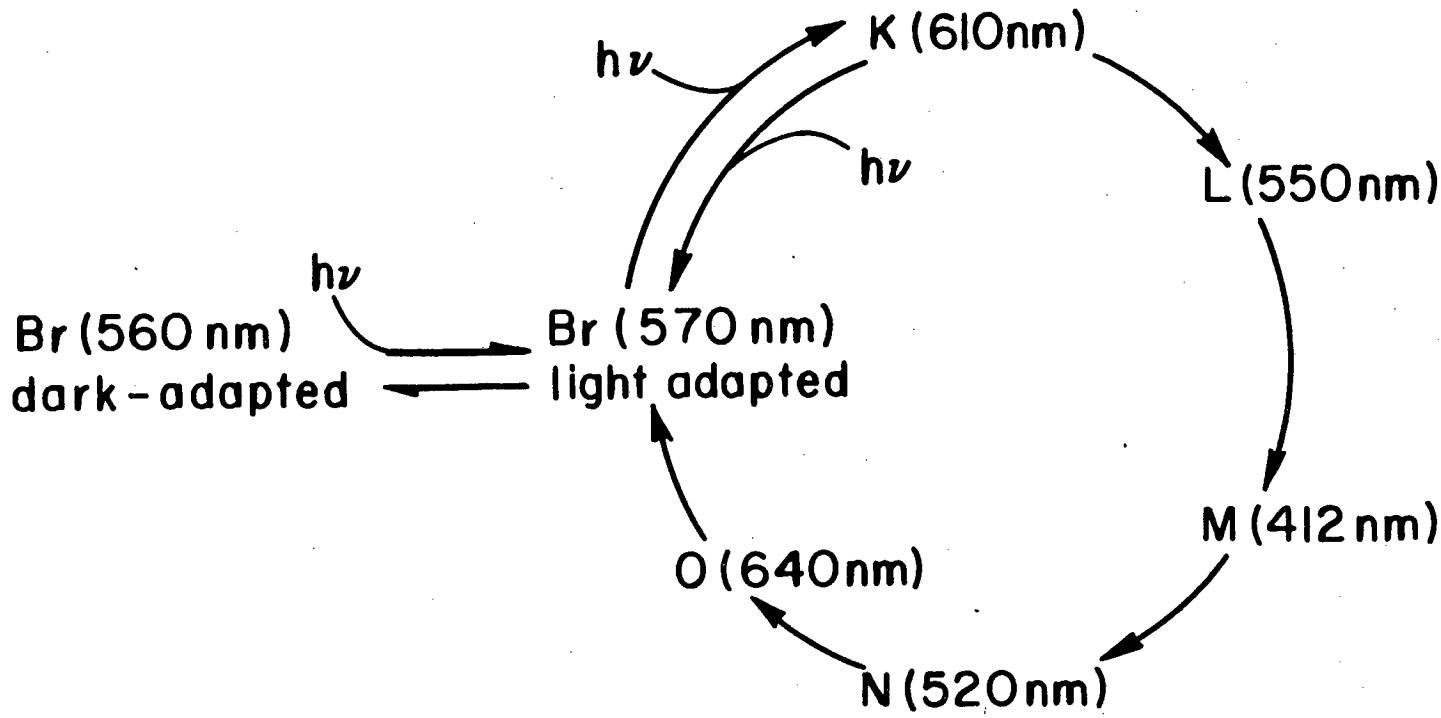

XBL829-4126

Fig. 1-6. Photocycle of purple membrane (Braiman and Mathies, 1982).

Mathies, 1980] strongly implies that a trans-cis conformational change occurs during the primary photochemical event.

The next photocycle intermediate, L_{550}, decays in ~40μs and the resonance Raman spectra are indicative of the cis conformation being maintained. The M_{412} intermediate shows changes in visible and Resonance Raman spectra. Model compounds have strongly implicated this (the M_{412} complex) as being in the 13-cis state [Braiman and Mathies, 1980]. The remaining intermediates in the photocycle have been studied using the same techniques as above, however, their kinetics are more complicated [Lozier, private communication]. There is some evidence that M is followed by N and O. There is also a possibility that a more complicated sequence of events than a linear chain of photo-intermediates exists, based on the difficulty of fitting the observed spectra [Stoeckenius, 1980].

One feature of the photocycle is the observation that the Schiff base exists in both a protonated and deprotonated form [Lewis et al., 1974]. Spectra observed using the Resonance Raman technique are consistent with Br_{570} being protonated and the M_{412} intermediate being deprotonated. This is also consistent with data obtained in the high salt-ether system [Oesterhelt and Hess, 1973] as well as results obtained by using a pH indicator dye to measure changes in pH [Lozier et al., 1975]. Although it is possible that the proton involved in the deprotonation of the base is actually translocated across the membrane, there is presently no strong evidence to support this hypothesis.

In an effort to localize any bulk channels for the transport of water Zaccai and Gilmore [1979] prepared PM in a state suitable for neutron studies by varying H_2O/D_2O mixtures in oriented multilayers. Assuming that their arguments are correct in terms of the absolute scale of the effects that they observed, they exclude the possibility of the existance of bulk water channels (10Å diam. pores) extending into the membrane by more than 5Å. It should also be noted that these structural analyses via neutron diffraction are subject to a range of problems already mentioned. Areas of exchangable water seemed to correlate well with the inter-trimer lipid regions of the protein. It may well be that the exchangable hydrogens that they are observing are associated with the head-groups of the various lipids found in PM. More recently [Rogan and Zaccai, 1981], these studies have been extended to D_2O-H_2O substitution at different relative humidities. The basic results encountered here were that at high relative humidities, the lipid associated water exchanged more rapidly and at lower relative humidities (47 percent) the protein associated hydrogens exchanged more rapidly. This was interpreted as being consistent with the Englemen model (to be discussed). Additionally, no bulk water channels were discovered at lower relative humidity.

There are many interesting thermodynamic questions that one can ask about bacteriorhodopsin. The main point of interest would be to describe the bioenergetics of the process by which proton translocation occurs. Assuming that a photon is absorbed by the retinal group, an energetically excited state is then transferred from a conformational change of the chromophore into a proton being transported

across the membrane. One interesting question concerns how many protons are transported across the membrane per photon or put another way, what is the quantum efficiency.

The best system devised, so far, for answering the question of quantum efficiency has been to make "envelope vesicles" in KCl where no prexisting chemical potential ($\Delta\mu_{H+}$) exists. Interferences from other physiologically connected processes are severed by having only bacteriorhodopsin present. Unfortunately, there is no great concensus on the numerical values of quantum efficiency obtained in such systems. Values of .64-.67 were obtained by Stoeckenius' group [Stoeckenius et al., 1979]. These numbers seem to be in good agreement with the value of .79 obtained by Oesterhelt and Hess [1973]. In addition, they can be reconciled with the result of .3 (M_{412}/photon) obtained by Ebrey's group [Becher and Ebrey, 1977], at low salt by considering the value of H^+/M412 to be around 2 [Govindjee et al., 1980]. Values as high as $2H^+$/photon [Ort and Parson, 1979] have been reported.

Another interesting question concerns the actual chemical nature of the proton transport chain. It is clear that the protons must have a way of getting through the membrane. A solid state model of proton conduction has been proposed [Morowitz, 1978; Nagle and Morowitz, 1978] in which a linear chain of hydroxyl groups can rotate. The injection of a proton at one end of the chain and the release of a proton from the other end could be driven by a conformational change of the protein. In fact, it is very possible that conformational changes in the protein exist. In an ultraviolet and visible absorption spectra study of PM and its intermediates Becher et al (1978) provide evidence for

changes in the protein structure. Their results suggest that approximately 60 percent of the tryptophanes and tyrosines in the protein move from a hydrophobic (interior) environment to a hydrophilic (exterior) environment either on bleaching or on converson of PM to L or M. However, a great amount of detail is not known about these changes. This absence of information about the conformation of protein is in contrast to the great amount of information that we have about the conformation of the chromophore at each step.

D. Current Models of Purple Membrane/Future Prospects

As we have seen above, there is a great deal of information that is known about PM. Assuming that the most interesting question about PM is, how does it work, a more primitive question which is necessarily answered first is: What is its structure Presently, based on the existent structural literature, several labs have attempted to piece together plausible models.

The starting point for all of these models is the Unwin and Henderson structure consisting of 7 α-helices oriented transverse to the membrane. Assuming that the carboxyl terminus of the polypeptide chain is on the cytoplasmic side implies that the amino terminus is on the extracellular side. According to the above facts the polypeptide chain will snake its way back and forth through the membrane. Thus, as the primary structure is known, at this level of structural resolution one could look at the amino acid sequence and try to figure out which amino acids are part of the helical regions and which amino acids are in the interhelical, or connecting regions. In addition, observed cleavage points must be located in the connecting regions.

The first assignment of helical and connecting linkages was done by Ovchinnikov's group [1979]. Their model suffers from several problems. In their model they have buried many hydrophilic and charged amino acids in the membrane. Glutamic acids, aspartic acids, and lysines are shown in what one would think of being a primarily hydrophobic environment. This has also been discussed by Engelman et al. in a related model which will be considered in more detail below.

The problem of buried charge-groups was addressed by Engleman and Zaccai [1980] in a neutron study of PM. Selective deuteration of valine and phenylalanine was used to locate the major distribution of these specific amino acids in the projected structure of the membrane. These studies seemed to indicate that the majority of the valine containing structures were on the outside of the protein and the majority of the phenylalanine structures were on the inside of the protein. Models of the 7 α-helical regions demonstrated that the majority of the charged groups would be oriented in the same direction as the phenylalanine, towards the interior of the protein. Thus, Engleman and Zaccai refer to the membrane as being an "inside-out" structure with the hydrophobic regions being directed toward the outside and the hydrophilic regions being directed toward the inside.

In another paper, Engleman et al. [1980] argue that the buried charges will form ion pairs in the membrane, resulting in stabilization of the structure. They propose an arrangement of 7 α-helices, and indicate which regions of the primary structure correspond to regions of the α-helices. It should be noted that their helices are somewhat shorter than those of Ovchinnikov. Based on the lengths of

α-helices and the total helical scattering power in the Unwin and Henderson structure these authors also attempted to assign their helical regions to specific locations in the structure. Another criterion used was that the helical connections should not cross each other. Out of a total of 5040 possibilities they chose one structure that they felt to be the most probable.

More recently, Katre et al. [1981a], have used information about the chromophore location to assess the reasonability of the Engleman model. In addition, they cited the work of Agard and Stroud [1982] that determined some of the inter-helical connections. On the basis of the neutron experiments of King [1980] combined with the above results they decide, in agreement with Engelman et al., that the 4 models seen in Figure 1-7 are of the greatest probability. This probability aspect should be emphasized as, at present, there is no unambiguous single interpretation of all of the facts.

Another interesting kind of model building has been undertaken on the basis of the resonance Raman studies. In this case, the great amount of similarity between the rhodopsin present in the visual system and that of purple membrane has led authors to try to explain both systems. Both Honig [Honig et al., 1979] and Warshel [1978] conclude that a cis-trans isomerization could store energy as a charge separated pair. In the mechanism of Honig, a trans --> cis isomerization of the chromophore cleaves a salt bridge and thus separates a pair of charges in the interior of the protein. A negative counterion such as the carboxylate of an aspartic or glutamic acid is proposed to be located 3Å away from the protonated shiff base nitrogen. In the mechan-

ism of Warshel, a similar sequence of events is postulated to occur as well as some changes in the pK's of several amino acids lining a channel which provide a pathway for the proton translocation.

Although a great deal of information is known about purple membrane, it is also true that a substantial amount of information has yet to be discovered. While the primary structure is known quite well, and assuming the membrane consists of 7 α-helical segments, we still have very little knowledge of how these helices are connected. Engleman et al. [1980] have ruled out a great many possibilities, but we cannot say that all of them are implausible. It thus becomes of great interest to determine the connections between the helical regions. The possibility of determining the location of connecting links was a primary motivation of the experimental work presented in this thesis.

At a more primitive level one could ask: Why were connecting regions not seen in the Unwin and Henderson three dimensional structure? One possible answer is that although the resolution of their map was 7Å in the plane of the membrane, it was only 14Å, in the perpendicular direction. Assuming that the connections between helices are parallel to the plane of the membrane, the effect of this degraded resolution would probably be to wash out the connections. With respect to this point, the anisotropic resolution would also degrade the appearance of structures of this type inside the membrane. Thus, any side chains between helices or the retinal group itself would be difficult, if not impossible, to see.

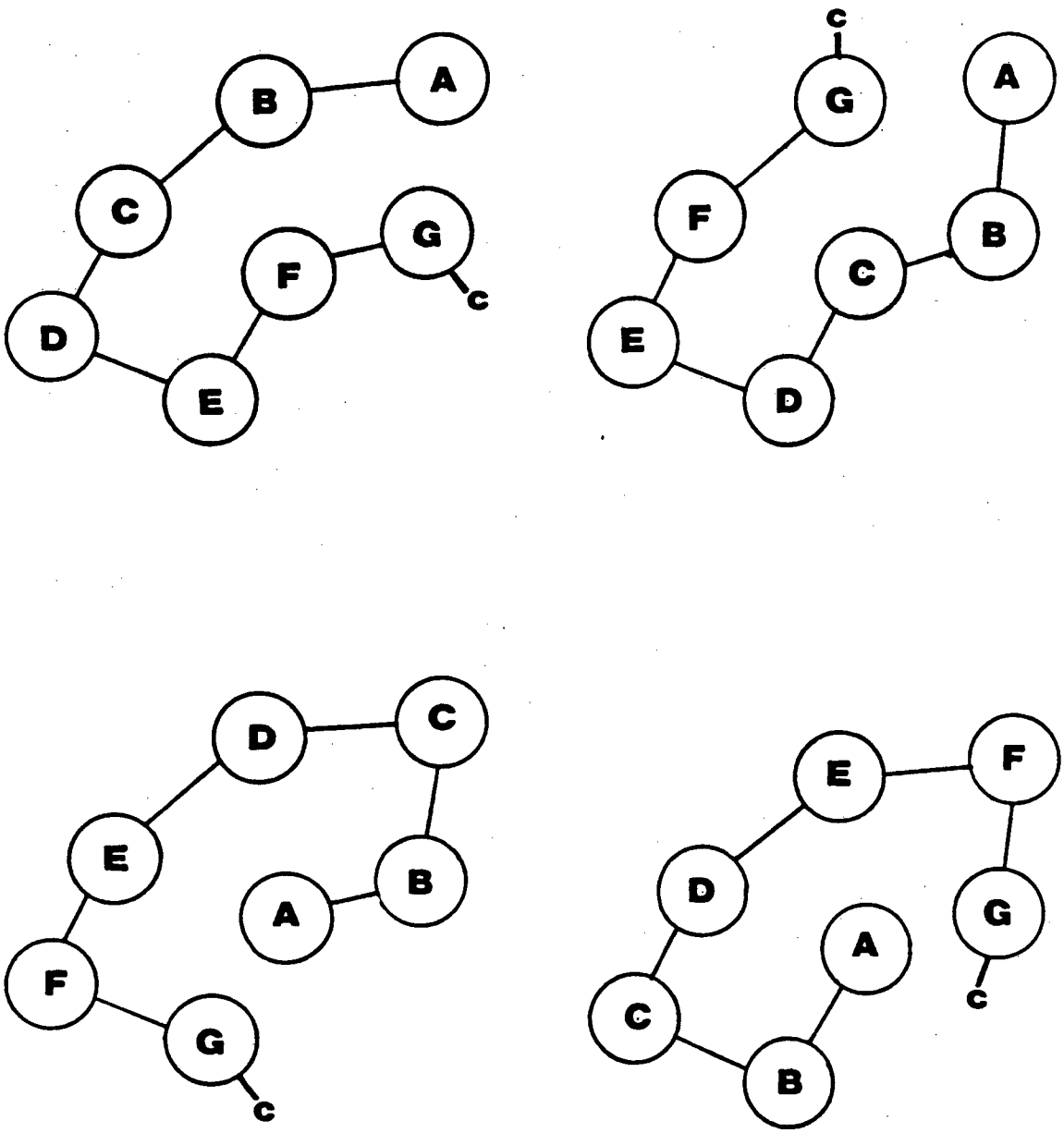

XBL 8211-3267

Fig. 1-7. Connectivity models of Agard and Stroud (1982).

Another possibility is that the connecting regions between the helices are not "crystallographic." That is to say, their position and/or structure varies from unit cell to unit cell, in the natural state. Based on some of the proteolytic cleavage patterns, it is quite reasonable that the carboxyl terminus, the amino terminus, and amino acids 65-73 are exposed to the aqueous phase. The flexibility of the polypeptide chain in these regions could be great enough to be consistent with the hypothesis that these regions would not be seen on a crystallographic map.

As a third possibility, one cannot rule out that the way the membranes were prepared for the electron microscopic studies led to a disorder of the linking regions. The technique that was used to preserve the structure of PM in the vacuum of the microscope was to embedd the membranes in glucose. Although the next chapter will discuss the preparation of specimens for electron crystallography more thoroughly, it should be mentioned here that the glucose embedment may interact strongly with the surface groups of bR and disorder some of the originally "crystallographic" surface structure.

Our approach to answering these experimental difficulties has been to prepare PM in a frozen hydrated state. The notion that the frozen state is closer to the "true" state is consistent with the idea that by flash freezing one can accurately preserve the structure. Thus, the hypothesis that some of these linker regions would be observable in a frozen hydrated preparation is a reasonable one. An additional benefit of such a preparation is the increased contrast of protein-ice versus protein-glucose. If some of these linker regions protrude into

the aqueous phase a fair amount, the lower density of ice would definitely be an asset.

It may ultimately prove to be true that the greatest advantage in having a reliable frozen hydrated preparation of PM may be the ability of flash freezing the membranes. I think it is clear that the real mechanism of how PM works will only come from a detailed understanding of the various intermediates in the photocycle. At present, it is also clear that the retinal photo-isomerizes upon being exposed to light. We have also seen that all of the subsequent reactions can proceed in the dark. This leads one to ask: How is this energy stored? It is possible that a conformational change of some part of the protein-retinal complex may store this energy. To be more specific, we might be able to discover the structure of the M intermediate by stimulating light adapted membranes with a laser pulse and flash freezing a millisecond later. A Heuser type apparatus [Heuser, 1976] could be the most successful way of proceeding.

There is also a possibility that the crystallinity of the specimen may prove to be the limiting factor in observing parts of the structure of PM. Thus, the flexibility of portions of the molecule may limit the obtainable crystallographic information. In the case of electron microscopic examinations, for 3-dimensional studies, limitations due to the cone of missing data or the extreme flatness required for coherent superposition of the structure at high tilts may also limit our knowledge [Hayward and Stroud, 1981]. It is therefore most likely that a complete understanding will only be possible by combining insights gained from many different experimental techniques.

CHAPTER II

PRESERVATION OF BIOLOGICAL SPECIMENS FOR HIGH RESOLUTION ELECTRON MICROSCOPY

A. Introduction

In contrast to the great amount of knowledge that we have obtained in the last 20 years about the atomic and molecular structure of water soluble proteins our present day knowledge of membrane bound and embedded proteins is extremely limited. Electron microscopy (EM) offers a unique method for obtaining this kind of information providing certain technical requirements can be satisfied. Existing methods of EM which rely heavily on the use of fixed, embedded and stained specimens have proven to be inadequate to reveal details of molecular structure below the size scale of 20Å.

One obstacle in observing the natural structure of biological specimens in the electron microscope is the loss of solvent and concurrent disruption of structure that occurs when specimens are placed into a vacuum. Many of the attempts at solving this problem have been designed to replace the aqueous phase with something that has a lower vapor pressure at room temperature. In these cases, the process of replacing the solvent may subject the specimens to a range of physical stresses which can explain the lack of preservation of the minute details of structure. The main exception to this statement, as mentioned in the last chapter, is the glucose embeddment technique of Un-

win and Henderson [1975] which has led to the first views (projected and 3-dimensional) of a membrane protein at a resolution of approximately 7Å. However, the possibility that glucose disorders some parts of the structure is still open (see Conclusions).

The approaches taken in this lab toward the high resolution elucidation of biological structures have been to use low temperatures in conjunction with the glucose technique [Hayward, 1978; Hayward and Stroud; 1981] as well as ice embedment [Taylor and Glaeser, 1976; Hayward et al., 1978]. In the ice embedment technique the specimens are frozen in liquid nitrogen (LN_2) outside the column of the microscope and then inserted into the microscope for examination. Thus, in addition to a microcope stage that is cold enough to prevent ice sublimation, a cold specimen transfer device is necessary to prevent the condensation of atmospheric water onto the specimen and to keep the specimen cold [Taylor and Glaeser, 1975].

A fortunate side effect of the low temperature is the great improvement in radiation resistivity of cold specimens to the electron beam. Initial work on catalase was able to demonstrate a threefold increase in diffraction spot lifetime [Taylor and Glaeser, 1976]. Subsequent studies using PM have been able to demonstrate a 5-7 fold increase in the lifetime of a great many reflections [Hayward and Glaeser, 1979].

Another constraint in the preparation of specimens is that they must be very thin (<500Å) in order to get the very easily scattered electron beam through with single scattering. In the case of the high resolution imaging of membrane structures the membranes themselves are

less than 100Å thick. This requires that the combined thickness of the support medium (carbon films) and the embedment medium (glucose or ice) is limited to about 400Å. We are thus limited to preserving our structure by using a necessary but correspondingly sparing amount of embedment.

In this chapter I will chronicle some of the past attempts to determine the structure of various biological systems via different preparatory techniques. In the case of 2-dimensional crystals a suitable measure of the preservation is provided via the existence of high resolution information in the optical or electron diffraction pattern. The detection and analysis of such patterns can also lead to the discovery of structural information as contained herein.

The last section of this chapter will describe a technique for the routine preparation of PM in ice without glucose. Existence of reflections to a resolution of 3.2Å in the diffraction patterns recorded from reconstituted membranes is evidence of the preservation of minute detail. It is expected that advantages over the glucose technique may possibly result from the increased contrast that exists between protein-ice versus protein-glucose as well as the increased order of some of the surface groups.

B. Techniques for the Preservation of Structure at Intermediate Resolution

As mentioned above, the primary problem in examining biological specimens in the electron microscope is due to the loss of water. I would like to differentiate between the actual process that accomplishes the loss of water and the absence of water itself. One

problem that occurs during the drying of specimens is that a receding layer of water will pass the specimen through a gas-liquid interface. Thus, although the specimen structure may be maintained in the dehydrated state, the process of drying will disorder it. Two techniques of early researchers were invented to circumvent this problem, the freeze drying technique of Williams [1953], and the critical point drying technique of Anderson [1952].

In the freeze drying technique the first step is to flash freeze the material of interest. The rapidity of freezing is an important parameter. Slow freezing can lead to the formation of ice crystals which will submit the material to severe forces which may ultimately lead to deformation [Merryman, 1974]. In the next step, either the pressure can be lowered or the temperature of the specimen can be raised leading to the sublimation of the water. Using a method of spraying micro droplets onto a cooled surface to insure rapid freezing, Williams was able to show a substantial improvement over air drying in the preservation of red blood cell ghosts and intact bacteria.

More recently, in an effort to obtain more detailed structural information, researchers have prepared crystalline biological specimens (T-layer cylinders, and T-even polyheads) via both the Williams microdroplet technique and a method based on the adherence of specimens to collodion film [Kistler and Kellenberger, 1977; Kistler et al., 1977]. Specimens that were freeze dried were then shadowed with either tungsten or uranium dioxide. One observation of these investigations was that on a gross morphological level the empty cylindrical structures were always collapsed either onto themselves or onto the supporting

film. The actual mechanism of this collapse, however, could not be identified. On a finer morphological level optical diffraction patterns of the shadowed periodic specimens were limited to a resolution of 25-30Å. In addition, when images that were filtered either optically or using the computer were compared to images of negatively stained specimens that were processed in the same manner, complimentary information about the surfaces was obtained.

Attempts have also been made to preserve catalase crystals via freeze drying for high resolution electron microscopy [Lepault and Dubochet, 1980]. Resolution obtained by these researchers has been limited to 8.5 Å in contrast to the resolution of 2.8Å obtained using frozen hydrated crystals.

In the critical point drying technique the water in the biological material is first replaced by a liquid whose critical temperature and pressure are of a suitable nature. This is necessary because the critical temperature of water is 374°C which is too high to be of a practical use in the method. One implementation of the method employs a series of ethyl alcohols of increasing concentrations. The alcohol is then replaced by amylacetate which, in turn, is replaced by liquid carbon dioxide. The critical temperature and pressure of carbon dioxide are 36.5°C and 1080 lbs/in^2, respectively. The specimen, immersed in liquid carbon dioxide under pressure, is then passed through the critical temperature of carbon dioxide. At or above this temperature the liquid and the gas became a single fluid phase, which can then be bled off. After release of the gas, the specimen, now dry, can be inserted into and viewed in the electron microscope.

This technique, like the freeze drying one, has been used very successfully on a moderate resolution basis. It was, however, observed that specimens prepared in this manner showed a characteristic type of dehydration artifact: flagella that were stretched between surfaces and allowed to be free between these surfaces were flattened at the point of surface contact [Anderson, 1954]. It was hypothesized that structures which are freely suspended under vacuum vibrate as a result of their thermal energy and collapse irreversibly upon the support.

An additional limitation of this technique in the case of membrane bound structures arises from the fact that the solvents that are used to replace water are strong protein denaturants. They may also extract lipids from the membranes.

In addition to the above methods, a rather common one that can be used even at room temperature is to administer uranyl acetate or phosphotungstic acid (PTA) to a specimen. The popularity of both of these techniques is due to the fact that not only is structural detail preserved but it is also contrast enhanced via the strong scattering of the uranium or tungsten atom. Negative staining, as this method is commonly known, works by filling in the hydrated areas of the structures of interest. Optical diffraction patterns of specimens prepared by this method may go to 15Å in fortuitous cases. However, systematic changes in the intensities of some reflections indicate [Glaeser, 1971; Unwin, 1974] that some stain redistribution may be taking place under electron bombardment leading one to question the validity of the information obtained. The greatest factors limiting the information ob-

tainable from negatively stained specimens are most probably the non-uniform stain penetration, and the interaction of stain with the specimen itself. This lack of strain penetration may be a serious limitation of the technique when trying to stain structures such as membranes. In particular, purple membrane does not stain well. This is probably due to its lack of large aqueous channels.

C. Techniques for the Preservation of High Resolution Information

It is not surprising to see that, due to the limitations of the preservation techniques described above, many researchers have tried to maintain the aqueous environment itself in the electron microscope. This can be accomplished by either lowering the temperature of the specimen and thus lowering the vapor pressure of the water, or by raising the column pressure in an environment local to the specimen.

In an effort aimed at the latter approach, a group led by Parsons [Parsons, 1974] was able to obtain electron diffraction patterns of catalase [Matricardi et al., 1972] to a resolution reported to be 2 angstroms. Specimens were kept hydrated by maintaining them in an atmosphere of saturated water. This was facilitated by building a small chamber in the microscope with 100μ apertures on either side of it. Another layer of 200μ–400μ apertures were placed around the first. The gas escaping from the inner set of apertures was pumped out of the pole piece gap by a liquid nitrogen trap and mechanical pump. The remaining gas was pumped away by the vacuum system of the microscope. Thus, this small set of apertures allows electron beam penetration but prevents large amounts of water from evaporating into the microscope column. There are several present limitations of the technique. One

concerns the problem of Brownian motion at room temperature in non-cyrstalline specimens. Another one is that there is presently no way to obtain high resolution phases via imaging as no high resolution stage exists.

Although the technique of Heide and Grund [1974] was not used to obtain very high resolution it probably could have been if the authors had been interested in using it as such. Their method deserves special note in this thesis as it contained all of the essential ingredients that were utilized in the method that I developed. This includes such procedures as sandwiching the specimen between two layers of foil and insertion of a specimen that was pre-cooled into the column of the microscope. An interesting feature of their technique was the use of nitrogen gas in the transfer device which allowed the frost free transfer of the specimen to the column. These investigators were mainly concerned with the observation of whole bacteria. Their claims of seeing no crystalline water leads one to suppose that they were able to freeze the specimens fast enough to prevent damage from crystalline ice. One cannot be sure, however, as no quantitative assay such as optical diffraction could be implemented. They did have problems with the water being too thick to allow the electron beam through. This was solved by raising the specimen temperature in order to allow some quantity of water to sublime.

Control of the thickness of the surrounding ice was also a problem in the method of Taylor and Glaeser [private communication]. Using a 100B JEOL microscope [Taylor and Glaeser, 1975] these authors were able to freeze specimens outside of the microscope and insert them at LN_2

temperature into the column. Excellent high resolution diffraction patterns of catalase were obtained as well as high contrast images [Taylor and Glaeser, 1976]. It was during these studies that it became apparent that there was a large degree of contrast as a result of embedding catalase in ice. This contrast is likely due to the density difference in the interior regions of catalase crystals that are filled with water versus the density of protein. In support of this hypothesis is the sensitivity of the crystalline structure to dehydration [Matricardi et al., 1972].

The method used by Taylor and Glaeser [1973] to prepare crystalline specimens consisted of preparing carbon films coated with a layer of silicon oxide (SiO). As this layer was hydrophilic it retained a layer of water. In an effort to control the rate of evaporation of water, folding grids were used to sandwich the specimen between two layers of carbon film. Excess water was drawn off with filter paper and specimens were immediately plunged into LN_2. Although some good quality diffraction patterns were obtained by using this method reproducability was definitely a problem [Taylor, private communication].

In a subsequent modification of this technique, specimens in water were placed onto carbon coated grids and allowed to dry at a controlled rate in a humidity box [Taylor, 1976]. When grids were judged to be of an appropriate thickness as examined in a phase contrast optical microscope they were quick frozen by insertion into LN_2. THis method was more reliable than the previous one, however, reproducability was again a problem.

The resolution of the maps obtained using these techniques were primarily limited by the availability of high resolution phases. Mechanical instability of the specimens was observed which limited the resolution to around 12Å. These problems were later overcome by moving the microscope to an environment with less vibration and by the construction of a high resolution cold state [Hayward and Glaeser, 1980].

The glucose embeddment technique of Unwin and Henderson [1975] allowed these authors to utilize their existing microscope facility to obtain room temperature diffraction patterns and images of PM to 7Å. As the results of these studies have already been discussed I will not reiterate them here. The technique itself is quite simple and consists of mixing the sample with a 1 or 2 percent solution of glucose and allowing the mixture to dry down onto a carbon coated grid. The result of this procedure is that a reasonable number of PM's are covered with a layer of glucose of sufficient thickness to keep the crystalline membrane hydrated, but thin enough to be reasonably electron transparent. A necessary requirement of this technique is that the support film must be hydrophobic [Hayward, private communication].

A double film technique was used by Talmon et al. [1980] to examine thin dispersions of bovine lecithin. Samples were frozen in LN_2 outside of the microscope between polyimide films and transferred to a cold stage at low temperature. No ice crystals could be seen by using this technique and the vesicles themselves appeared to be intact. Again, no quantitative estimate could be made as to the extent of specimen preservation.

An interesting monolayer technique was developed in order to study the orientation of PM on polylysine as a function of pH. A different technique than glucose embedment for the preservation of PM was necessary because both Hayward and Henderson [personal communication] were unable to prepare PM oriented on polylysine in glucose. The specimen preparation developed by Hayward et al. [1978] was to take polylysine coated grids and apply PMs at a range of different pH. These grids were then placed into a solution of 5 mM CaCl at Ph 8-9. Several drops of castor oil were then applied to the surface followed by a drop of 2 percent stearic acid in hexane. As the hexane evaporated, a surface film of stearic acid was formed through which a submerged grid was withdrawn. Grids were then frozen in LN_2 and placed into a JEOL 100B microscope for diffraction which extended to approximately 4Å. Catalase was also prepared via this method as a test specimen and some partial disordering was evidenced on diffraction patterns that went to a resolution of 4.2Å.

D. Physical Parameters Important in High Resolution Specimen Preservation

In the previous sections we have examined various attempts at maintaining the structures of crystalline biological specimens in the electron microscope. As has been demonstrated above, due to the radical change in specimen environment that occurs when samples are introduced into the microscope, specimen preservation concerns critical parameters that must be controlled. It is certainly a worthwhile exercise to try to determine the specific physical parameters that influence the preservation of specimens.

In my opinion, the most important factors associated with good preparation of specimens are the elimination of surface tension effects, the maintenance of specimen hydration, and the minimization of strong interactions with support films. We have already seen how the critical point drying method of Anderson and freeze drying technique of Williams helped to circumvent some of the problems associated with surface tension collapse. It is most likely that the disorder induced by air drying specimens is attributable to surface tension effects. In our case, it remains an open question as to whether the protein-lipid lattice is strong enough to resist these kinds of deformations. As an intermediate case, we can imagine that some parts of the structure may denature and others not.

The maintenance of the hydration of specimens is often confused with the process involved in removing water. The question of whether specimens that are normally immersed in an aqueous mileau can survive in the absence of water is a different one than asking if the removal of water disorders them. As an example, a relatively open structure such as a vesicle may be dehydrated using the critical point drying technique and the end result will be a collapsed vesicle. This does not mean that the surface tension effects collapsed the vesicle.

An important factor, necessary for high resolution work, is the existence of crystallinity. At present, high resolution images have only been obtained from crystalline materials. This is because the radiation sensitivity of biological materials prevents high resolution information to be extracted from a single unit cell [Glaeser, 1975]. The advantage of using crystalline arrays is that the multitude of

similar units allows the "constructive reinforcement" of the high resolution information and at the same time permits exposure of a subcritical dose to any individual unit.

The ideal specimen for high resolution electron crystallography would be a perfectly rigid, flat, 2-dimensional crystal. The extent to which crystals that we observe fit this criteria limits the applicability of the technology. The ridigity of the crystal would presumably allow it to resist deformations inherent in the preparative process. The flatness is necessary to insure that the same projected view of each of the individual units is taken. Small departures from flatness will have much more drastic effect on the coherence of tilted views. Current limitations to a 3-dimensional structural analysis of PM seem to be a result of this effect [Hayward and Stroud, 1981].

The ideal support film for the purpose of 2-dimensional crystal analysis should be very flat, mildly "sticky," and extremely stable in the electron beam. Assuming that the specimen is already a 2-D crystal in solution, as explained above, the flatness is necessary for the preservation of coherence. A great deal of time has been dedicated to studying the surface characteristics of support films. The initial requirements of all surfaces is that the specimen adhere to the support film surface. However, this interaction should not be so strong as to disorder the crystalline structure of the specimen. In the case of carbon films, it is thought that they are hydrophilic immediately after preparation and then become more hydrophobic with time. This increase in hydrophobicity is assumed to be due to the adherence of hydrocarbons present in the atmosphere.

In the case of purple membrane it seems to stick equally well to both hydrophilic and hydrophobic films. As mentioned before, other attempts to prepare PM by means other than adherence to carbon have made use of polylysine as a substrate. Membranes adhere very well to carbon coated with this chemical and in fact will change their orientation as a function of pH [Fisher et al., 1977, 1978]. As already mentioned, this was exploited by Hayward et al. [1978] to determine the orientation of PM in vivo with respect to the Unwin and Henderson model.

Finally, support films should be more radiation resistant than the specimens that one is observing. As a limiting case, we can imagine that a radiation sensitive support film will deform under electron bombardment. If the film and the specimen are in close contact, the specimen itself may be forced to disorder. In a comprehensive review of specimen supports [Baumeister and Hahn, 1978] the radiation sensitivity of various plastic support films is reviewed. Interestingly enough, the most common supports nitrocellulose and polyvinylformal are the most sensitive to radiation. Other supports such as polyvinyl carbazole and polystyrene are much more radiation resistant. This is probably due to their increased content of aromatic groups. Hayward et al [1978] observed a change in defocus and specimen induced drift in frozen glucose purple membranes. The use of thicker carbon films was able to reduce these effects to the point of allowing high resolution images to be taken. Thus, although thin carbon films have been traditionally advocated for contrast reasons, the thicker ones may be necessary, due to radiation induced effects.

E. A Method for Obtaining High Resolution Electron Diffraction Patterns of Purple Membrane

Given the above mentioned parameters as a guide to the preservation of specimens in the electron microscope various strategies for accomplishing in vivo-like preparations are possible. We have approached this problem by formulating a technique whose main objective has been to promote rapid freezing of the specimen embeded in a thin coat of water. As the membranes themselves are also extremely thin the rate of freezing is not a problem. Insertion of sandwiched specimens into liquid nitrogen did not ordinarily result in the observations of nitrogen bubbles on the specimen in support of this remark. As far as controlling the ice film thickness goes, the following method, illustrated in Figure 2-1 was found to give consistently good results.

One ordinarily starts by evaporating some carbon onto freshly cleaved mica. Small pieces of mica can be placed at variable distances from the carbon electrodes. Those being closer will have more carbon evaporated onto them, the ones further away will have less. Using this methodology, it was quite easy to achieve a range of carbon thicknesses which subsequently led to good specimen preservation. Carbon films obtained in this manner were then floated off onto distilled water. Correct thickness of the film was judged by the smoothness of the surface, thin films would tend to shred and break up, thick films were extremely cracked. Next, a copper grid (ordinarily 200 mesh) was inserted into the distilled water, up through the carbon, and allowed to dry.

The next step consisted of applying purple membranes at room temperature in the presence of light. Depending on the concentration the membranes were allowed to sit in solution on the grid for up to 5 minutes. Longer periods of time were used to get better coverage, however, for single crystal patterns 10-20 membranes in a grid square were sufficient. The grid was then placed back down into the distilled water and the membrane solution was then washed off before bringing the grid up through the carbon film for the second time. The result of this procedure was to sandwich the specimen between two layers of carbon films.

Only grids that were found to have a lens of water on both sides were used for further experimental work. At first this lens of water is continuous between both sides of the grid, however, after some evaporation the rim of the grid will divide the lens into two, one on each side. It is then possible to blot off the water on the back side of the grid with filter paper at this point. It was necessary to wait as the lens slowly evaporated, rendering the specimen a purplish-orange color. Throughout this process the grid was monitored with an ordinary incandescent bulb placed around 8 inches from the object. The shiny surface of the grid was always indicative of a layer of water that was found to be too thick upon freezing. Usually several tries per batch of carbon films resulted in the preparation of frozen samples on grids that were either too thick or too thin. Some experience then led to the preparation of specimens that were of the correct thickness to allow collection of good diffraction patterns.

FROZEN HYDRATED PREPARATION

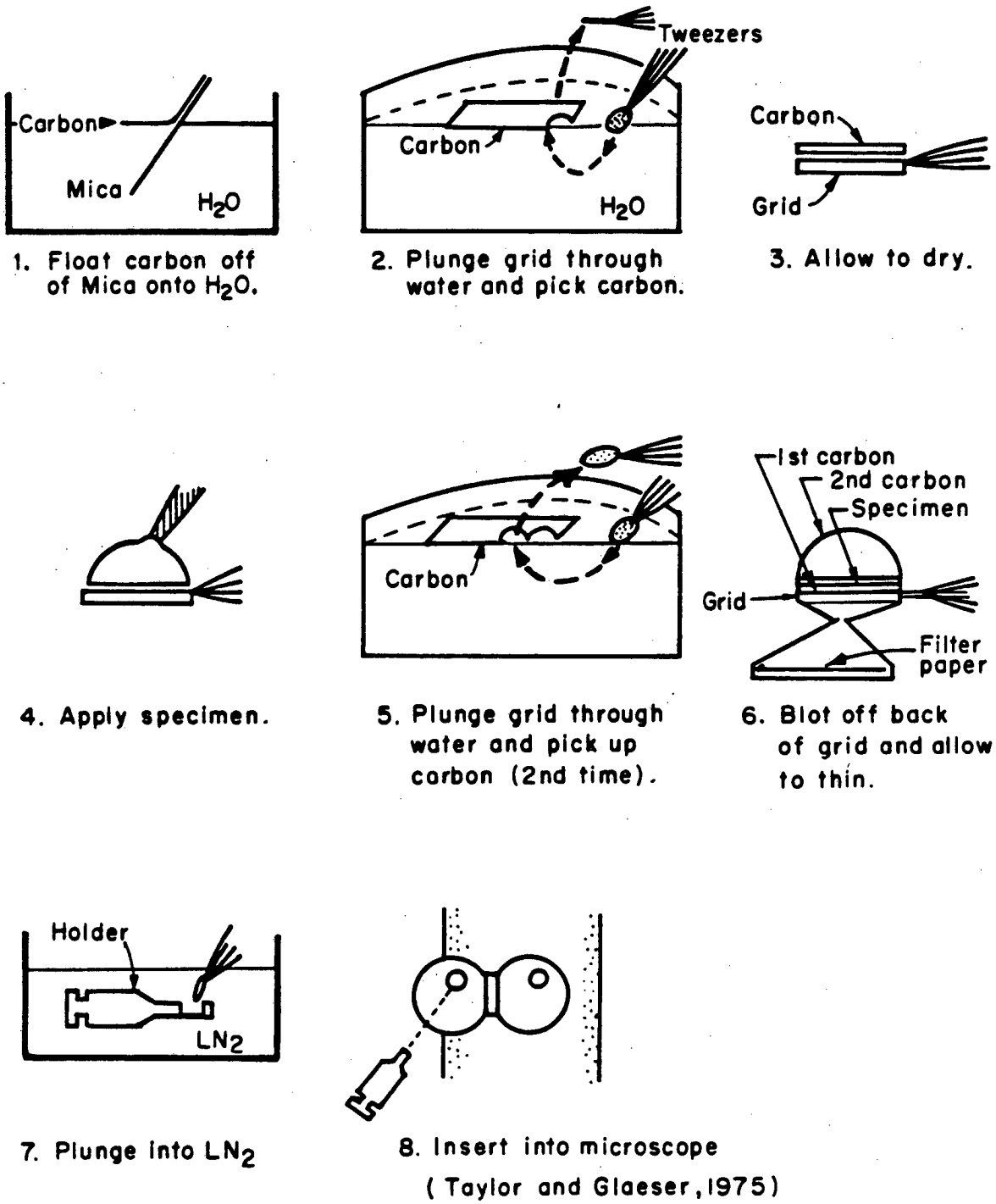

XBL822-3611

Fig. 2-1. Illustration of the frozen hydrated preparation.

When the specimens were judged to be of the correct thickness they were then inserted into LN_2. Frozen specimens were then transferred into the cold stage of a JEOL 100B microscope via a cold transfer device.

In Figure 2-2 we can see the appearance of a typical specimen prepared in this manner that has led to high resolution diffraction. Contrary to what one might expect, this specimen is not submerged in a pool of ice but rather it seems to be delineated by crisp outlines around its circumference. Specimens that were capped with ice that was thicker than this did not usually diffract as well. An example of this type of specimens is shown in Figure 2-3. A distinguishing factor of the membranes that led to high resolution patterns was their shaded appearance. This shaded appearance was interpreted as being due to a layer of bound water that was retained by the membranes.

The method has also been used on other crystals with some success such as gap junctions [Unwin, private communication] and catalase. Its principle advantages are that it does not require any technology other than that included in the standard repertoire of most electron microscopists. The greatest area of improvement over previous methods is that it allows for the controlled evaporation of solvent from the specimens. Assuming that there is a critial time interval t_c in which specimen preservation may be accomplished, t_c is greater for slowly evaporating solvent. This would increase the probability of success. There is really no special dependence of the technique upon the pH because of the inert composition of the carbon film.

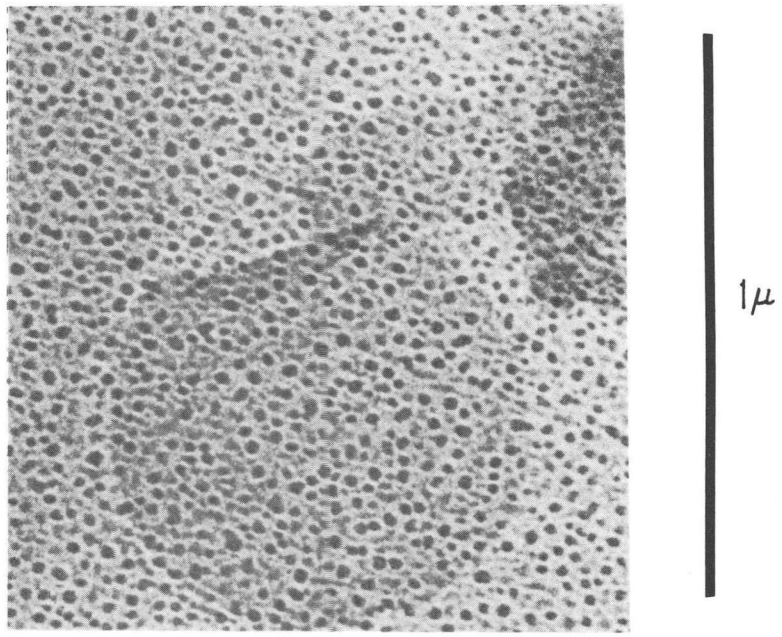

Fig. 2-2. Example of purple membrane in ice that led to high resolution diffraction patterns.

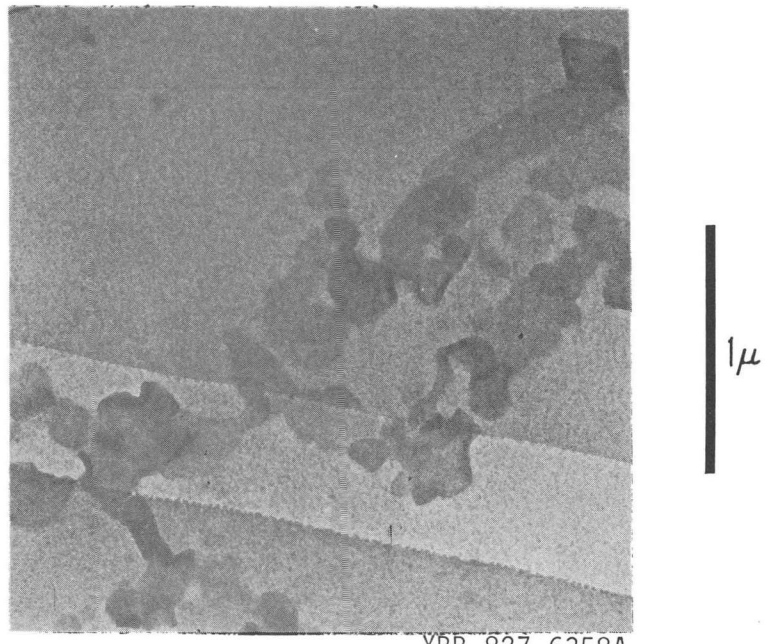

XBB 827-6358A

Fig. 2-3. Example of purple membrane in ice that did not lead to high resolution diffraction patterns.

There is, however, a possible problem in using specimens that are very sensitive to ionic strength. This is because as one waits for the lens of water to evaporate, the solutes are concentrating. This concentration may be many fold over the initial conditions leading to possible alterations in the drying environment.

In this chapter we have reviewed various aspects of specimen preparation in electron microscopy. The contributions of various researchers were usually aimed toward perfecting the preparation of specific specimens that they were interested in. The technique discussed above works quite well with purple membrane and seems to hold promise for other specimens. I would not be surprised, however, if the number of preservation techniques developed by clever researchers for specific problems was close to the number of problems themselves.

CHAPTER III

COMPUTER PROCESSING OF DIFFRACTION PATTERNS: SCANNING AND SCALING

A. Scanning of Diffraction Patterns

In order to accurately derive a set of intensities from photographs of diffraction patterns it is necessary to first convert the partially blackened emulsion to a 2-dimensional array of optical densities. The scanning microdensitometer that is used for this purpose consists of a good quality optical microscope interfaced to a photomultiplier tube whose output is then converted to a 10-bit number by an analog to digital converter. This number can be proportional to the amount of light transmitted (transmission mode) or to the logarithm of the light transmitted (optical density mode). The user is allowed to control the size of the sampled area via selection of an aperture, and the selection of the locations of the sampled areas is controlled by a computer program.

An important question arises with regard to the size of the aperture needed in order to "correctly" sample the diffraction pattern. It is clear that we are interested in sampling the patterns in such a way so as to not lose any information or bias the results systematically. This can be accomplished quite easily by sampling with very small spots that are closely spaced. However, it does not make sense to collect more data than we need in order to determine the quantity of interest. This is because the amount of data processing and time spent scanning will then be increased.

A complication arises when one is measuring optical densities from a densitometer that is recording the transmission of light. Optical density is defined to be equal to the logrithm of the ratio of incident to transmitted light intensity. As the logarithm of the average is not the same as the average of the logarithm an error will result unless the optical density is uniform within the area of the sampling of the light spot. This effect is commonly referred to as the Wooster effect [Wooster, 1964]. A careful study of the magnitude of this effect has been considered by Mathews et al. [1972]. To state their results breifly, these authors concluded that in examining a diffraction spot that could be enclosed in a box of 800μ x 600μ a 100μ scanning aperture and 100μ intersample distance was adequate to keep the error due to all effects to less than 1.5 percent.

It is therefore apparent that as long as the ratio of the Gaussian shaped diffraction spot size to the aperture size is 10 or greater the requirements of the Wooster effect can be fulfilled. In scanning the purple membrane patterns for this study, a square aperture of 5μ was used with a 5μ distance between scanned points. Although the diffraction spot sizes were found to vary (the more intense reflections have larger radii) the diameters of the weaker reflections were never less than 50μ. Another reason for using this small scanning aperture was to maintain compatibility with the set of scanned glucose patterns that were donated by Dr. S. Hayward [private communication]. Scans were preformed on strips of the photographs that were 40 apertures wide by 3500 long [see Appendix A]. Half pictures of diffraction patterns were usually scanned in a time of about 45 minutes. Scans were

performed on half patterns in order to minimize the effects of instrumental variation such as aperture drift, etc.

B. Processing of Diffraction Patterns

I would now like to describe how the relevant information was extracted from the scanned diffraction patterns. That is to say, once the patterns have been scanned, the next step is to input the data into a computer program that will generate a set of intensities I(h,k) for every reflection on the plate. A set of programs was implemented ('DIFPROC') in order to calculate these parameters. This set of programs was designed to be run on a VAX 11-780 computer (Digital Equipment Company) in an interactive mode. No knowledge of computer programming is required to use these programs as a meta-language of simple instructions has been devised. For information about the specific use of the system the reader is referred to Appendix A which contains a users manual.

After reading into computer memory one fourth of a plate as described in the appendix, the diffraction patttern was indexed by first locating the centers of several reflections and then fitting a least squares lattice to these locations. For a P3 lattice, a pseudo-orthorhombic indexing scheme will predict the spot locations once the lengths of the a* and b* vectors have been established. In visually examining these patterns the large intensity of the (4,3) reflection was always a good index of the handedness and the radical change of the (2,4) and (4,2) reflections about the equatorial plane provided a convenient way of monitoring tilt [Hayward and Stroud, 1981]. Several

predicted values of spot locations were then compared with the actual spot locations and were usually found to be within several pixels.

A square array was then defined around each of the lattice points with a size large enough to include all of the reflection. Two background areas of the same size were also defined at an equal distance away from the spot location along the lattice. Figure 3-1 shows the geometry inherent in these choices. Integrated intensities were then determined for the backgrounds by applying a parabolic correction to convert from optical density to electrons/μ^2 [Section C]. The values in a given background area were summed and an average value/pixel was then calculated. An average value of the two background areas was then taken. This value was subtracted from each of the parabolically corrected intensities for the reflection and the resultant values were integrated to get the intensity of the diffraction spot.

The accuracy of the resulting data was evaluated by calculation of the RSYM value (see Appendix A). Symmetry related reflections were compared and whenever large discrepancies observed, they were explored by first examining the predicted locations of the reflections. When necessary, corrected locations were then entered. The accuracy of this "manual correction" procedure is supported by some of the very low values of RSYM that were obtained on a great many of the more intense reflections.

C. Response of the Photo-Emulsion to Electrons

In deriving a set of intensities, I(h,k), from a photoemulsion of a recorded diffraction pattern, the conversion from optical density to a number proportional to the number of electrons striking the emulsion

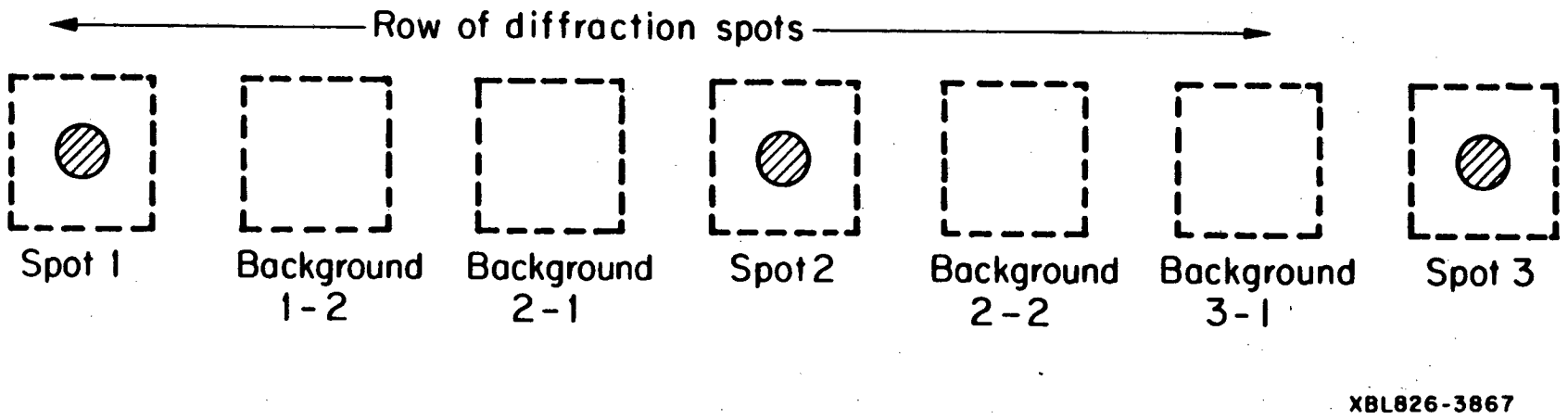

Fig. 3-1. Geometry of areas used for the backgrounds and spot locations in "Difproc".

is necessary. Although it is true that at low electron exposures the photoemulsion has a linear response to the incident electron beam the reasearcher can also gain a considerable amount of useful data recorded in the nonlinear part of the response curve by calibrating the relationship over an extended range. What then is the relationship between the blackening of the photoemulsion and the number of electrons that strike a plate This question has been authoritiatively addressed in a review by Valentine [1966]. The basic theory for understanding the answer to this question is governed by the single hit law. Stated succintly, if a silver halide grain of mean cross-sectional area A is irradited by E electrons per unit area then, from a Poisson distribution, the fraction of all crystals hit at least once is $F = 1-e^{-EA}$, with mean number of hits = EA. Combining this equation with an expression for the uniform attenuation of light by the developed emulsion leads to

$$D = D_s \ (1-e^{-EA})$$

where D_s = saturation density reached after a prolonged exposure to electrons (D = observed density).

A considerable simplifcation to this equation can be accomplished by expanding the exponential in a power series:

$$e^{-x} = 1 - x + \frac{x^2}{2!} - \frac{y^3}{3!} + \ldots$$

$$e^{-EA} = 1 - EA + \frac{(EA)^2}{2} - \frac{(EA)^3}{3!} + \ldots$$

$$D = D_S(EA - \frac{(EA)^2}{2} + \frac{(EA)^3}{6})\ldots \quad = D_S EA - D_S(\frac{E^2A^2}{2}) + \frac{D_S E^3 A^3}{6} \ldots$$

Thus, provided that E is small, and neglecting higher order terms the expression can be simplified to:

$$O.D. = C_0 + C_1\,[E] + C_2[E]^2$$

where

C_0 = a term due to the fog level which has been added here to correct for the "DC" offset of the data

$C_1 = +D_S A$

$C_2 = \frac{-D_s A^2}{2}$

A convenient way of checking the validity of this equation is to record a series of photographic plates that have been exposed to electrons at a fixed dose rate and variable increment of time. Cumulative dose then becomes proportional to exposed time. A least squares fit of data to a parabolic equation will determine the coefficients of the resultant curve. Results of such a procedure are shown in Figure 3-2. As can be seen, a good fit is obtained over a broad region of the data. At higher optical densities, due to the slope of the curve, the small variations in recorded optical density will lead to large variations in the calculated number of electrons. It was therefore decided to truncate the curve in a region close to the linear range in order

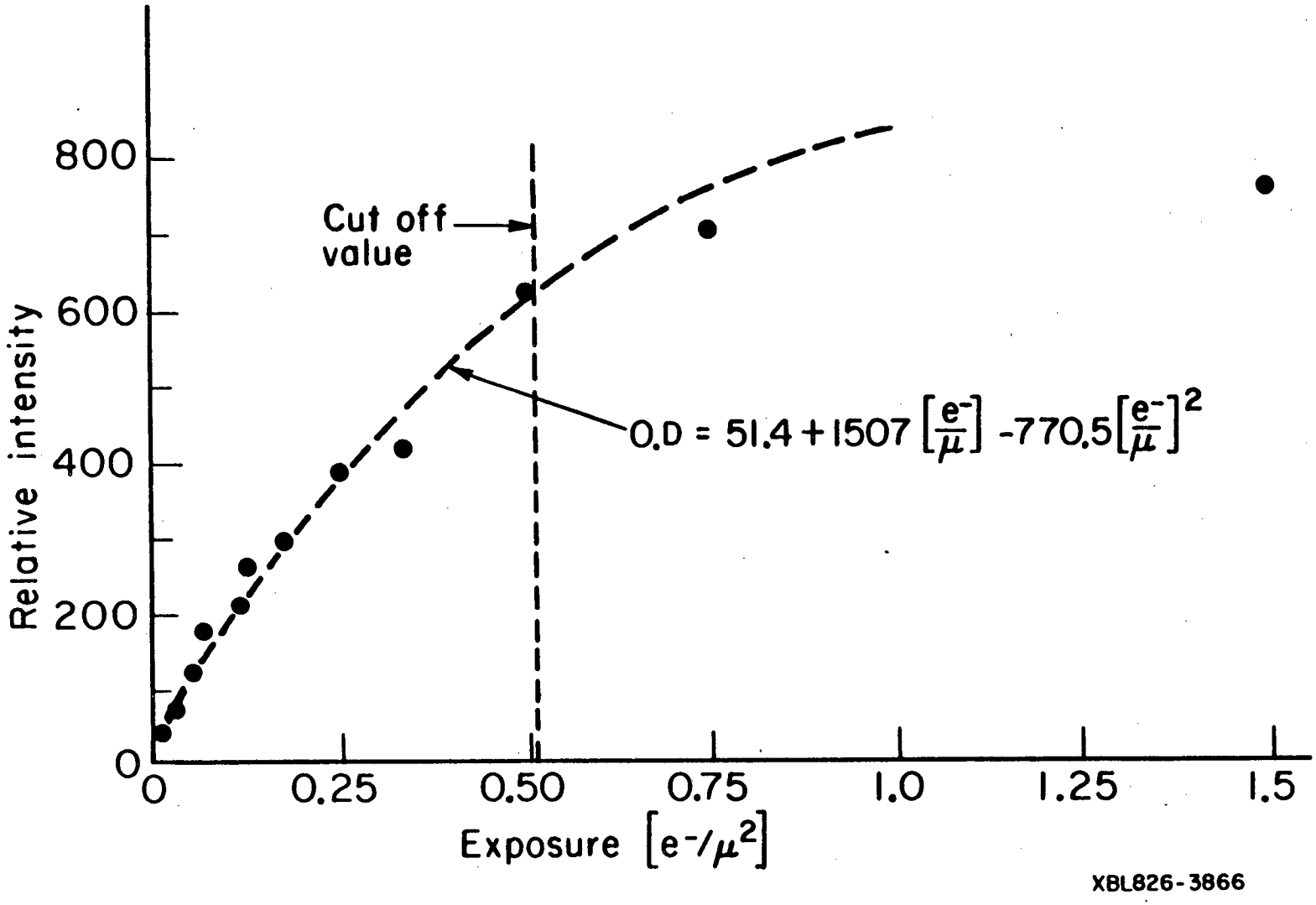

Fig. 3-2. Least squares fit of calibration data to a parabolic equation.

to minimize this effect. A point was chosen that was referred to as a cut-off value. Individual reflections that had optical densities that exceeded this amount were not considered further. In practice, the quadratic equation was inverted in order to obtain the electron dose for a given optical density.

Therefore, along with each set of diffraction patterns a set of calibrated exposures was taken in order to convert the optical density to a quantity proportional to the number of electrons striking the emulsion at each point.

D. Scaling of Diffraction Patterns

There are several factors that necessitate the collection of more than one electron diffraction pattern for a given state of a specimen. Probably the most important factor in our case is the limited dose that the specimen can tolerate due to its' radiation sensitivity. Variations in emulsion thickness and uniformity as well as scanner noise inherent in the analog to digital conversion process will also contribute to the noise of data collected from any one plate. The size of a given crystal will also limit the number of electrons in a given reflection. In our application, we are interested in scaling data sets together for two purposes: 1) to increase the signal to noise by combining similar data sets, and 2) to compare data sets in order to visualize any "differences" which may occur between them. Of the two, the first is by far the simpler application. In this case, the variance of the mean is expected to decrease as 1/N where N is the number of data sets. In the second case, the variance of the signal, ΔF, follows a more complicated distribution (Chapter 4).

As an example, a particularly simple form of the equation that has numerous applications in x-ray crystallography is $I_1(h,k) = KI_2(h,k)$. This would be physically realistic if data of the same crystal were collected by different investigators, each having his own diffractometer, or for scaling multiple films that have been taken together from the same exposure [Mathews et al., 1972].

In our case, we would like to include the possibility that different data sets are more "perfectly crystalline" than others. This difference can be visualized as a pertubation e^{-2BS^2} that multiplies one of the data sets where S is frequency and B a "temperature factor." Thus, we have assumed that $I_1 = I_2Ae^{-2BS^2}$. The physical ramification of this equation would be that one of the diffraction patterns fades exponentially more rapidly than another one as a function of resolution. Thus,

$$I_1 = I_2Ae^{-2BS^2}$$

$$\longrightarrow \frac{I_1}{I_2} = Ae^{-2BS^2}$$

$$\longrightarrow \ln\left(\frac{I_1}{I_2}\right) = \ln A - 2BS^2$$

In this case, a system of linear equations CX = D can be generated:

$$\text{where } C = \begin{bmatrix} 1 & S_1^2 \\ \vdots & \vdots \\ 1 & S_N^2 \end{bmatrix}, \quad X = \begin{bmatrix} \ln A \\ -2B \end{bmatrix}; \quad D = \begin{bmatrix} \ln \frac{I_1(S_1)}{I_2(S_1)} \\ \vdots \\ \ln \frac{I_1(S_N)}{I_2(S_N)} \end{bmatrix}$$

This system can then be solved via a least squares technique by minimizing the quantity $\Sigma(D_i - C_i X)^2$.

It should be noted that this scaling technique can be described as "difference Wilson scaling." In the case of Wilson scaling, as before, including a contribution due to thermal vibrations leads to [Blundel and Johnson, 1976]:

$$K \langle I \rangle = f_j^2 \exp - 2B\ S^2$$

where B = average isotropic temperature factor. $\langle I \rangle$ = average of observed intensities, K = absolute scale factor.

Ordinarily, for statistical reasons, one considers these scattering factors to be averaged only in a band of S^2. Finally, a graph of ln $[\langle I \rangle / f_j^2]$ versus S^2 should give a straight line of slope -2B and intercept -lnK because

$$\ln \frac{\langle I \rangle}{f_j^2} = -\ln K - 2B\ S^2$$

Problems can arise in using this methodology due to the breakdown of the assumptions made in the derivation. Departures from a random distribution of atoms, especially at low resolution may lead to a poor fit to the data.

The determination of the absolute scale factor K and temperature factor B are the chief result of this technique. After determining these parameters data sets may be placed on the same scale by multiplication of the reflections by the reciprocal of these expressions or by choosing an average K and B to which all of the data are then scaled.

In the case of purple membrane, the limited resolution obtainable and the relatively small unit cell size limit the total number of reflections. The effect of this is to cast the statistical assumptions necessary for absolute Wilson scaling in a doubtful light.

The relative scaling scheme is a way of circumventing the statistical assumptions that are necessary by treating the ratio of the intensities of the reflections on a one by one basis. Assuming that we have 2 data sets and we take the value of <I> equal to only one reflection then the Wilson equation yields:

$$K(1) \cdot I(1) = f_j \exp(-2B_1 S^2)$$

$$K(2) \cdot I(2) = f_j \exp(-2B_2 S^2)$$

dividing one equation by the other

$$\frac{K(1)}{K(2)} \frac{I(1)}{I(2)} = \exp(-2S^2(B_1-B_2))$$

which is identical to the previous expression for relative scaling if

$$A = \frac{K(1)}{K(2)} \text{ and } B = 2(B_1-B_2)$$

Thus, A is a relative scale constant and B is proportional to a relative temperature factor ΔB.

An additional consideration in the analysis of any data is the fact that some of the data may be more reliable than others. In our case, the more intense reflections are more reliable. This can be seen in a graph of RSYM versus I (Figure 3-3). Incorporation of this fact into the scaling program can be accomplished by using a weighting scheme. Thus, in the case of relative scaling, one may alter the least squares system of linear equations that one is attempting to solve to be:

$$\vec{w} \; (\bar{C}\bar{X} = \bar{D})$$

so that we seek to minimize:

$$\sum_i w_i \, [C_i x_i - D_i]^2$$

An interesting situation arises in the scaling of the glucose-hydrated data sets. This is because we are trying to place data that are believed to be different on the same scale. In our case, we have no <u>a priori</u> way of knowing what the expected differences will be. Fur-

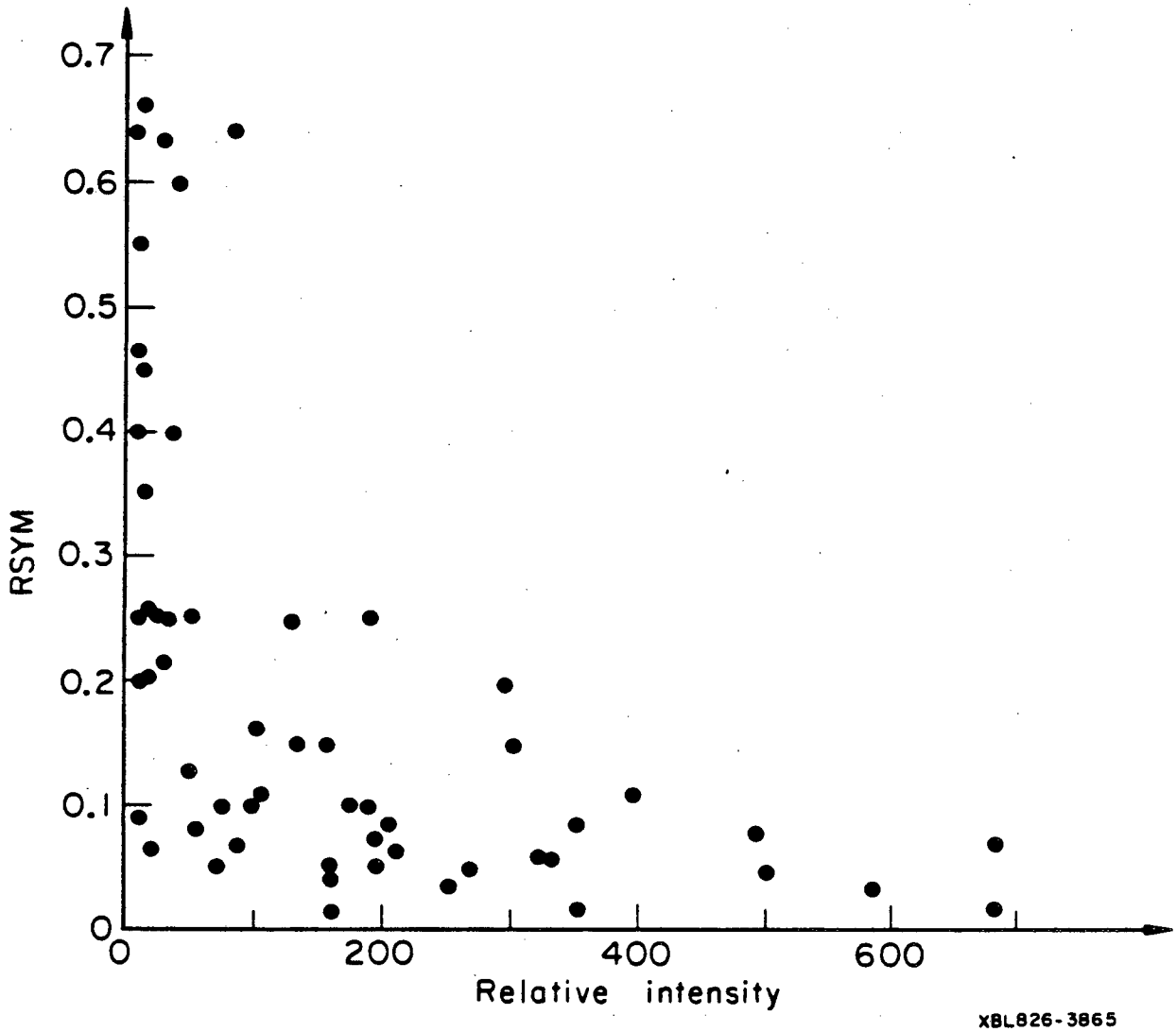

Fig. 3-3. RSYM vs. intensity for individual reflections (all data).

thermore, incorrect scaling may leads to "ghosts" of the original structure (holes or peaks) in the difference maps, that have very little to do with the true differences.

An easy way of illustrating this effect is to consider the result of an incorrect scaling for two identical sets of data. Multiplying one of the sets by the incorrect scale factor of 2 and subtracting the sets would yield the original data, clearly not the difference data which should be zero in this case.

Mathematically, assuming that our real space glucose structure is $\rho_G(r)$ and the hydrated structure $\rho_H(r)$ what we are most interested in is the difference structure $\Delta\rho = \rho_G(r) - \rho_H(r)$. Talking Fourier transforms of both sides $\rightarrow \Delta F = F_G - F_H$.

A convenient method for determining whether a scaling is "correct" or scaled correctly was devised by Kraut (1962). This method consists of comparing the numerical value at the origin of the difference Patterson, i.e., the Fourier transform of $(F_G-F_H)^2$ to that at the origin of the difference between Patterson functions, i.e., the Fourier transform of $(F_G^2-F_H^2)$. For the ideal case, these two values should be equal. Any deviation from equality can be corrected by multiplying one of the data sets by a scale factor which is derived in Kraut's article. In processing the data of this study, I have elected to calculate these scale factors on an <u>a posteriori</u> basis after least squares scaling of the data as described above. It is interesting to note that the otimal scalings, as determined by the least square technique, gave Kraut scale factors that were very close to 1. This has also been found by Arnone et al. (1971).

The above relative Wilson scaling algorithm was applied to the data that was output from the "Difproc" processing system. Another system of computer programs was designed and implemented which allowed the user to combine either glucose-glucose, hydrated-hydrated, or glucose-hydrated data sets. The results obtained will be discussed more fully in the final section.

The interplay between the final difference Fourier and the scaling used cannot be emphasized enough. Questions like: What are the objective criteria of a good scaling when there is no a priori knowledge of differences (i.e., heavy atom binding stochiometry), and how does the choice of scaling affect final interpretation, will be addressed in the conclusions where it will be shown that the Kraut factor in addition to the least squares method provides a convenient and sensitive test for proper scaling.

CHAPTER IV

DIFFERENCE FOURIER TECHNIQUES

A. Methodology and Goals

The basic objective of the difference Fourier technique is to calculate an estimation of the difference between two similar structures. In our case, we are interested in comparing the structure of PM in the frozen hydrated state with PM in the glucose embedded state. This is easily accomplished by using the difference technique if one has the amplitudes of the two structures and the phases of one of the structures. One advantage of the difference Fourier technique is that only one set of phases is necessary. Another advantage, that we shall see, is that it is sensitive to small changes in structural variation.

Mathematically, we form a difference structure by taking an inverse transform of the difference amplitude paired with the set of phases. Thus,

$$\Delta\rho(x,y) = \mathcal{F}^{-1} (F_2 - F_1) e^{i\theta} \qquad (1)$$

where F_1 = structure 1 amplitude; F_2 = structure 2 amplitude; and θ = phase of one structure.

There are many instances where the difference Fourier technique is useful. An important application would be to observe matter in one of the structures that is not present in the other. This is illustrated

in Figure 4-1. Examples of use of the difference Fourier synthesis for this purpose are the binding of azide ion to myoglobin (Stryer et al., 1964), the binding of competitive inhibitors to enzymes (Henderson et al, 1969), and the refinement of the location of heavy atoms. Difference Fouriers are also sensitive to conformational changes that occur in the structure. These changes may be due to the binding of small substrates (Moffat, 1971), or to alterations in the chemical environment (Perutz, 1970). Small shifts in the structure can be identified by the appearance of a peak located next to a trough (Figure 4-2). Examples of these uses will be covered in more depth later in this chapter.

A necessary understanding of the expected magnitude of the heights of the observed peaks is a prerequisite to the interpretation of a difference Fourier map. In particular, given a peak in a difference map, one would like to determine whether its height is consistent with certain molecular models. In addition, it is not obvious that the difference Fourier is a good approximation to the true differences between the two structures. These questions can be answered in a precise way.

Following Blundell and Johnson (1976), and with reference to Figure 4-3, we would like to determine the error between the calculated difference $(F_2-F_1)\ \exp i\theta_1$, and the true difference $F_2 \exp i\theta_2 - F_1 \exp i\theta_1 = F_\Delta \exp i\theta_\Delta$.

Using the cosine rule for the triangle illustrated in Figure 4-3

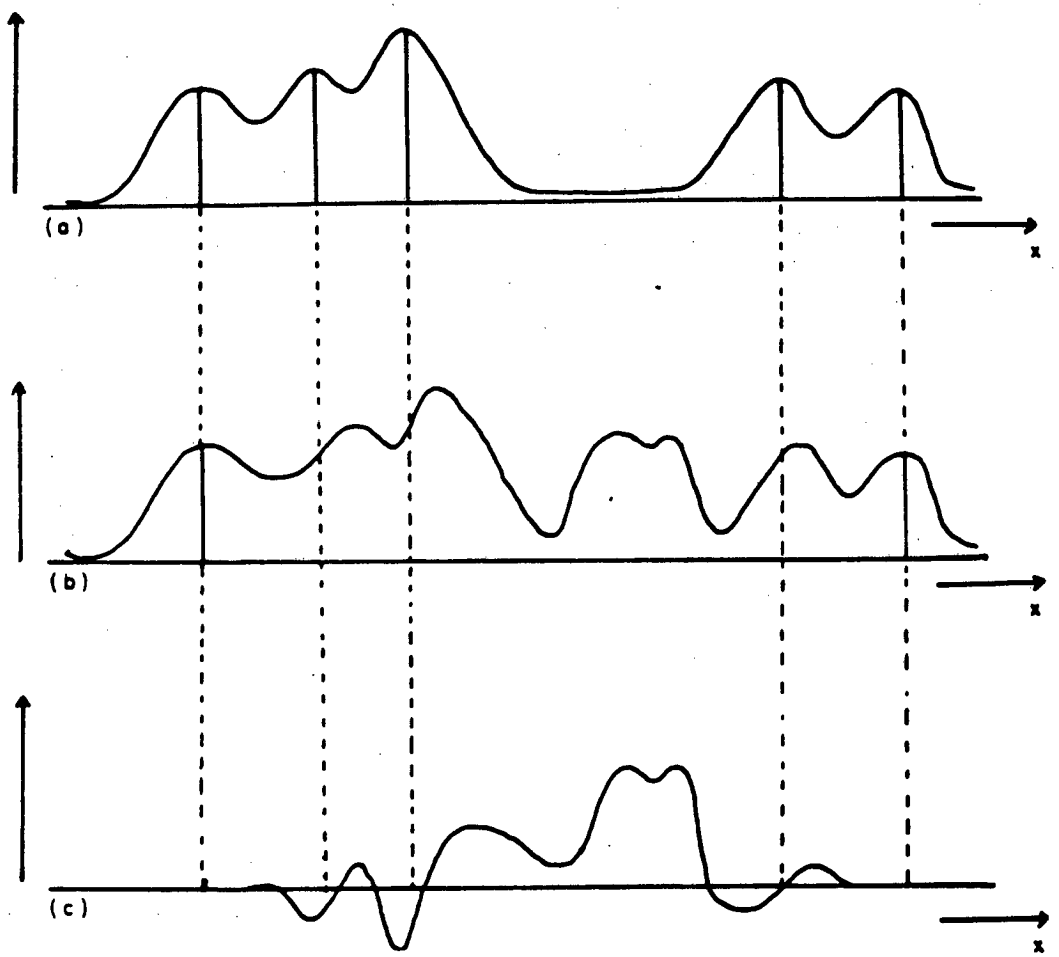

XBL 829-11681

Fig. 4-1. Example of the result of subtracting structure (a) from structure (b) to yield structure (c).

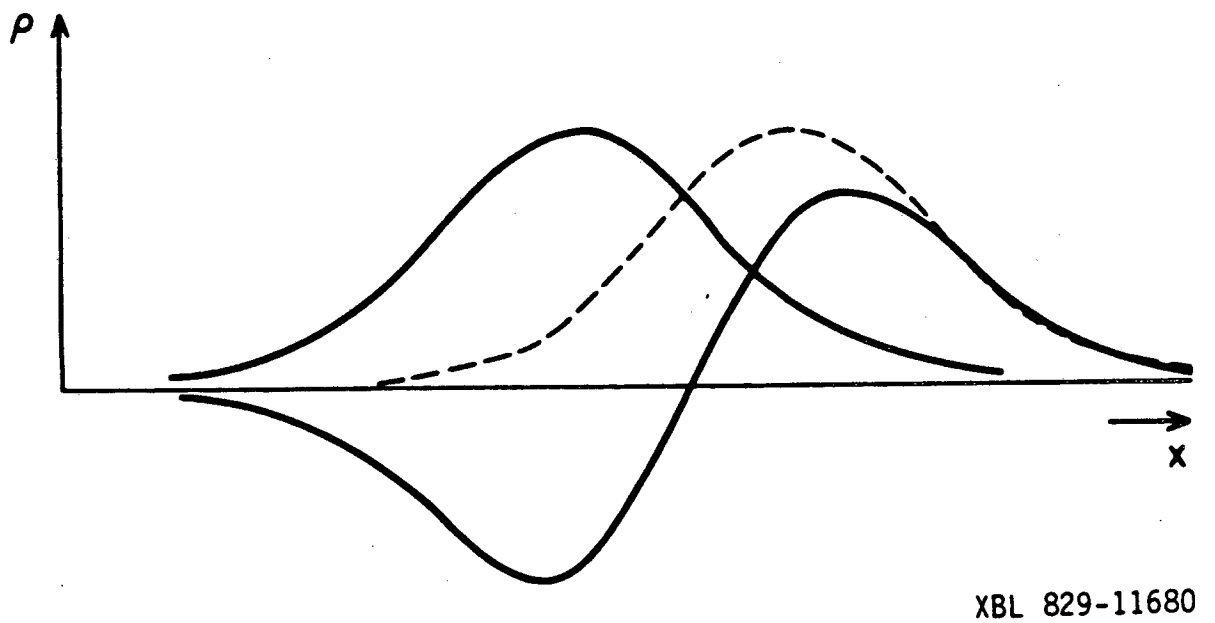

Fig. 4-2. Illustration of how a shift in structure can lead to a trough next to a peak in the subtracted map.

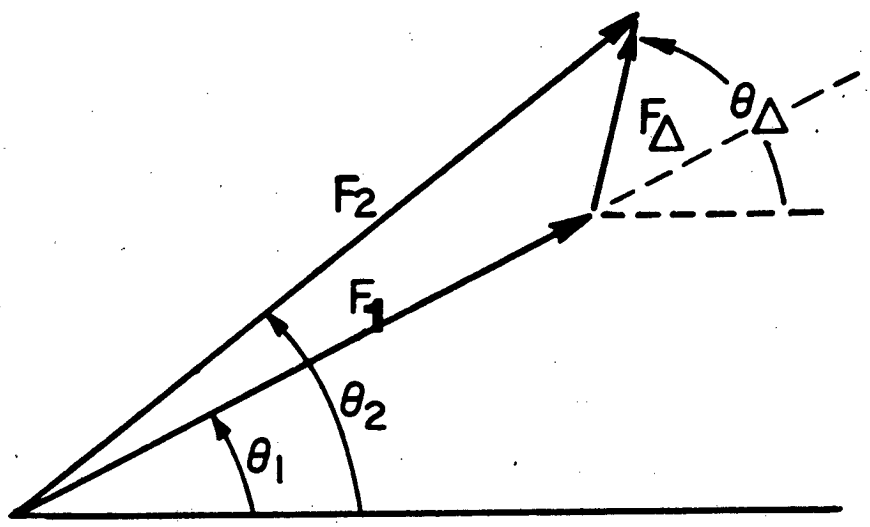

XBL829-4125

Fig. 4-3. Vector diagram for a difference map.

$$(F_2-F_1) = \frac{(F\Delta)^2}{F_1+F_2} + \frac{F_1F_\Delta \cos(\theta_\Delta-\theta_1)}{F_1+F_2} \qquad (2)$$

and using $\cos(\theta_\Delta-\theta_1) = 1/2\,[\exp i(\theta_\Delta-\theta_1) + \exp -i(\theta_\Delta-\theta_1)]$ then

$$(F_2-F_1)\exp i\theta_1 = \frac{F_\Delta^2 \exp i\theta_1}{F_1+F_2} + \frac{F_1F_\Delta \exp i\theta_\Delta}{F_1+F_2} + \frac{F_1F_\Delta \exp i(-\theta_\Delta+2\theta_1)}{F_1+F_2} \qquad (3)$$

This sum of three terms can be analyzed in the following way; term 1 will give a very small noise structure (correlated somewhat to the original structure) since $F_1 + F_2 >> F_\Delta$. Term 2 is half the true difference map since $F_1 \cong F_2$, and term 3 will average out to some noise level since θ_Δ and θ_1 are uncorrelated. Thus, the difference map will consist of half the true difference structure $(F_\Delta/2)\exp i\theta_\Delta$ plus some noise.

In principal it is also a good idea to consider the reduction in the peak heights of the map that is caused by uncertaintiy or error in the phases θ. Hayward and Stroud (1981) have recently extended the concepts of Blow and Crick (1959) in order to synthesize a "best" (minimal error) map in the case of the phases derived from images collected in electron microscopy. As in the x-ray case, they define a figure of merit m to be associated with each reflection. In analogy, the difference Fourier should contain the factor of m as a weighting term so that

$\Delta\rho = \mathcal{F}^{-1}\,[m\,(F_1-F_2)\exp i\theta_1]$ represents the "best" Fourier.

The effect that m has on the final difference map has been considered by Henderson and Moffat (1971). These authors have shown that the mean contribution to the structure factor is $m^2 \Delta F$. Thus, peak heights will be reduced on the average by a factor of m^2.

B. Error Analysis of the Difference Fourier Method

In examining the results of a difference Fourier synthesis the experimentalist is confronted with the task of interpreting the collection of hills and valleys as structural additions, subtractions or alterations. The peaks and troughs in this map may or may not contain information that is statistically significant based on the quality of the data. A useful approach in examining such maps is to calculate an expected noise level in the resultant difference map and compare this level with the heights of the observed peaks. Assuming that the errors are distributed with a somewhat gaussian distribution, peaks whose absolute value are greater than 3.5 standard deviations above the noise have less than a .5 percent chance of being due to random error.

One of the first attempts at calculating the noise level in the real space map was by Henderson and Moffatt (1971). Later on, Blundell and Johnson (1976) argued that Henderson's final formula was obtained by arbitrarily dividing his next to last equation by a factor of 2. In their book, they present a rigorous treatment of the error and also mention that in a more recent derivation by Henderson (1973, private communication) a similar formula to theirs has been obtained.

The starting point for the error estimation is the attribution of the error in the difference map to three sources: 1) errors in the measurements of intensities which contribute to errors in the difference between amplitudes; 2) errors inherent in the use of the coefficients $(F_2-F_1)\exp i\theta_1$ instead of the true differences $F_\Delta \exp i\theta_\Delta$; 3) errors in the measurement of the original set of phases of the parent structure.

In order to estimate the contribution $\langle E(\Delta\rho)^2\rangle_{\Delta I}$ to the total real space mean squared error $\langle E(\Delta\rho)^2\rangle_T$ which arises from errors in the measurement of the intensities, we note that from the definition of the Fourier transform, and considering the error due to only one term in reciprocal space,

we first define

$$\rho_s = \frac{1}{V} F\exp(-2\pi i\bar{s}\cdot\bar{r})$$

and

$$\Delta\rho_s = \frac{1}{V} (F_2-F_1)\exp(-2\pi i\bar{s}\cdot\bar{r})$$

Now, assume we measure values

$$F_{1m} = F_1 + E(F_1) \text{ and } F_{2m} = F_2 + E(F_2)$$

where F_1 and F_2 are the "true" values of their respective structures. Then the measured difference structure is

$$\Delta\rho_{ms} = \frac{1}{V}(\Delta F_m)\exp(-2\pi i\bar{s}\cdot\bar{r})$$

where $\Delta Fm = F_{2m} - F_{1m} = [F_2 + E(F_2)] - [F_1 + E(F_1)]$.

Define the error in $\Delta\rho$ to be

$$E(\Delta\rho_m) = \Delta\rho_m - \Delta\rho$$

so that

$$E(\Delta\rho_{ms}) = \frac{1}{V}[F_{2m}-F_{1m}) - (F_2-F_1)]\exp(-2\pi i\bar{s}\cdot\bar{r})$$

$$= \frac{1}{V}[E(F_2)-E(F_1)]\exp(-2\pi\bar{s}\cdot\bar{r})$$

taking the square and averaging over the whole unit cell

$$\langle E(\Delta\rho_{ms}{}^2)\rangle_{\Delta I} = \frac{1}{V^2}[E(F_2) - E(F_1)]^2$$

$$= \frac{1}{V^2}(F_{1m}-F_1)^2 - 2(F_{1m}-F_1)(F_{2m}-F_2) + (F_{2m}-F_2)^2]$$

Now, by taking many measurements at a given reflection the second term will cancel as the measurements of F_1 and F_2 are statistically uncorrelated.

Therefore,

$$\langle E(\Delta\rho_{ms}{}^2)\rangle_{\Delta I} = \frac{1}{V^2}(\mathrm{Var}\bar{F}_1 + \mathrm{Var}\bar{F}_2)$$

Finally, to get the total error due to all Fourier coefficients used in the Fourier synthesis, we sum over all s (Blow and Crick, 1959) so that

$$<E(\Delta\rho)^2>_{\Delta I} = \frac{1}{V^2} \sum_s [\mathrm{Var}\overline{F}_1] + [\mathrm{Var}\overline{F}_2]$$

In order to approximate the error in using the coefficient $(F_2-F_1)\ \exp i\theta_1$ instead of $F_\Delta \exp i\theta_\Delta$, we can examine more closely the three terms derived before in equation number 3. As argued previously, term number 1 is close to zero because F_1 and $F_2 >> F_\Delta$. Thus, if $F_2 \cong F_1$

$$(F_2-F_1)\exp i\theta_1 \cong \frac{F_\Delta}{2} \exp i\theta_\Delta + \frac{F_\Delta}{2} \exp i(-\theta_\Delta + 2\theta_1) \qquad (5)$$

Here, as before, the first term is half the true difference structure. On the other hand, the second term is a noise term. In order to estimate the mean squared contribution of the second term to the noise in the real space structure we average its square over the entire unit cell. If we let $< E(\Delta\rho)^2>_{\Delta F}$ be equal to the mean square error in real space due to the second term then:

$$<(E\Delta\rho)^2>_{\Delta F} = \frac{1}{V} \sum_V (E\Delta\rho)^2 dv$$

$$= \frac{1}{V^3} \sum_V \left[\sum_s \frac{F_\Delta}{2} \exp i\ (2\theta_1-\theta_\Delta)\exp\ (-2\pi i\overline{s}\cdot\overline{r})\right]^2 dv$$

$$= \frac{1}{V^3} \sum_V \left[\sum_s \frac{F_\Delta}{2} \exp i\ (2\theta_1-\theta_\Delta)\exp(-2\pi i\overline{s}\cdot\overline{r}) \quad . \right.$$

$$\left. \sum_{s'} \frac{F_\Delta}{2} \exp i\ (2\theta_1-\theta_\Delta)\exp\ (-2\pi i\overline{s}'\cdot\overline{r})\right] dv$$

We note that

$$\sum_V \exp(-2\pi i(\overline{s}+\overline{s}')\cdot\overline{r})dv = 0 \text{ if } s \neq -s'$$

$$= V \text{ if } s = -s'$$

therefore, doing the summation over real space first gives the result that

$$<(E\Delta\rho)^2>_{\Delta F} = \frac{1}{4V^2} \sum_s F_\Delta^2 \quad .$$

Since

$$F_2 - F_1 \simeq F_\Delta \cos(\theta_\Delta - \theta_1),$$

it follows that

$$<(F_2-F_1)^2> = <F_\Delta^2 \cos^2(\theta_\Delta - \theta_1)> = F_\Delta^2/2 \quad .$$

because

$$<\cos^2(\theta_\Delta - \theta_1)> = \frac{1}{2}$$

so that

$$<(E(\Delta\rho)^2)>_{\Delta F} = \frac{2}{4V^2} \sum_s (F_2-F_1)^2 = \frac{1}{2V^2} \sum_s (F_2-F_1)^2$$

Although not examined by Blundell and Johnson, the errors due to measurements in the phases are correctly treated by Henderson-Moffat. In analogy with Blow and Crick (1959) these authors showed the errors in the phase can be accounted for by multiplying the term $(F_1-F_2)^2$ by a factor of $(2-m^2)$.

In conclusion, the error due to these three factors can be summarized as

$$<E(\Delta\rho)^2>_T = <E(\Delta\rho)^2>_{\Delta I} + <E(\Delta\rho)^2>_{\Delta F}$$

$$<E(\Delta\rho)^2>_T = \frac{1}{V^2} \sum_s [\mathrm{var}(\overline{F}_2) + \mathrm{var}(\overline{F}_1) + (\frac{2-m^2}{2})(\overline{F}_1-\overline{F}_2)^2] \qquad (9)$$

Here, I have emphasized the fact that each F is an average of many symmetry related values by placing a bar over the F. To estimate the relationship between var($\overline{F}$), the variance in the average of the intensities, and var(F) we note that

$$\mathrm{Var}(\overline{F}) = \mathrm{Var}\left(\frac{F_1+F_2+\ldots F_N}{N}\right)$$

$$= \mathrm{Var}\left(\frac{F_1}{N} + \frac{F_2}{N} + \ldots \frac{F_N}{N}\right) = \frac{1}{N^2}\,\mathrm{Var}(F_1) + \frac{1}{N^2}\mathrm{Var}(F_2)+\ldots\frac{1}{N^2}\mathrm{Var}(F_N)$$

$$= \frac{N}{N^2}\,(\mathrm{Var}(F)) \text{ if } F_1, F_2 \ldots F_N \text{ are all distributed similarly}$$

$$= \frac{\mathrm{Var}(F)}{N}$$

An interesting exercise is to compare our final equation to that derived by Blow and Crick (1959) in their treatment of the total mean squared error obtained, in a normal Fourier map, when the phases are obtained by the method of isomorphous replacement.

$$\langle \mathrm{error}(\Delta\rho)^2 \rangle = \frac{2}{V^2} \sum_S [\overline{F}\,(1-M^2) + \mathrm{var}(\overline{F})] \qquad (10)$$

A result of the fact that $\Delta F \ll F$ is that the mean squared error in the difference map is much smaller than that of the normal Fourier map, as long as var(F) is not the dominant term.

C. Examples of the Use of the Difference Fouier Technique

An interesting example of the use of the difference Fourier technique is that of Stryer et al. (1964). These authors were interested in determining the location of the binding site of azide

ion to metmyoglobin. At that time they were able to exploit the availability of a three dimensional structural data set (phases and amplitudes) on whale metmyoglobin to a resolution of 1.4Å. It is also of interest to note that this was the first example of the use of a difference Fourier in protein crystallography.

The binding of the azide ion to whale myoglobin is easily accomplished by adding sodium azide in a molar ratio of 10:1. Spectrophotometric titration of the heme-azide absorption band indicated that over 99 percent of the metmyoglobin was complexed with the azide. Crystallization of the azide-metmyoglobin complex was then accomplished in the same manner as that of the native protein. Intensity data were then collected from the three dimensional crystals and a difference Fourier synthesis was calculated, i.e.:

$$\mathcal{F}^{-1} \quad [\Delta F_{expie} \text{ (metmyoglobin)}]$$

Difference maps of several sections are shown in Figure 4-4. As can be seen, there is a large positive peak in the top structure and a large negative peak in the bottom structure. The interpretation of these peaks is shown in Figure 4-5. As illustrated, the azide ion will displace a water molecule at the sixth coordination position of the heme iron, and there is a concomitant loss of a single sulphate ion bound at the surface of the molecule 9Å from the azide site. Other positive peaks in the difference map are situated at points occupied by the heavy atoms that were used in the phase determination

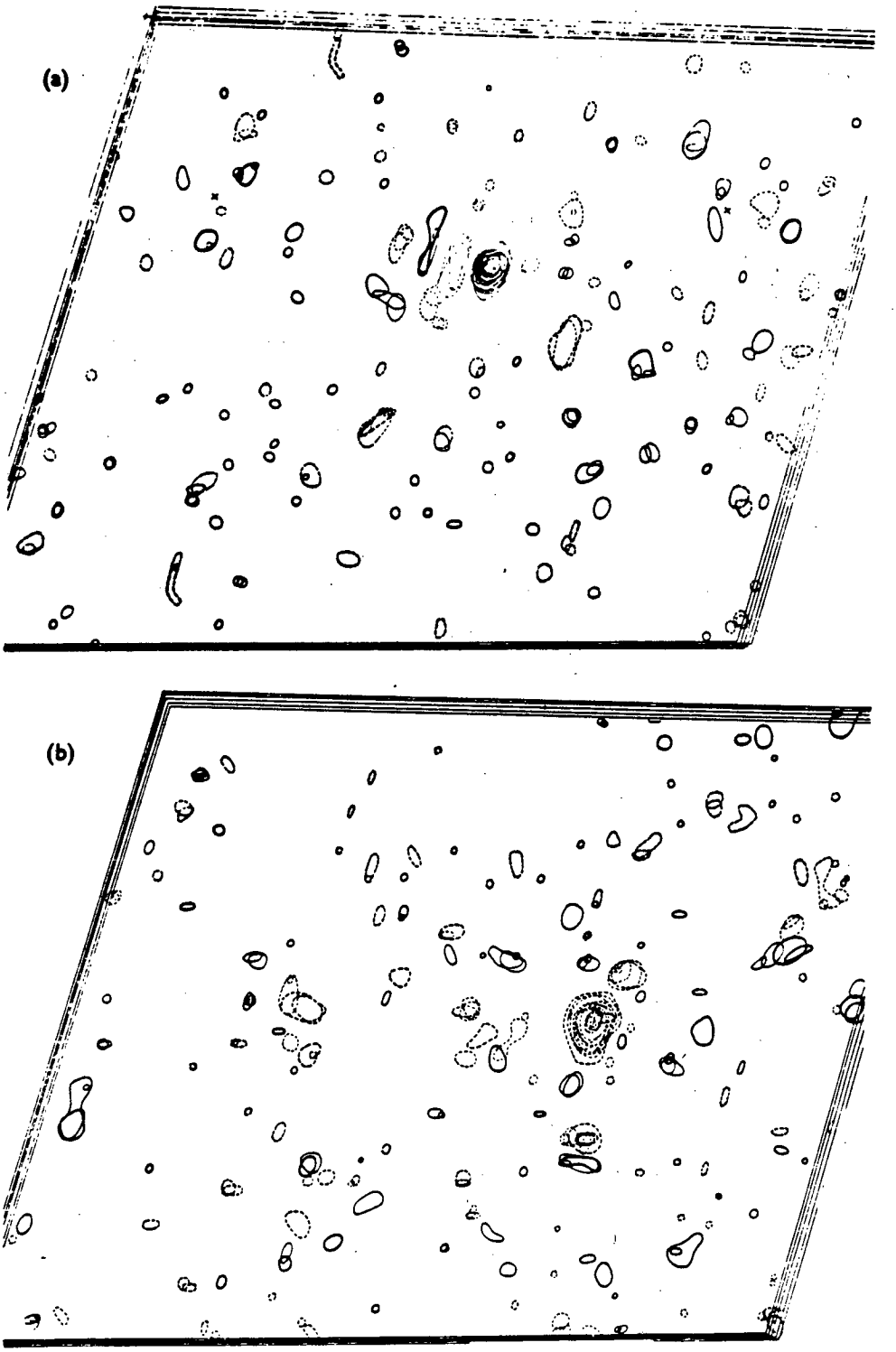

XBL 829-11683

Fig. 4-4. Difference map of metmyoglobin. Solid contours indicate additional electron density, dashed contours indicate a loss of density.

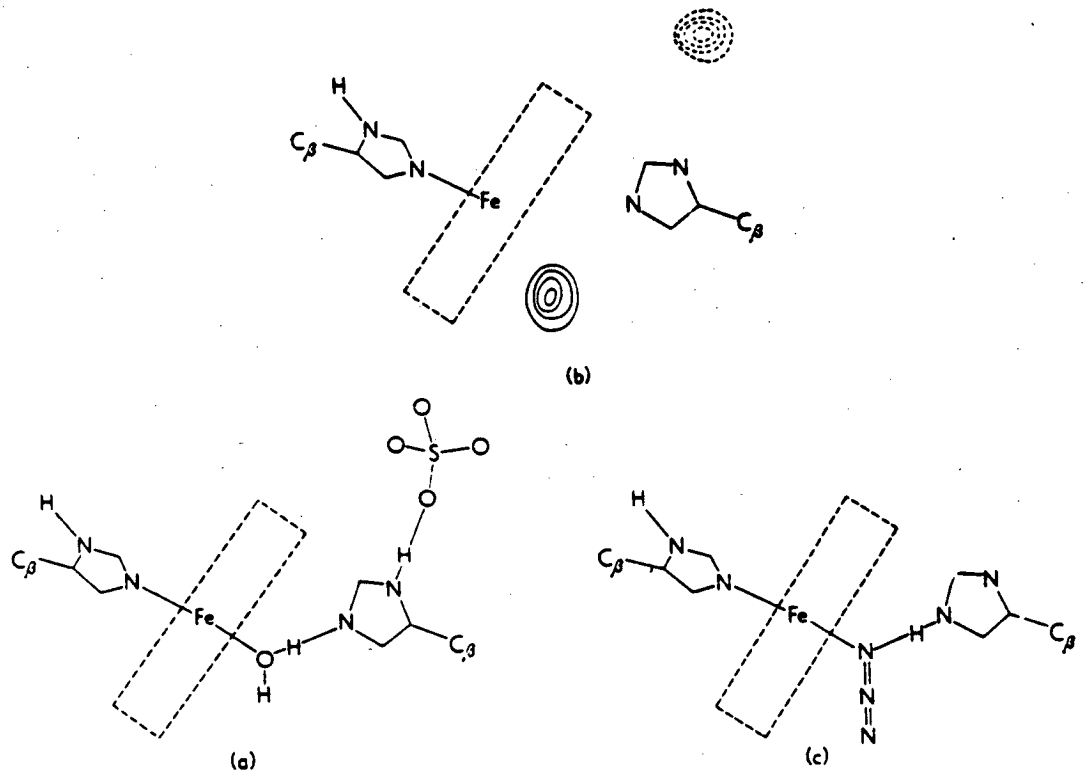

XBL 829-11684

Fig. 4-5. Molecular interpretation of the difference map shown in figure 4-4.

via the isomorphous replacement method. It was therefore considered unlikely that peaks which were less than 2/3 the azide peak represented added density in the azide derivative. No error analysis was performed in conjunction with this study.

A comparison of the magnitude of the peak expected from the additional azide is consistent with the above interpreation. The positive peak had a magnitude of .75 el./$Å^3$ while the negative peak had the same value. The expected peak height, as quoted by these authors, was 1.5 el./$Å^3$. We have already seen that the heights in the difference Fourier synthesis are reduced by half. Therefore, the observed reduction in the difference Fourier synthesis of azide metmyoglobin agrees with the theoretical expectation. The above example illustrated the use of the difference Fourier synthesis for a simple structural addition/subtraction. In the next example I would like to show how the method can be used to observe conformational alterations.

In this case, the structure of the reaction complex of carboxyhaemoglobin with the spin label N-(1-oxyl 2,2,6,6-tetramethyl-4-piperidinyl) iodoacetamide (spinCOHb) was studied (Moffat, 1971). Considerable interest in the location of the spin label was due to the large amount of electron paramagnetic resonance (EPR) spectroscopic data that had been recorded by McConnell and coworkers. Although the EPR studies were able to yield a great deal of information about the conformational changes occurring in partially oxygenated species, the amount of structural perturbation induced by the spin-label itself may

have altered the properties of the system. Although a number of spin labels had been under consideration, the iodoacetamide label (Figure 4-6) was potentially the most informative since haemoglobin reacted with this compound retained a large degree of cooperativity in the O_2-binding curve.

Diffraction data from crystals reacted with the spin label were collected to a resolution of 3.5Å and difference Fourier maps were generated between it and the native horse oxyhaemoglobin. These maps were able to reveal that the label which reacted at CYS F9 (93)β was able to maintain two orientations; one strongly immobilized and the other weakly immobilized. The strongly immobilized orientation displaces the Tyr HC2 (145)β and the C-terminus of the β chain. The weakly immobilized orientation is free in solution at the surface of the molecule and seems to have little effect on the structure.

Composite sections of the horse oxyhaemoglobin 2.8Å Fourier (Perutz, Muirhead, Cox and Goodman, 1968) are shown in Figure 4-7(a) and (b) with the corresponding sections of the 3.5Å spin-COHb difference Fourier in (c) and (d). As can be seen, the perturbations produced by the spin label are very complex. In this example, the difference Fourier is contoured in increments of root mean square error. I will next outline some of Moffat's interpretations.

A very striking feature of the map is the large positive peak at "f", interpreted to be one of the spin label orientations. The smaller positive feature "O" was the other, reduced in height by its superposition on the negative peak associated with the phenol ring of Tyr

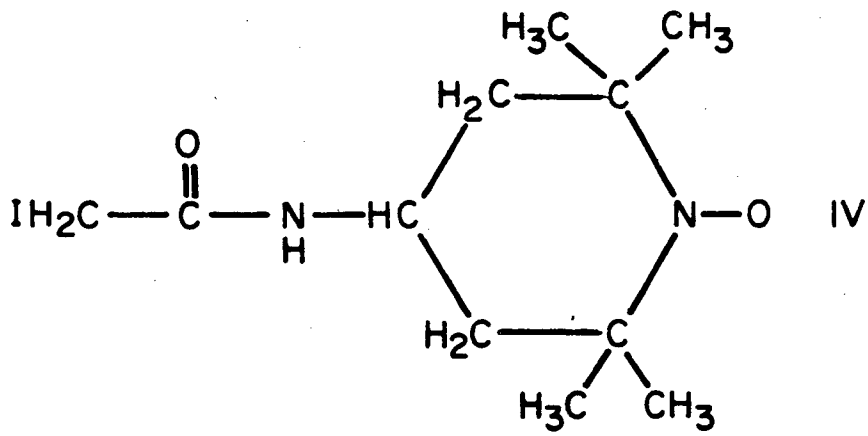

XBL 829 - 4127

Fig. 4-6. Iodoacetamide label used by McConnell (Moffat, 1971).

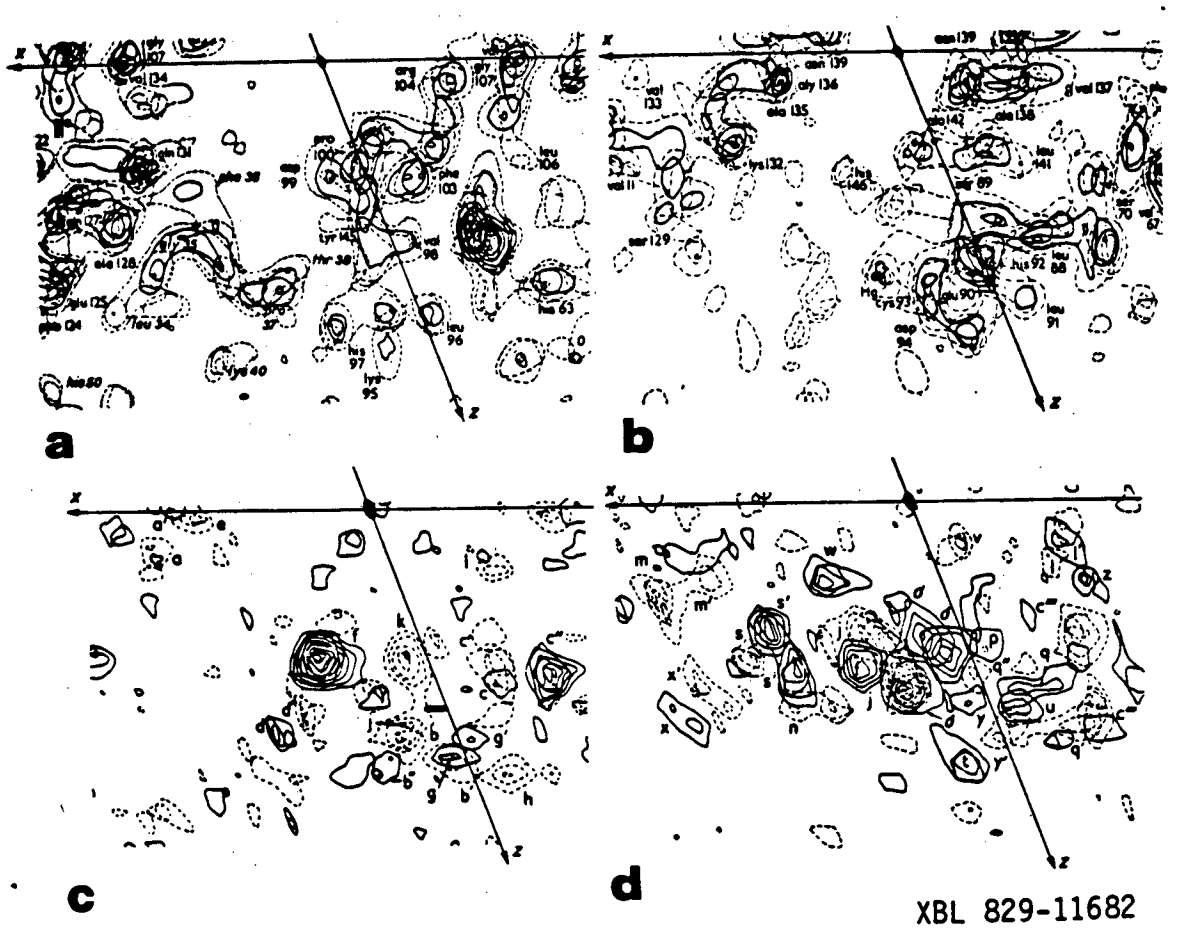

Fig. 4-7. Composite sections of horse oxyhaemoglobin at 2.8Å (a,b) with the corresponding sections of the 3.5Å spin Co-Hb difference Fourier (c,d).

HC2 (145)β, which has been displaced to give rise to the large negative feature j. Feature j is also accentuated by the displacement of the Cys F9 (93)β. Many other features of the F helix are displaced, arising from a slight twist of the F helix about its axis, counter-clockwise as seen in Figure 2(b). In addition to a distortion of the main chain from Asp FG1 (94)β, to Val F64 (98)β which includes some of the haem contacts and part of the $\alpha_1\beta_2$ interface (b', t, and k) an imidazole of residue FG4(97)β has moved .25Å (band b") as has the side chain of Leu FG3(96)β (g and g'). The N-terminus of the β-chain is displaced (x and x') and it adopts a new conformation in the internal cavity (s and s"). Therefore, in summary, "the distortions induced by the presence of the spin label are both numerous and extensive, the largest concentration of them in the environment of the heam groups of both the α and β chains, the F helix of the β chain and the FG region of the $\alpha_1\beta_2$ interface."

An outstanding feature of the interpretation of this map is the minute size of the shifts (.2Å) that can be seen relative to the resolution of 3.5Å. Thus, the location or displacement of a peak can be determined to greater detail than the actual width of the peak itself. This may appear at first to be somewhat surprising and indeed did surprise some of the earliest investigators. As part of a careful investigation of the conformations of haemoglobin, Perutz states, "When Dr. H. Muirhead and I measured the atomic coordinates of methaemoglobin using a plumb line and an electron density map drawn on the scale of 1Å = 5mm we did not believe our resolution of 2.8Å to be

sufficient to determine the displacement of the iron atoms out of the plane of the porphyrin ring. But by drawing the maps on a scale of 1Å = 2cm and viewing them in Dr. F. M. Richards' reflecting box it was clear that we had underestimated the information contained in them" (Perutz, 1970). What surprised them so much was that a distance of .3Å could be accurately measured in exact agreement with the displacement of the iron atom in metmyoglobin.

In this chapter I have outlined the basic methodology used in the difference Fourier technique. As demonstrated above, the technique can provide tremendous accuracy with a minimum of computational complexity, once a set of phases is accurately known. The technique is most useful for comparing two different structures, when the difference pertubation is small.

The history of the use of difference Fourier techniques in x-ray crystallography is extensive. As mentioned above it can be used in the refinement of the location of heavy atom positions that are needed to "phase" diffraction patterns. However, the physiological information that can be obtained by comparing the same molecular structures that are in different functional states are probably the most exciting application of the technique.

As briefly touched upon above, the difference technique has played a major role in understanding the different states of haemoglobin and the allosteric interactions of the α and β subunits (Perutz; 1970). Studies of the mechanisms of enzymes have been greatly facilitated by using diffrence techniques (Fersht, 1977). In a great many cases enzymes can be crystallized with and without inhibitors. This can

often give valuable information about both the location of the active site and the sometimes subtle changes that accomplish catalysis.

It is also interesting to ask about the limitations of the technique. One limitation that we have considered in detail concerns the noise level. Obviously good phases and accurate intensities are a prerequisite. However, the third parameter in equation number 10 is the noise term inherent in using the difference coefficient (F_2-F_1) expiθ in place of the true difference. We have seen that this value is approximately equal to $\Sigma \frac{(F_2-F_1)^2}{2V^2}$. If all of the real space difference is concentrated at one peak then the magnitude of the peak will be approximtely $\Sigma \frac{(F_2-F_1)^2}{2}$. Thus, if we have a large volume, the single peak will be more significant. It is also clear that a difference map is limited by the resolution of the data as well as the spectra of the difference structure. A movement of .5Å will certainly not be visible on a 7Å difference map, however, a 1Å movement may be, depending on the quality of the data. Significant difference peaks on a 7Å map may not be interpretable in terms of specific amino acids, however, they can be analysed in terms of the movement of α-helices or β-sheet. If there are many complicated movements that are close together, as in the Moffat map considered in this chapter, adjacent troughs and peaks may "washout " at lower resolution.

With respect to purple membrane, the recent availability of a set of phases (Hayward and Stroud, 1981) to 4Å allows the computation of projected difference maps to that resolution. In particular, the

results obtained when PM is prepared using a frozen hydrated method can be compared with the results obtained from the glucose technique via difference Fouriers. It will be shown in the Results and Conclusions sections that valuable information is revealed as a result of this process.

results obtained when PM is prepared using a frozen hydrated method can be compared with the results obtained from the glucose technique via difference Fouriers. It will be shown in the Results and Conclusions sections that valuable information is revealed as a result of this process.

CHAPTER V. RESULTS AND CONCLUSIONS

A. Microscopy

Using the methodology described in Chapter 2 to prepare frozen hydrated specimens, several electron diffraction patterns were collected whose resolution extended to 3.8 Å. Membranes isolated from the R1 strain of Halobacterium halobium were used (kindly donated by Dr. W. Stoeckenius) and were stored at 4°C in distilled water with .2 percent sodium azide. All membranes used were pelleted and resuspended several times prior to microscopy.

After freezing in LN_2 membranes were transferred to a liquid nitrogen stage (maintained at -135°C) using a cryotransfer device (Taylor and Glaeser; 1975). Grids were scanned at low magnification by defocusing a projection lens (P1) in diffraction mode (Hayward, 1978). Dose rate was monitored by a solid state detector and was 3-4e^-/Å-minute. When promising areas of specimens were found in the field of view a small condensor aperture was rapidly inserted, the projector lens was focused, and a 20-30 second exposure was taken.

The initial procedure of finding good areas and exposing the specimen did not take more than 5 seconds. Therefore, the total dose received by the specimen was never more than 2.4e^-/Å. This level of exposure was considered to be "safe" as studies of the rate of fading of powder patterns obtained using this frozen hydrated technique were not appreciably different from the frozen glucose studies of Hayward et al. (Jaffe, unpublished observations).

The recording medium for all of the frozen hydrated studies was electron image plates. Exposed plates were developed for 12 minutes

in full strength D19. Electron image plates were chosen over faster photographic films because of their uniform fog level and rigidity. The latter factor was very helpful for densitometer scanning.

Prior to scanning and data processing plates were evaluated by visual inspection on the basis of their symmetry and resolution. It is of special note that the absence of a selected area aperture facilitated the symmetry of the patterns as no asymmetry due to objective lens defocus was introduced. The rapid change in the intensity of the (4,2) reflection near the equator provided an excellent index of the tilt of the patches for even small angles (Hayward and Stroud, 1981). An example of one of the patterns is shown in Fig. 5-1.

B. Data Processing

Three relatively good diffraction patterns were selected, based on the above criteria, for further processing. As previously described, these patterns were scanned on a Perkin-Elmer scanning microdensitometer with an aperture size of 5μ square at 5μ intervals. These patterns were then processed through the "Difproc" family of programs (Appendix A) in order to extract the intensites of the recorded reflections. In addition, three glucose diffraction patterns (donated by Dr. S. Hayward) that were scanned under identical conditions were then processed through the same set of computer programs. At the conclusion of this stage of the processing, each reflection's intensity and (H,K) coordinates, as determined by the program, were output to a file in the memory of the computer. One such file existed for each of the plates bringing the total number of files to 6.

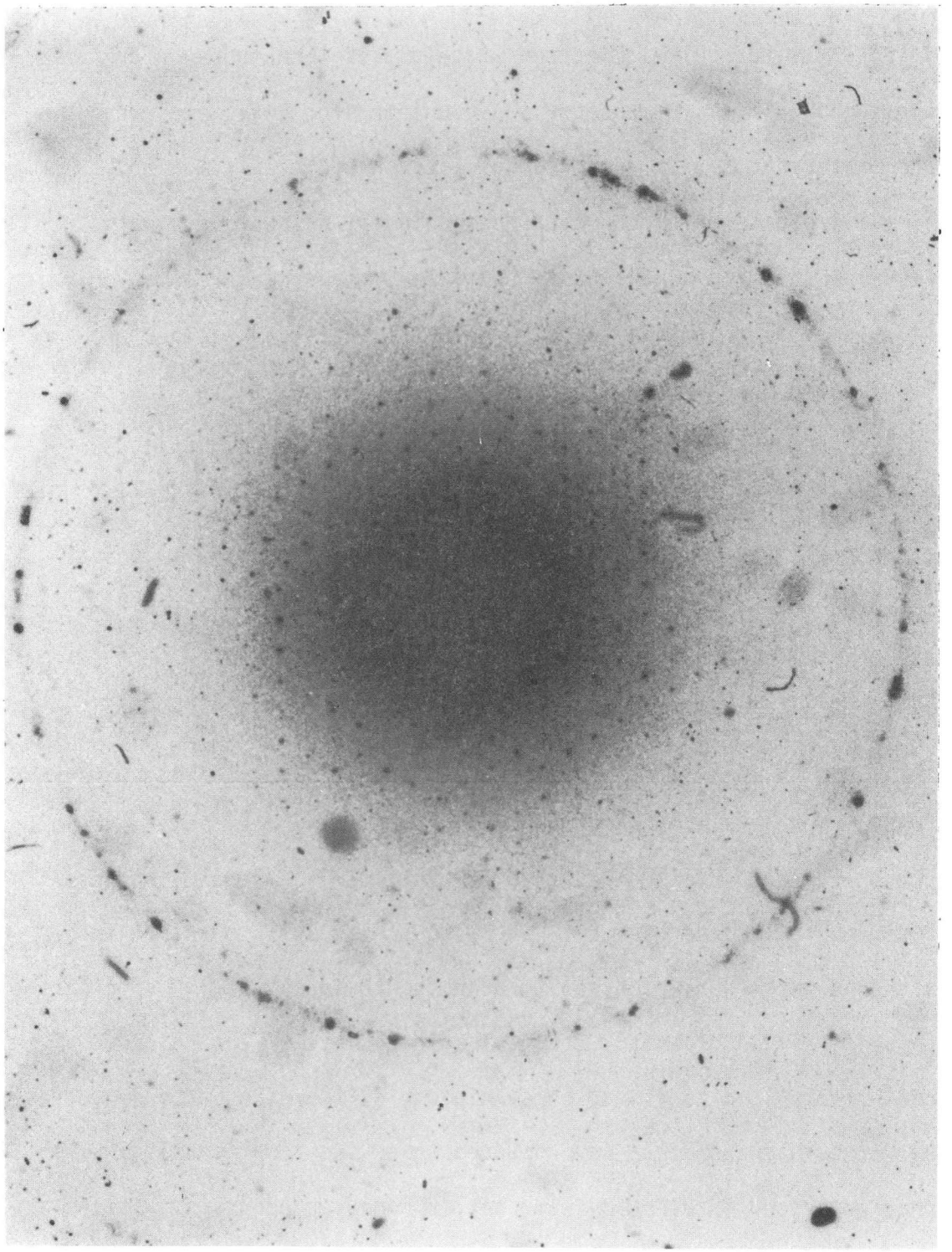

XBB 829-8095

Fig. 5-1. Example of a diffraction pattern.

These individual plate data provided the input for another system of computer programs that scaled data sets together. Various statistical parameters such as RSYM and the variance of the amplitudes were also calculated. One user option was a maximum RSYM level that was allowable in order for data to be included. The sets of three similar data (glucose and hydrated) were then combined into two master data sets using the relative Wilson scaling scheme that was described in Chapter 3. The two master data sets were then scaled against each other and a difference structure factor was calculated. By first pairing these difference amplitudes to the appropriate phases from the Hayward and Stroud (1981) data set and then taking an inverse Fourier transform a real space difference structure was obtained.

In figure 5-2 we can see a picture of the final difference map. The scaling interval in the drawing is 1 contour interval = 1 standard deviation of the noise as computed by the noise equation (9) in Chapter 4. Probably the most striking feature of the map is the large positive density that occurs in the inter-trimer regions (i.e., on the 3-folds). Although the largest of these peaks is only 2.9 standard deviations above the noise we have interpreted these positive densities as being glucose. In figure 5-3 I have illustrated the reasoning behind this hypothesis. As we can see, all other things being equal, the dense glucose minus less dense ice will show up as a positive peak in the difference map. Furthermore, a reasonable interpretation of this difference map is that there is a depression in the inter-trimer regions. In other words, it appears that this map infers that the protein sticks out above the plane of the lipids.

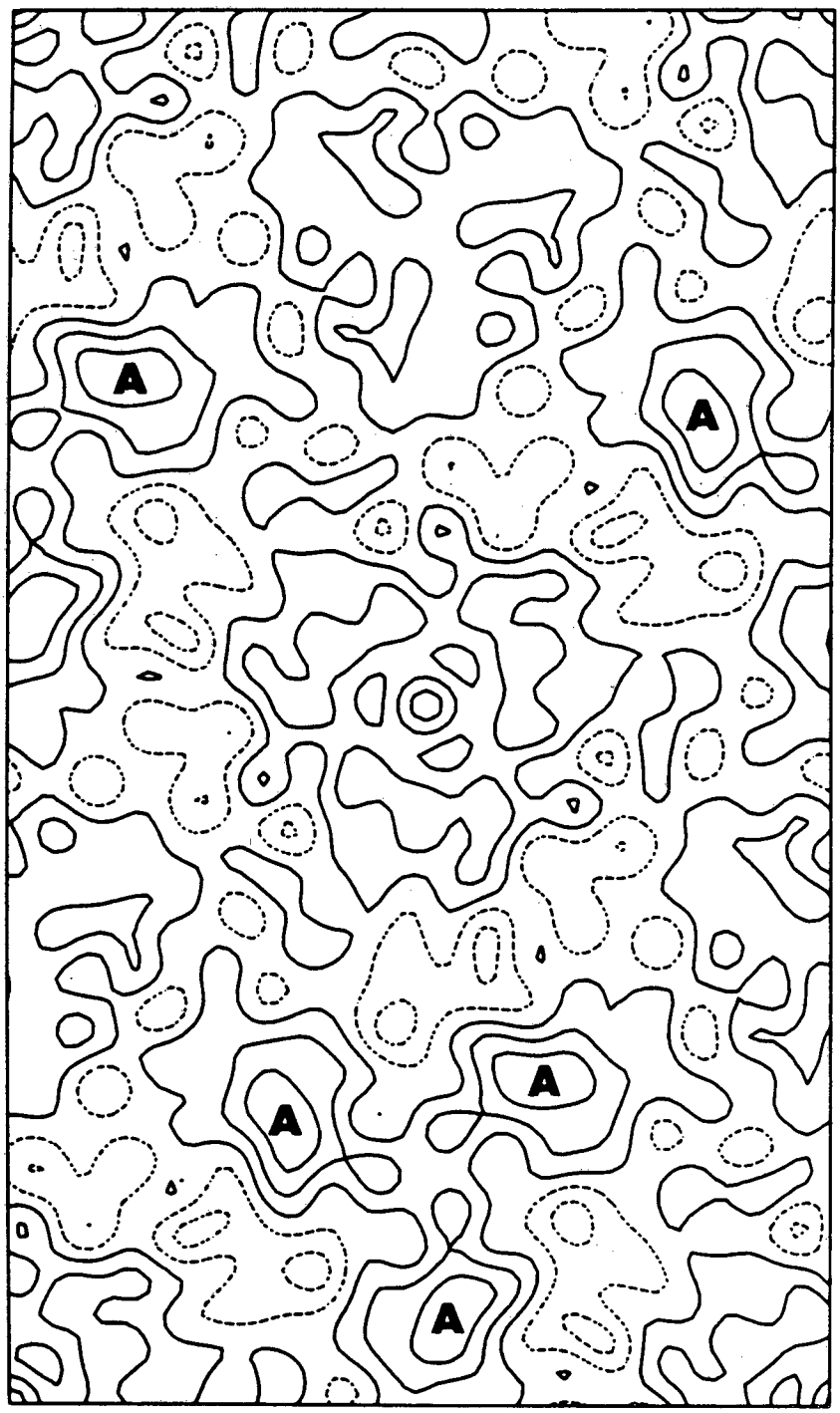

XBL 8211-3266

Fig. 5-2. Picture of the final difference map to 5.4A resolution.

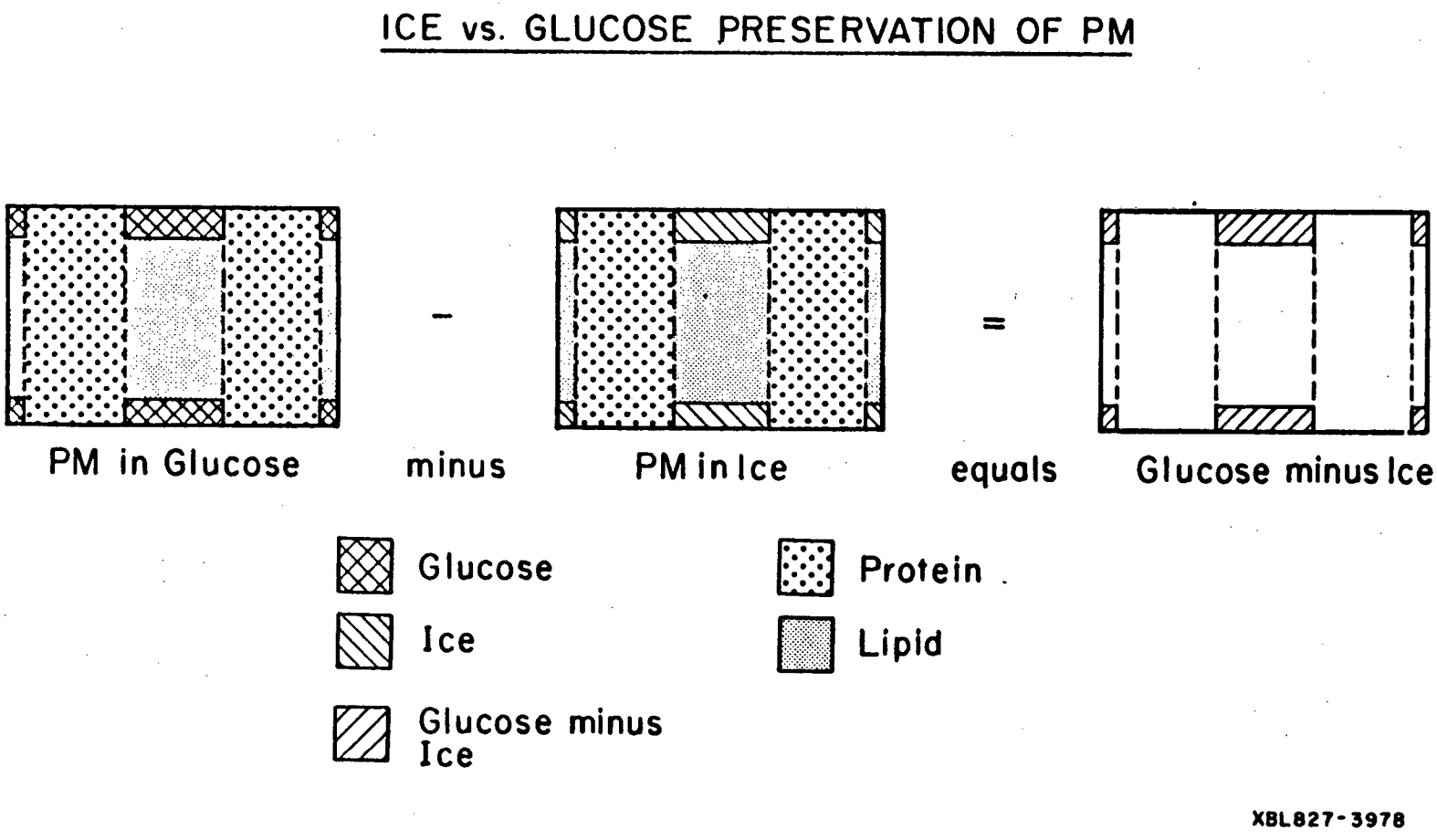

Fig. 5-3. Reasoning behind the hypothesis that the glucose peaks are positive in the difference map.

It is certainly worthwhile to examine the validity of the generation of this difference map before proceeding with the interpretations. Towards this goal, computational controls were performed. To examine the validity of the scaling itself, alternate scalings were employed. To aid in the interpretation of the final difference map, difference maps were performed between the individual plates in similar data sets, i.e., glucose-glucose and hydrated-hydrated.

In Figure 5-4 we can see the effect that systematically varying the scaling intercept and slope of the relative scaling has on the final difference map. In these examples the least squares program was modified to allow the user to determine the intercept (C_0) and the program chose a slope that led to a least squares solution (C_1). Note that $C_0 = A$ and $C_1 = -2B$ in the notation of Chapter 3. As judged by the disappearance of the strongest feature of the map, the inner three helices, the optimal scaling by the least squares program seems to be very reasonable. Another fact supporting this scaling as being the most reasonable is that its Kraut factor is closest to the optimal value of one. Kraut scale factors are also noted in Figure 5-4 on the scaling plots.

In Figure 5-5 we can see the results of scaling the similar individual plate data against each other. It is interesting to note that in any of these scalings we do not see the same type of distribution of positive and negative peaks as in the final difference

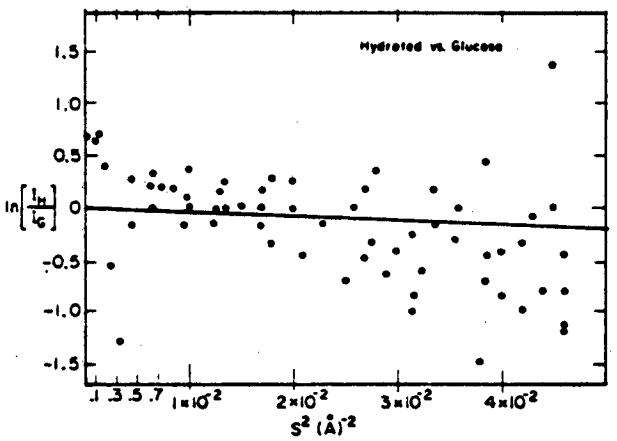

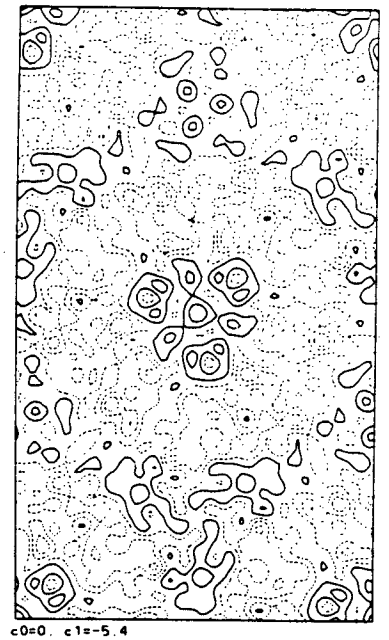

Fig. 5-4(a). Kraut = .91

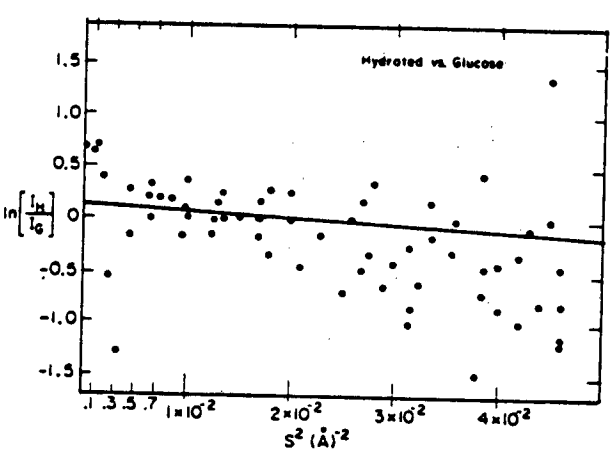

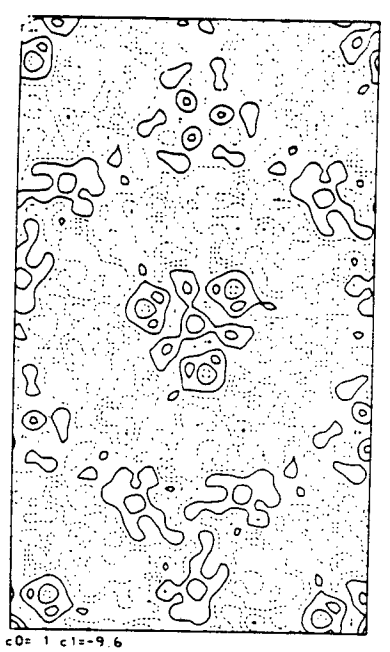

Fig. 5-4(b). Kraut = .89

Fig. 5-4. Effect of systematically varying the slope of the Wilson plot.

XBL 8211-3262

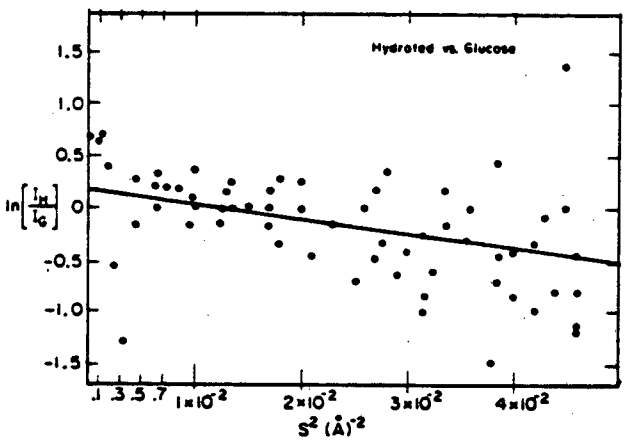

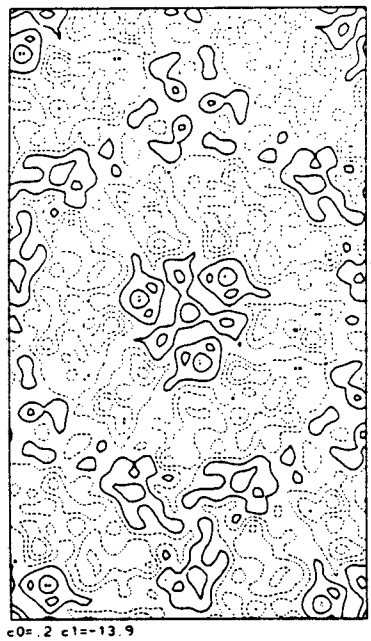

Fig. 5-4(c). Kraut = .97

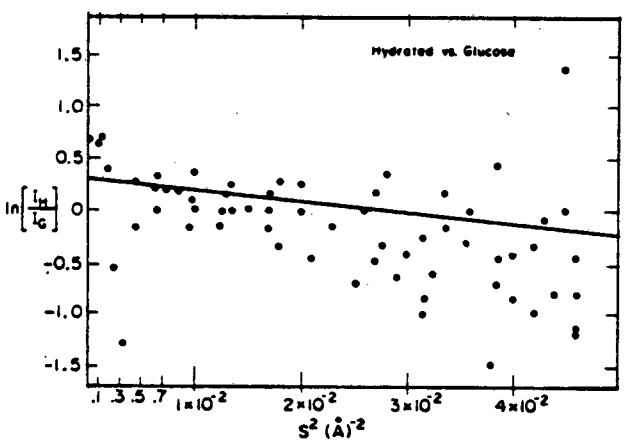

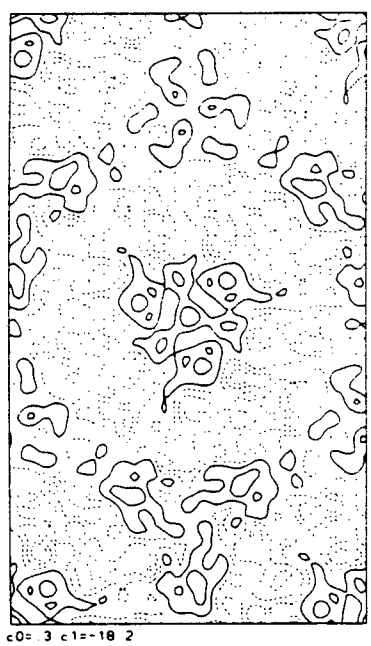

Fig. 5-4(d). Kraut = .97

XBL 8211-3263

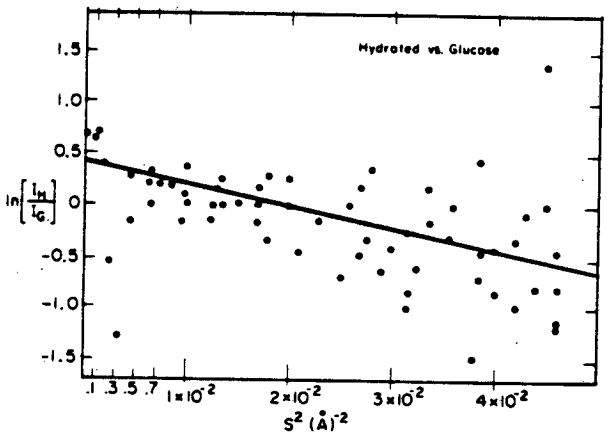

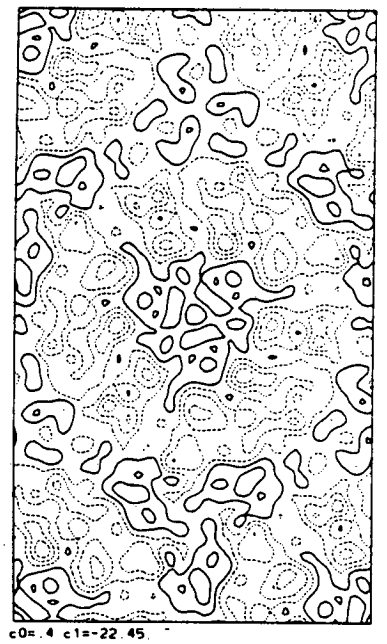

Fig. 5-4(e). Kraut = .93

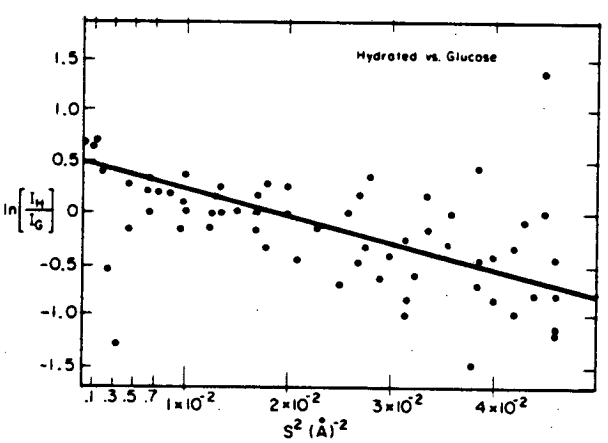

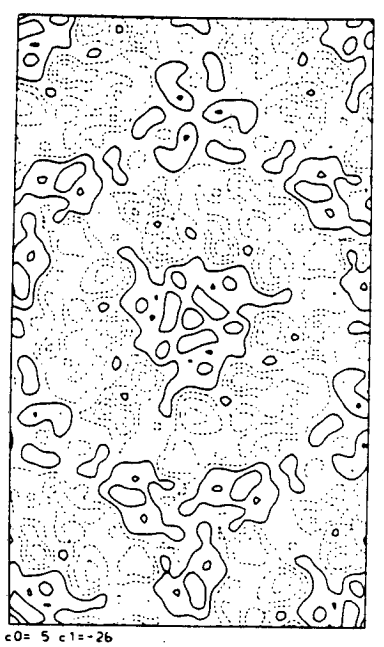

Fig. 5-4(f). Kraut = .92

XBL 8211-3264

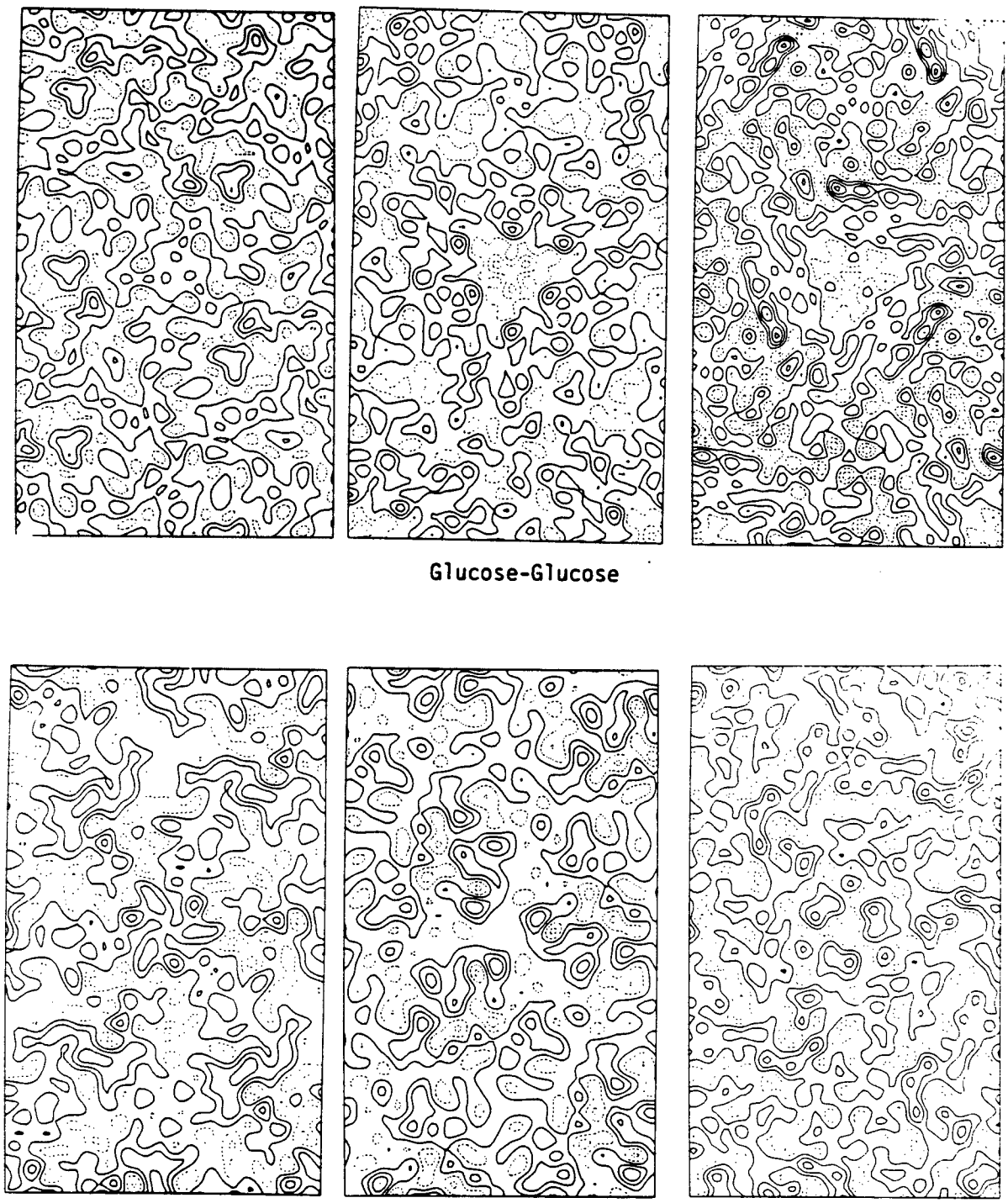

Figure 5.5 Effects of scaling similar data sets.

map. As already stated, in the final map the large positive peaks occur near the 3-fold origins surrounded by a fairly negative region.

It should also be noted that in the illustrations of figure 5-5 the data was not contoured in increments of a standard deviation but rather so that there were 7 contour levels between the minimum and maximum value. This arbitrary scaling is of minor concern as we are interested in the qualitative features.

C. Interpretations

The region that is occupied primarily by protein in the PM structure displays several interesting negative features in the difference map. It should be strongly emphasized here that the height of these peaks above the noise is somewhat less than those of the positive peaks. The deepest trough here is only 2.4 standard deviations above the noise level. Several interesting hypothesis for the origin of these peaks may be that they are due to an elongation of the helices (i.e., the middle of the inner three) or that they may represent linker regions between the helices. Two of the negative peaks in the outer region would be ideally situated for this to be true. Further interesting interpretations would be more worthwhile if the signal from these peaks was actually more above the noise level.

Indeed, it is anticipated that additional experiments will reduce the noise levels by improving the extent of statistical definition.

As a final exercise, it is interesting to try to determine the magnitude of the depth of the surface features of PM that are

indicated by the positive peaks. For this purpose, as illustrated in Figure 5-6, I have divided the membrane into two regions, a lipid and a protein region. The sizes of these regions were determined by assuming that the lipid occupies around 27 percent of the area of the membranes (Hayward and Stroud, 1981).

A value for F_0 of the membranes was determined such that the ratio of the density of protein to lipid was 1.3. Next, the average density of matter in the lipid region of the difference map was calculated and an estimate was made of the relative thickness of a glucose layer that could give rise to such a feature. Using this reasoning we can also estimate the depth of the largest positive feature, peak A in Figure 5-2. By making the above assumptions, and also assuming that the height of the peaks in a difference Fourier are reduced by half, this feature was estimated to correspond to an 8 percent change in membrane thickness. Interestingly enough, this corresponds to the change one would expect to observe for a single glucose molecule and is testimony to the sensitivity of the difference Fourier.

D. SUMMARY

In this thesis I have demonstrated how the difference Fourier technique which has been in common use in x-ray crystallography, can be applied to the analysis of electron diffraction patterns. This work has resulted in the first example of the determination to high resolution of a frozen hydrated structure. Several new and significant steps were required in order to achieve these rsults:

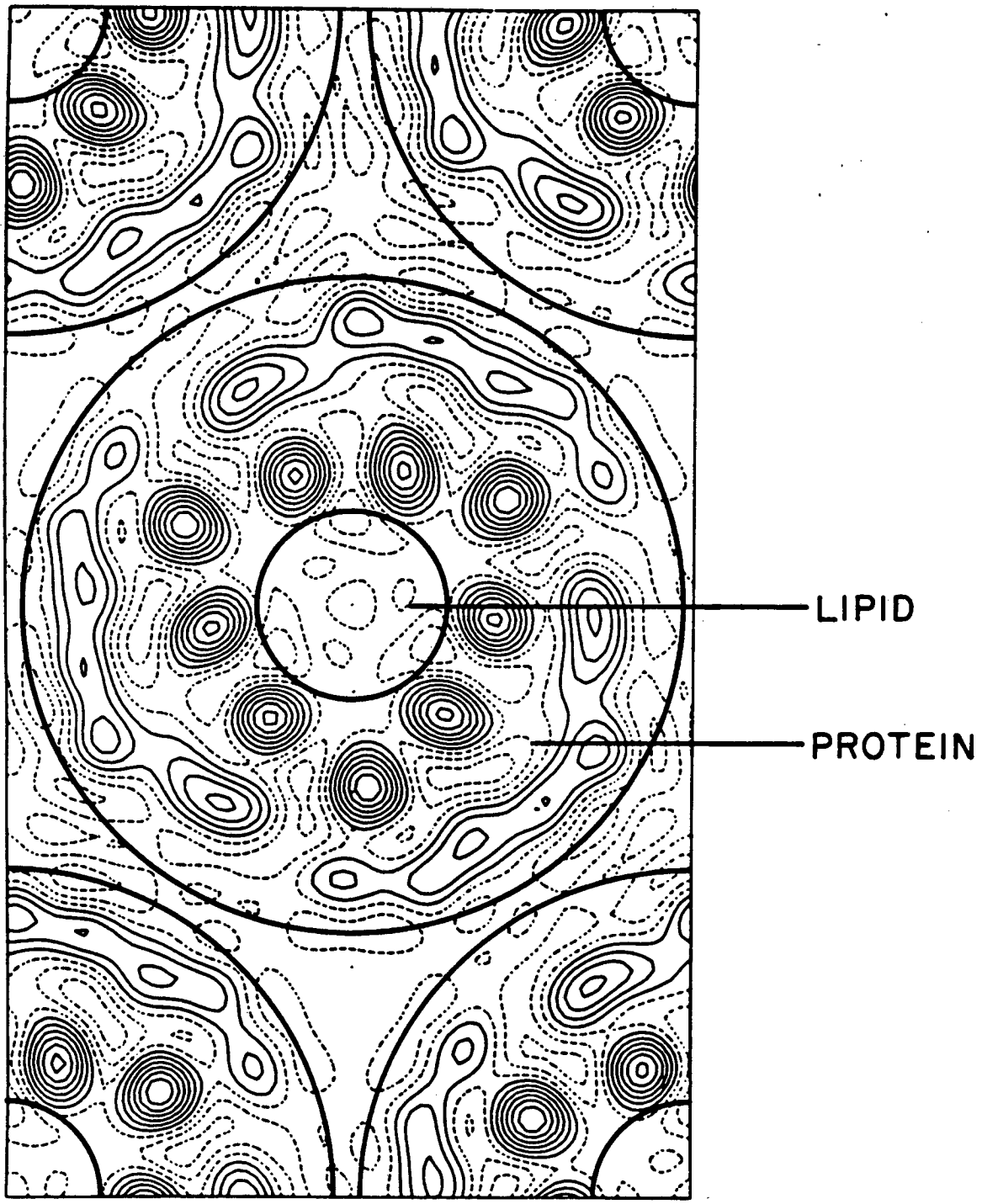

XBL8210-4147

Fig. 5-6. Example of the two regions used to determine the area occupied by lipid and protein.

1) A new method of specimen preparation was developed in order to observe bacteriorhodopsin in a frozen hydrated state. The structural work reported here was permitted by the reliability of the specimen preparation.

2) A method of scaling the glucose versus the frozen hydrated diffracted intensities was developed using a relative Wilson technique. This included a weighting scheme to account for the reliability of the data.

3) An alternative check on the scaling was provided by computing a Kraut scale factor. Various scaling parameters were adjusted to determine how sensitive the final results are to deviations from the optimal value of this scale factor.

4) The scaling methodologies of 2 and 3 were compared. The least squares estimate based on the relative Wilson scaling was found to agree quite well with the optimal value as determined by the Kraut scale factor.

5) Several topological features of purple membrane have been revealed as a result of the difference in contrast between ice and glucose. In particular, statistically significant depressions in the inter-trimer areas, are evidenct in the difference maps.

6) Higher resolution features that are not statistically significant at the present time, but which show extensive spatial correlations, occur in interesting regions of the protein structure. These higher resolution features may produce statistically significant electron dense matter when we are able to decrease the level of noise in our data, but this will require that additional patterns be collected and processed.

APPENDIX A

A Guide to the Use of the "DIFPROC" System

Purpose of System

The purpose of the "Difproc" processing system is to allow the user to obtain a set of intensities, I(h,k) as a function of X, Y location on a plate. Input to the program is a computer tape of data collected from EM plates that have been scanned on a Perkin-Elmer scanning microdensitometer. The units of I are unimportant as long as they are proportional to the number of electrons/reflection. Accurate determination of intensities is a very important ingredient in performing difference Fouriers. The "Difproc" family of programs is designed to allow the user to interactively index a given pattern by using the computer to locate the spots and to determine the set of I (h,k) once they have been found.

General Description: Input-Output of Flow Chart of Typical Session

Once the program has been engaged, the operator will type in the name of the file containing the scanned data in response to the request by the computer. This will be the input data to the program. The next thing that needs to be done is to inform the program of the 3 parameters of the scan; 1) number of scan lines/frames; 2) number of data per scan lines; and 3) the number of frames. These parameters are illustrated in Figure A-1. An additional user option is the ability to skip a number of frames before reading the data into computer memory. This is because a scan can exceed the amount of available memory. Thus, half pattern scans can then be broken in half

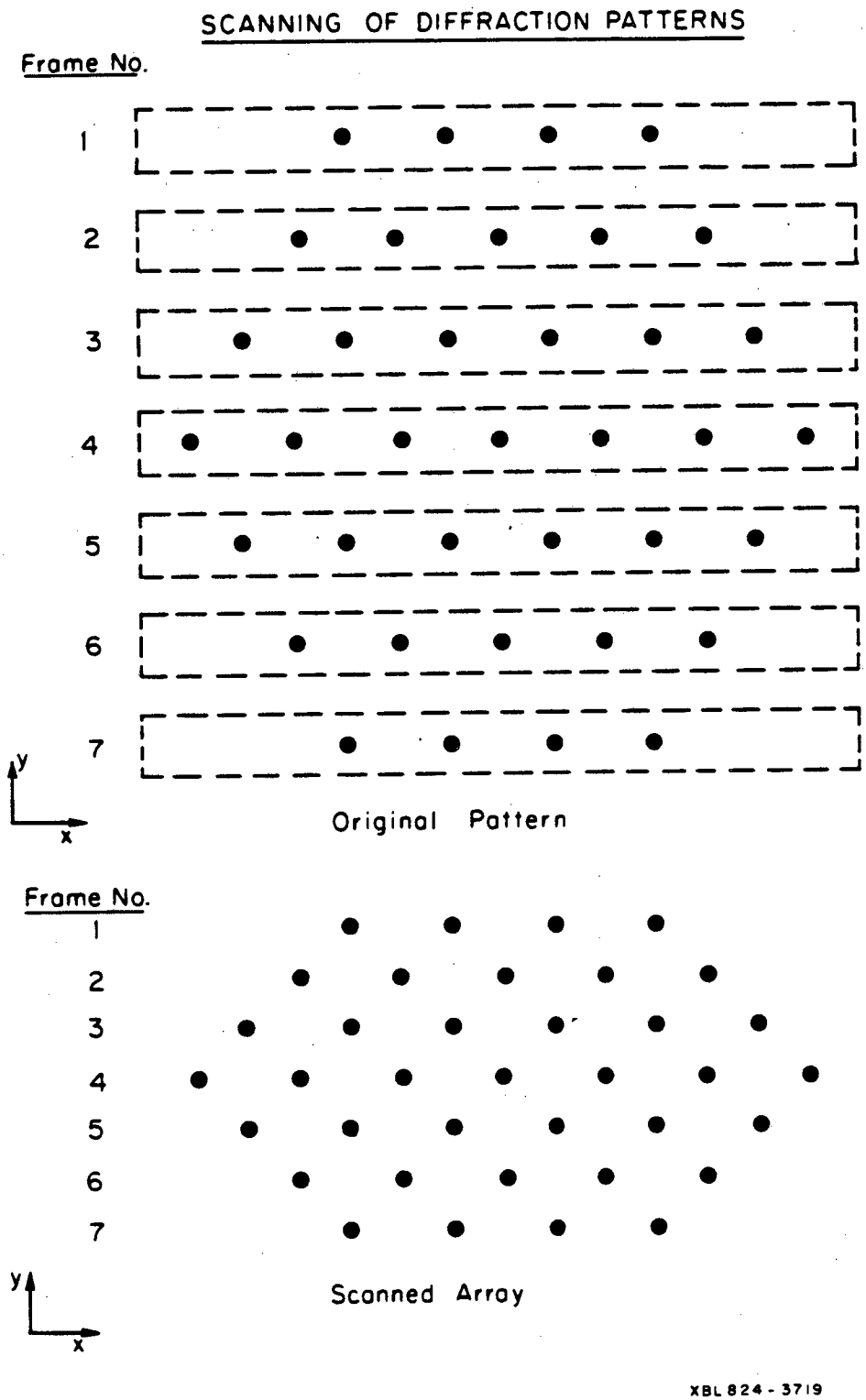

Fig. A-1. Example of the result of scanning diffraction patterns.

again to yield quadrants. After entering the number of frames the user wishes to skip the program will then be ready to accept commands in the command language. Ordinarily, the next thing to do will be to index the pattern. That is to say for every H,K reflection, the program will help the user to determine its' x and y location.

The approach that has been taken here is to allow the user to determine the location of each reflection by visually scanning an intensity modulated display of the data. The current version of Difproc gives the user the option of using the screen of a VT-100 display or a printer in a print-plot mode. If one is using a VT-100 the command 'VTWIND' is entered. The program will then request an x, y location, an input array size (necessarily square), and an output array size (necessarily square). The input array is reduced in dimension by an integer fraction to match the output size which is then displayed on the respective device. Successive use of this command allows the user to roam around different parts of the scanned image at different magnifications to determine the exact (visually approximated) location of the h,k reflections.

For example, assume that an input data of 7 frames, 40 lines/frame, and 3500 data points/line have been input. The program will store these values in an array of dimension 280 (y) by 3500 (x). Assuming that the spots are located centrally with respect to each scan line (see Figure A-1 for a typical example) would infer that the y locations of the reflections would be 20, 60, 100, 140, 180, and 220. Now, we would like to display a square area around (825, 100)

having a diameter of 200 pixels. So far, the response to the "WINDOW" prompt would be 825, 100, 200... If we wanted to reduce this array to a size of 50 x 50 (factor of 4) we would enter a 50 last. If we wanted to reduce this array to a size of 20 x 20 (factor of 10) we would enter a 20 last.

The next step generally taken is to index the entire lattice that is in bounds on the area of the plate that is in memory. (It is usually necessary to split a scan of a plate into several sections because the entire data set will not fit into memory of the computer that is available to the program). Several accurate determinations of H and K as well as their x and y locations are entered by using the command 'LTCREF.' At least three non-colinear points are necessary; however, any larger number may be submitted. It is usually a good idea to input four to six values that are spaced as far apart as possible. The entire lattice is then calculated by entering the appropriate command: 'ABCALC'.

There are two remaining parameters that should be input before the intensity of each spot can be determined: 1) The area around each x,y location to be considered as included in the reflection and 2) the relationship between the Optical Density (O.D.) at a point and the number of electrons striking the emulsion at that point. For convenience, the present version of Difproc assumes that the size of the area to be integrated around each reflection is independent of the reflection under consideration. The program will ask for the radius of this circular area upon entering the 'ABCALC' command. To input

the second group of parameters the command 'CALSCN' is invoked. The program will then ask for the A0, A1 and A2 values in the parabolic correction procedure as well as a saturation value. Data that are above the saturation value will not be used. In fact, if the program encounters data above the saturation value in a given reflection it will ignore that reflection in subsequent processing. One can now invoke the integration of background areas around all reflections and subsequent subtraction of backround areas by use of the 'SCNINT' command.

It has usually been helpful to compute RSYM* values for the data reflections to determine if the lattice has been indexed correctly, because low values of RSYM are generally indicative of a successful run. This can be accomplished by invoking the 'RSYM' command. Based on the results of this procedure one can either decide to look at the aberrant reflections using 'WINDOW' to see if they are being indexed correctly or write the data file out for further processing. Usually several iterations of this process are necessary to get optimal results. A particularly useful feature for looking at reflections that do not seem to be consistent is the 'DISPLAY' or 'VTDISP' command. This command is very similar to window except that the first 2 parameters to be entered are the H and K location of the given reflection. If the lattice has been indexed incorrectly and the major peak of the reflection is not sitting on the predicted lattice location the actual location can sometimes be discovered lying close to the predicted lattice point. 'DISPLAY'ing a large enough area

around each point allows the user to re-index the lattice more accurately.

Data files can be output onto disk by invoking the 'SAVE' command. The program will prompt for the name of the output file which will contain the output. The current version of Difproc will output H, K and intensity. The steps in the entire procedure are outlined in Figure A-2.

$$*\mathrm{RSYM}\ (h,k) = {}_{i}\ \frac{I_{i}(h_i,k_i) - \bar{I}(h,k)}{I_i(h_i,k_i)}$$

where I_i are symmetry related and $\bar{I}$ are the average intensities over i.

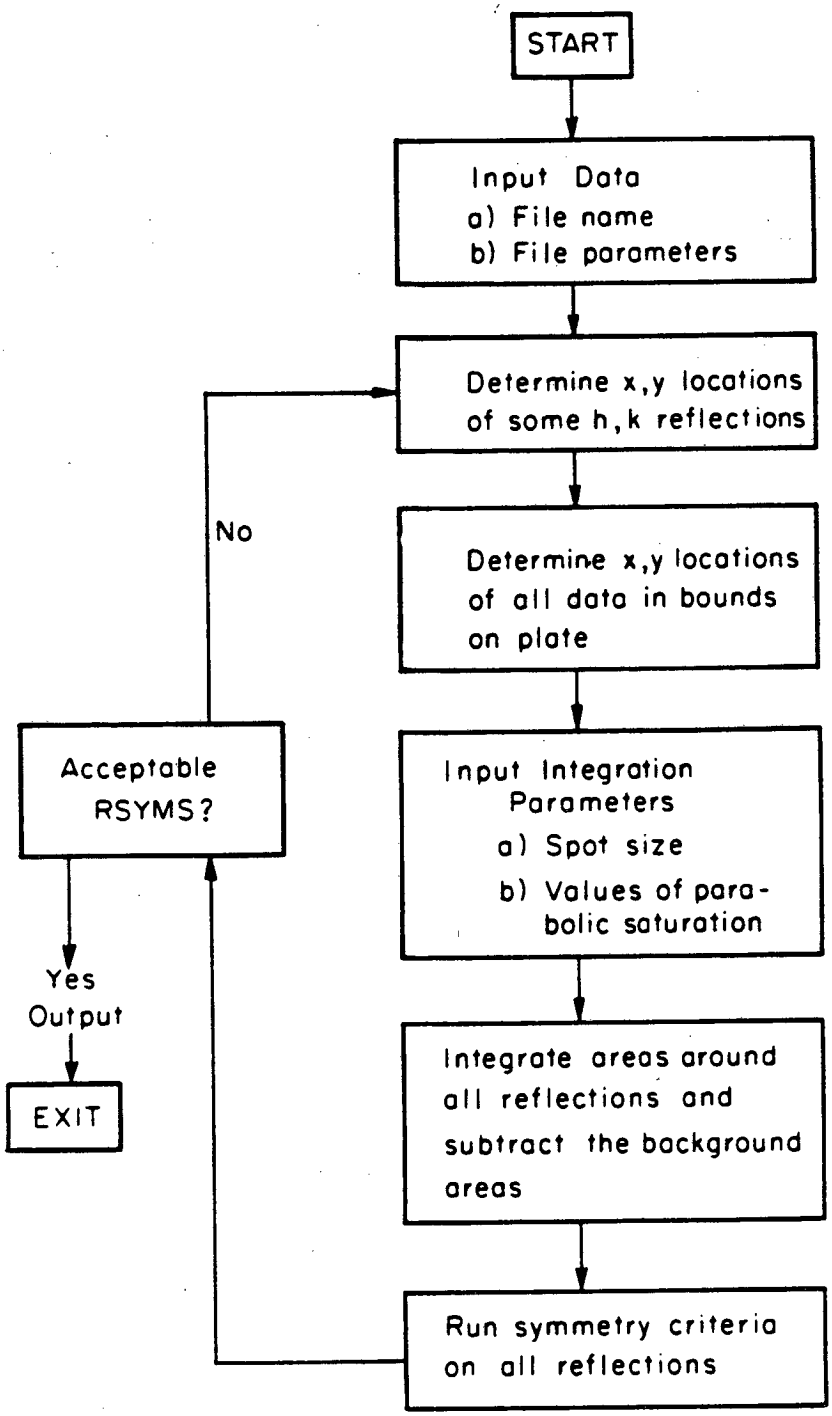

Fig. A-2. Basic steps in processing diffraction patterns.

XBL823-3700

DIFPROC COMMANDS

'WINDOW'
'VTWIND': This command will prompt for x and y origin, the diameter of a square boundry around these origins, and an output square diameter to be displayed. 'WINDOW' will print an intensity modulated printer picture and 'VTWIND' will display an intensity modulated picture on a VT100 terminal. Maximum width of the output fields are 132 and 18.

'LEVELS' This command is meant to be used with the above window command to get minimum and maximum clip levels for displaying the data. The routine will also set levels for the 'DISPLAY' command below.

'LTCREF' This command is used as a prelude to the calculation of the lattice vectors. It can be invoked any number of times and it will prompt the user for the H, K number indices and the X and Y location of the reflection in the input matrix.

'ABCALC' This command will take the values entered in the 'LTCREF' and solve a system of equations for refining orthorhombic lattice. X and Y locations of reflections will be determined for all values within the scan.

'DISPLAY'
'VTDISP' These commands are used to display the area around a given h,k reflection as indexed by the 'ABCALC' command. It is identical to the above "WINDOW" and "VTWIND" command except that instead of giving an X and Y origin the user inputs an H and K value. This command is used to see how well the lattice has been indexed by the least squares technique by comparing the actual and predicted values of reflections. As before, maximum width of the fields is 132 and 18.

'SCNINT' This command will perform the integrations using the input radii and X and Y locations that have already been input. Background subtractions will be performed and parabolic corrections will be applied to all points (background and spots).

'CALSCN' This command must be entered before the scan integration is performed. IT will prompt for a_0, a_1 and a_2 in the parabolic equation $[e^-] = a_0 + a_1 [O.D.] + a_2 [O.D.]^2$.

'RSYM' This command is meant to be used to evaluate the results of the lattice vector calculations and subsequent spot integrations. It will take the output of these two procedures and display the RSYM of given symmetry related reflections for a given plate. Its main use is a further check on the correct indexing of the lattice, however other experimental situations (tilt, focus) may affect the symmetry relatedness of the reflections.

'HEADER' Used to decode the PDS header this command will output all of the X and Y locations for the individual frames as well as the general scan parameters.

'QUIT' The command will terminate the session without saving any files.

'SAVE' This command will terminate the session, and will prompt for a file name and 60 character command which is placed at the beginning of the file.

REFERENCES

1. Agard, D. A. and Stroud, R. M., "Linking Regions Between Helices in Bacteriorhodopsin Revealed," Biophy. J. 37, 589-602 (1982).

2. Anderson, T. F. "Stereoscopic Study of Cells and Viruses in the Electron Microscope." Amer. Naturalist 86, 91-100 (1952).

3. Arnone, A., Bier, C. J., Cotton, F. A., Day, V. W., Hazen, E. E., Richardson, D. C., Richardson, J. S. "A High Resolution Structure of an Inhibitor Complex of the Extracellular Nuclease of Staphylococcus Aureus." J. Biol. Chem. 246, 2302-2316 1971.

4. Becker, B., Tokunaga, F. and Ebrey, T. G., "Ultraviolet and Visible Absorbtion Spectra of Purple Membrane Protein and Photocycle Intermediates," Biochemistry 17, 2293-2300 (1978).

5. Baumeister, W. and Hahn, M. "Specimen Supports," Principles and Techniques of Electron Microscopy, 8, 1-112 (1978).

6. Bayley, H., Huang, K.S., and Radhakrishnan, R., Ross, A. H., Takagaki, Y., and Khorana, H. G. "Site of Attachment of Retinal in Bacteriorhodopsin." Proc. Nat. Acad. Sci., 78, 2225-2229, (1981).

7. Becher, B. and Ebrey, T. G. "The Quantum Efficiency for the Photochemical Conversion of the Purple Membrane Protein." Biophys. J. 17, 185-191 (1977).

8. Blaurock, A. L. and King, G. L., "Asymmetric Structure of the Purple Membrane," Science 196, 1101-1104 (1977).

9. Blaurock, A. L., "Bacteriorhodopsin: A Trans-Membrane Pump Containing α-helix." J. Mol. Biol. 93, 139-158 (1975).

10. Blaurock, A. E., Stoeckenius, W., Oesterhelt, D., and Scherphof, G. L. "Structure of the Cell Envelope of Halobacterium halobium." J. Cell Biol. 71, 1-22 (1976).

11. Blaurock, A. and Stoeckenius, W. "Structure of the Purple Membrane," Nature New Biology, 233, 152-5 (1971).

12. Blow, D. M. and Crick, F.H.C. "The Treatment of Errors in the Isomorphous Replacement Method," Act. Cryst. 12, 794-802 (1959).

13. Blundell, T. L. and Johnson, L. N. "Protein Crystallography," 404-419, Academic Press, 1976.

14. Bogomolni, R. A., Hwang, S. B., Tseug, Y.-W., King, G. I., Stoeckenius, W. "Orientation of the Bacteriorhodopsin Transition Dipole." Biophys. J. 17, 98a, (1977).

15. Braiman, M. and Mathies, R. "Resonance Raman Evidence for All-Trans to 13-Cis Isomerization in the Proton-Pumping Cycle of Bacteriorhodopsin," Biochemistry 19, 5421-5428 (1980).

16. Braiman, M. and Mathies, R. "Resonance Raman Spectra of Bacteriorhodopsin's Primary Photo Product: Evidence for a Distorted 13-Cis Retinal Chromophore," Proc. Nat. Acad. Sci. 79, 403-407 (1982).

17. Bridgen, J. and Walker, I.D. "Photoreceptor Protein from the Purple Membrane of Halobacterium halobium. Molecular Weight and Retinal Binding Site," Biochemistry 15, 792-798, (1976).

18. Chou, P. Y. and Fasman, G. D. "Prediction of the Secondary Structure of Proteins from Their Amino Acid Sequence." Adv. Enzymol 47, 45-148 (1978).

19. Ebrey, T. G., Becher, B., Mao, B., Kilbridge, P., and Honig, B. "Exciton Interactions and Chromophore Orientation in the Purple Membrane." J. Mol. Biol. 112, 377-397 (1977).

20. Engleman, D. M., Henderson, R., McLachlan, A. D., and Wallace, B. A. "Path of the Polypeptide in Bacteriorhodopsin," Proc. Nat. Acad. Sci. 77, 2023-2027 (1980).

21. Engleman, D. M. and Zaccai, G. "Bacteriorhodopsin is an Inside-out Protein." Proc. Nat. Acad. Sci. 77, 5894-5898 (1980).

22. Fersht, A. "Enzyme Structure and Mechanism," 288-345, W. H. Freeman and Company (1977).

23. Fisher, K. A., Yanagimoto, k. and Stoeckenius, W. "Purple Membrane Bound to Polylysine Glass: Effects of pH and Light." J. Cell Biol. 75, 220a (1977).

24. Fisher, K. A., Yanagimoto, K. and Stoeckenius, W. "Oriented Adsorbtion of Purple Membrane to Cationic Surfaces," J. Cell. Biol. 77, 611-621 (1978).

25. Gerber, G. E., Gray, C. P., Wildenauer, D., and Khorana, H. G. "Orientation of Bacteriorhodopsin in Halobacterium halobium as Studied by Selective Proteolysis." Proc. Nat. Acad. Sci. 74, 5426-5430 (1977).

26. Glaeser, R. M., "Radiation Damage and Biological Electron Microscopy," in Physical Aspects of Electron Microscopy and Microbeam Analysis, B. Siegel, D. R. Beaman eds., 205-229, John Wiley and Son (1975).

27. Glaeser, R. M., "Limitations to Significant Information in Biological Electron Microscopy as a Result of Radiation Damage," J. Ultrastructure Res. 36, 466-482 (1971).

28. Govindjee, R., Ebrey, T. G. and Crofts, A. R., "The Quantum Efficiency of Proton Pumping by the Purple Membrane of Halobacterium halobium," Biophys. J. 30, 231-242 (1980).

29. Hall, C. E. "Introduction to Electron Microscopy," McGraw-Hill 371-376, (1963).

30. Hayward, S. B. and Glaeser, R. M.. "High Resolution Cold Stage for the JEOL 100B and 100C Electron Microscopes," Ultramicroscopy 5, 3-8 (1980).

31. Hayward, S. B., Grano, D. A., Glaeser, R. M. and Fisher, K. A. "Molecular Orientation of Bacteriorhodopsin within the Purple Membrane of Halobacterion halobium," Proc. Nat. Acad. Sci. 75, 4320-4324 (1978).

32. Hayward, S. B. and Glaeser, R. M. "Radiation Damage of Purple Membrane at Low Temperature," Ultramicroscopy 4, 201-210 (1979).

33. Hayward, S. B. and Stroud, R. M. "Projected Structure of Purple Membrane Determined to 3.7Å Resolution by Low Temperature Electron Microscopy." J. Mol. Biol. 151, 491-517. (1981).

34. Heide, H. G. and Grund, S. "A Deep Cooling Chain for the Transport of Hydrated Biological Objects into the Electron Microscope." J. Ultrastructure Research 48, 259-268 (1974).

35. Henderson, R., "Structure of Crystalline α-Chymotsypsin," J. Mol. Biol. 54, 341-354 (1970).

36. Henderson, R. "The Structure of the Purple Membrane from Halobacterium halobium, Analysis of the X-Ray Diffraction Pattern." J. Mol. Biol. 93, 123-138 (1975).

37. Henderson, R. "The Purple Membrane from Halobacterium halobium." Ann. Rev. Biophys. Bioeng. 6, 87-109 (1977).

38. Henderson, R., Jubb, J. S., and Rossman, M. G. "A Contracted Form of the Trigonal Purple Membrane of Halobacterium halobium." J. Mol. Biol. 154, 501-514 (1982).

39. Henderson, R., Jubb, J. S., and Whytock, S. "Specific Labeling of the Protein and Lipid on the Extracellular Surface of Purple Membrane," J. Mol. Biol. 123, 259-274 (1978).

40. Henderson, R. and Moffat, J. K. "The Difference Fourier Technique in Protein Crystallography: Errors and Their Treatment." Acta Cryst. B27, 1414-1422 (1971).

41. Henderson, R. and Unwin, P.N.T. "Three Dimensional Model of Purple Membrane Obtained by Electron Microscopy." Nature, 257, 28-32 (1975).

42. Henderson, R. "Membrane Protein Structure," in Membranes and Intercellular Communication, R. Balian, M. Chabre, P. F. Devaux eds., 232-248, North Holland Publishing (1981).

43. Heuser, J. E., "Ultrafast Freezing to Capture the Structural Changes that Underlie Neuromuscular Transmission," Excerpta Medica International Congress Series No. 404, Pathogenesis of Human Muscular Dytrophies, Proceedings of the Fifth International Conference of the Muscular Dystrophy Assoc. 62-72, (1976).

44. Heyn, M. P., Bauer, P. J., and Dencher, N. A. "A Natural CD Label to Probe the Structure of Purple Membrane from the Halobacterium halobium by Means of Exciton Coupling Effects." Biochem. Biophys. Res. Commun. 67, 897-903 (1975).

45. Honig, B., Ebrey, T., Callender, R. H., Dinor, V. and Ottolenghi, M. "Photo Isomerization Energy Storage, and Charge Separation: A Model for Light Energy Transduction in Visual Pigments and Bacteriorhodopsin," Proc. Nat. Acad. Sci. 76, 2503-2507 (1979).

46. Katre, N. V. and Stroud, R. M. "A Probable Linking Sequence Between Two Transmembrane Components of Bacteriorhodopsin," FEBS Letters, 136, 170-174 (1981a).

47. Katre, N. V., Wolber, P. K., Stoeckenius, W. and Stroud, R. M. "Attachment Site(s) of Retinal in Bacteriorhodopsin," Proc. Nat. Acad. Sci. 78, 4068-4072 (1981b).

48. Kellenberger, E. and J. Kistler. "The Physics of Specimen Preparation," in Advances in Structure Research by Diffraction Methods, W. Hoppe, R. Mason, eds., 49-81, Friedr. Viewig. E. Sohn. (1979).

49. Khorana, H. G., Gerber, G. E., Herlihy, W. C., Grant, C. P., Anderess, R. J., Nihel, K., and Biemann, K. "Amino Acid Sequence of Bacteriorhodopsin," Proc. Nat. Acad. Sci. 76, 5046-5050 (1979).

50. King, G. I., Mowery, P. C., Stoeckenius, W., Crespi, H. L. and Schoenborn, B. P. "Location of the Chromophore in Bacteriorhodopsin, Proc. Nat. Acad. Sci. 77, 4726-4720, (1980).

51. King, G. I., Stoeckenius, W., Crespi, H. L. and Schoenborn, B. P. "The Location of Retinal in the Purple Membrane Profile by Neutron Diffraction," J. Mol. Biol. 130, 395-404 (1979).

52. Kistler, J., Aebi, U. and Kellenberger, E. "Freeze Drying and Shadowing of Two-Dimensional Periodic Specimens," J. Ultrastructure Res. 59, 78-86 (1977).

53. Kistler, J. and Kellenberger, E. "Collapse Phenomena in Freeze Drying." J. Ultrastructure Res. 59, 70-75 (1977).

54. Kouyama, T., Kimura, Y., Konosita, K. and Itegami, A. "Location and Orientation of the Chromophore in Bacteriorhodopsin." J. Mol. Biol. 153, 337-359 (1981).

55. Kraut, J. C., Siegler, L. C., High, D. F. and Freer, S. T., "Chymotrypsinogen: A Three-Dimensional Fourier Synthesis at 5Å Resolution." Proc. Nat. Acad. Sci. 18, 1417-1424 (1962).

56. Krimm, S. and Dwivedi, A. M., "Infrared Spectrum of Purple Membrane: Clue to a Proton Conduction Mechanism," Science 216, 407-408 (1982).

57. Lemke, H. D. and Oesterhelt, D. "Lysine 216 is a Binding Site of the Retinyl Moiety in Bacteriorhodopsin," FEBS Letters 128, 255-260 (1981).

58. Lepault, J. and Dubochet, J. "Preservation of Biological Specimens after Freezing," Proceedings of the European Congress on Electron Microscopy 2, 648 (1980).

59. Lewis, A., Spoonhower, J., Bogomolni, R., Lozier, R., and Stoeckenius, W. "Tunable Laser Resonance Raman Spectroscopy of Bacteriorhodopsin." Proc. Nat. Acad. Sci. USA 71, 4462-4466 (1974).

60. Long, M. M., Urry, D. W., and Stoeckenius, W. "Circular Dichroism of Biological Membranes: Purple Membrane of Halobacterium halobium." Biochem. Biophys. Res. Commun. 75, 725-731 (1977).

61. Lozier, R. H., Boglomoni, R. A. and Stoeckenius, W. "Bacteriorhodopsin: a Light Driven Proton Pump in Halobacterium halobium." Biophysics J. 15, 955-962 (1975).

62. Mathews, B. W., Klopfenstein, C. E. and Colman, P. M. "A Computer Controlled Film Scanner for X-Ray Crystallography." Journal of Physics E: Scientific Instruments, 5, 353-359 (1972).

63. Matricardi, V. F., Moretz, R. C. and Parsons, D. F. "Electron Diffraction of Wet Proteins: Catalase." Science, 177, 268-270 (1972).

64. Merryman, H. T. "Freezing Injury and Its Prevention in Living Cells," Annual Rev. of Biophys. and Bioeng., 3, 341-363 (1974).

65. Moffat, J. K. "Spin-labeled Haemoglobins: A Structural Interpretation of Electron Paramagnetic Resonance Spectra Based on X-ray Analysis." J. Mol. Biol. 55, 135-146 (1971).

66. Morowitz, H. J. "Proton Semiconductors and Energy Transduction in Biological Systems." Am. J. Physiol. 235(3): R99-114 (1978).

67. Mullen, E., Johnson, A. H. and Akhtar, M. "The Identification of Lys 216 as the Retinal Binding Residue in Bacteriorhodopsin," FEBS Letters 130, 187-193 (1981).

68. Nagle, J. F. and Morowitz, H. J. "Molecular Mechanisms for Proton Transport in Membranes," Proc. Nat. Acad. Sci. U.S.A. 75, 298-302 (1978).

69. Oesterhelt, D. and Hess, B. "Reversible Photolysis of the Purple Complex in the Purple Membrane of Halobacterium halobium." Eur. J. Biochem. 37, 316-326 (1973).

70. Oesterhelt, D., Meentzen, M. and Schuhmann, L. "Reversible Dissociation of the Purple Complex in Bacteriorhodopsin and Identification of 13 Cis and all-trans-retinal as its Chromophores." Eur. J. Biochem. 40, 458-463 (1973).

71. Oesterhelt, D. and Stoeckenius, W. "Rhodopsin-like Protein from the Purple Membrane of Halobacterium halobium." Nature New Biology 233, 152-155 (1971).

72. Oesterhelt, D. and Stoeckenius, W. "Function of a New Photoreceptor Membrane," Proc. Nat. Acad. Sci. 70, 2853-2857 (1973).

73. Ort, D. R. and Parson, W. W. "The Quantum Yield of Flash-Induced Proton Release by Bacteriorhodopsin Containing Membrane Fragments," Biophys. J. 25, 341-353 (1979).

74. Ovchinnikov, N. G., Abdulev, N. G., Feigina, M. Y., Kiselev, A. V., and Lobanov, N. A. "The Structural Basis of the Functioning of Bacteriorhodopsin: An Overview." FEBS Letters, 100, 219-224 (1979).

75. Ovchinnikov, Y. A., Abdulaev, N. G., Fegina, M. Yu., Kiselev, A. V., and Lobanov, N. A. "Recent Findings in the Structure-Functional Characteristics of Bacteriorhodopsin." FEBS Letters, 84, 1-4 (1977).

76. Parsons, D. F. "Structure of Wet Specimens in Electron Microscopy," Science, 186, 407-414 (1974).

77. Perutz, M. F. "Stereochemistry of Cooperative Effects in Haemoglobin," Nature 228, 726-739 (1970).

78. Perutz, M. F., Murihead, M., Cox, J. M. and Goaman, L. G. C. "Three-Dimensional Fourier Synthesis of Horse Oxyhaemoglobin at 2.8Å: The Atomic Model." Nature 219, 131-139 (1968).

79. Racker, E. and Stoeckenius, W. "Reconstruction of Purple Membrane Vesicles Catalyzing Light-Driven Proton Uptake and Adenosine Triphosphate Formation." J. Biol. Chem. 249, 662-663 (1973).

80. Renard, M. and DelMelle, M. "Quantum Efficiency of Light-Driven Protein Extrusion in Halobacterium halobium: pH Dependence." Biophys. J., 32, 993-1006 (1980).

81. Rogan, P. K. and Zaccai, G. "Hydration in Purple Membrane as a Function of Relative Humidity." J. Mol. Biol. 145, 281-284 (1981).

82. Rothschild, K. J. and Clark, N. A. "Polarized Infared Spectroscopy of Oriented Purple Membrane." Biophys. J. 25, 473-488 (1979).

83. Sigrist, H. and Zahler, P. "Heterobifunctional Crosslinking of Bacteriorhodopsin by Azidophenylisothiocyanate." FEBS Lett., 113, 307-311 (1980).

84. Skau, H. B., Franks, F., Asquith, M. H. and Echlin, P. "Polymeric Cryoprotectants in the Preservation of Biological Ultrastructure." J. Microscopy, 110, 239-270 (1977).

85. Stoeckenius, W. and Kunaw, W. H. "Further Characterization of Particulate Fractions from Lysed Cell Envelopes of Halobacterium halobium and Isolation of Gas Vacuole Membranes." J. Cell Biol. 38: 337-357 (1968).

86. Stoeckenius, W. and Rowen, R. "A Morphological Study of Halobacterium halobium and its Lysis in Media of Low Salt Concentration." J. Cell. Biol. 34, 365-396 (1967).

87. Stoeckenius, W., Lozier, R. H., and Boglomoni, R. A. "Bacteriorhodopsin and the Purple Membrane of Halobacteria," Biochim. Biophys Acta, 505, 215-278 (1979).

88. Stryer, L., Kendrew, J. C., and Watson, H. C., "The Mode of Attachment of Azide Ion to Sperm Whale Metmyoglobin," J. Mol. Biol. 8, 96-104 (1964).

89. Talmon, V., Davis, H. T., Scriven, L. E. and Thomas, E. L. "Cold Stage Microscopy System for Fast-Frozen Liquids 50, 698-704, Rev. Sci. Instrum. (1979).

90. Taylor, K. A. and Glaeser, R. M. "Hydrophilic Support Films of Controlled Thickness and Composition." Rev. Sci. Instrum. 44, 1546-1547 (1973).

91. Taylor, K. A. and Glaeser, R. M. "Modified Airlock Door for the Introduction of Frozen Specimens into the JEM 100B Microscope." Rev. Sci. Instrum. 46, 985-986 (1975).

92. Taylor, K. A. and Glaeser, R. M. "Electron Microscopy of Frozen Hydrated Biological Specimens." J. Ultrastructure Res. 55, 448-456 (1976).

93. Unwin, P. N. T. and Henderson, R. "Molecular Structure Determination by Electron Microscopy of Unstained Crystalline Specimens," J. Mol. Biol. 94, 425-440 (1975).

94. Valentine, R. C. "The Response of Photographic Emulsions to Electrons." Adv. Optical Electron Microscopy 1, 180-203 (1966).

95. Wallace, B. A. and Henderson, R. "The Path of the Polypeptide of Bacteriorhodopsin: Electron Diffraction Studies of Purple Membrane." Biophys. J. 33, 261a (1981).

96. Warshel, A. "Charge Stabilization Mechanism in the Visual and Purple Membrane Pigments." Proc. Nat. Acad. Sci. 75, 2558-2262 (1978).

97. Williams, R. C. "A Method of Freeze-Drying for Electron Microscopy." Exptl. Cell Res. 4, 188 (1953).

98. Wilson, A. J. C. "The Probability Distribution of X-ray Intensities." Acta Cryst. 2, 318 (1949).

99. Wooster, W. A. "Microdensitometry Applied to X-ray Photographs." Acta Cryst. 17, 878-883 (1964).

100. Zaccai, G. and Gilmore, D. J. "Areas of Hydration in Purple Membrane of Halobacterium halobium: A Neutron Diffraction Study." J. Mol. Biol. 132, 181-191 (1979).

This report was done with support from the Department of Energy. Any conclusions or opinions expressed in this report represent solely those of the author(s) and not necessarily those of The Regents of the University of California, the Lawrence Berkeley Laboratory or the Department of Energy.

Reference to a company or product name does not imply approval or recommendation of the product by the University of California or the U.S. Department of Energy to the exclusion of others that may be suitable.

TECHNICAL INFORMATION DEPARTMENT
LAWRENCE BERKELEY LABORATORY
UNIVERSITY OF CALIFORNIA
BERKELEY, CALIFORNIA 94720